Nonequilibrium boundary-driven quantum systems: Models, methods, and properties

Gabriel T. Landi*

Instituto de Física da Universidade de São Paulo, 05314-970 São Paulo, Brazil

Dario Poletti†

Science, Mathematics and Technology Cluster and Engineering Product Development Pillar, Singapore University of Technology and Design, 8 Somapah Road, 487372 Singapore, Singapore

Gernot Schaller‡

Helmholtz-Zentrum Dresden-Rossendorf, Bautzner Landstraße 400, 01328 Dresden, Germany and Institut für Theoretische Physik, Technische Universität Berlin, D-10623 Berlin, Germany

(published 13 December 2022)

Recent years have seen tremendous progress in the theoretical understanding of quantum systems driven dissipatively by coupling to different baths at their edges. This was possible because of concurrent advances in the models used to represent these systems, the methods employed, and the analysis of the emerging phenomenology. A comprehensive review of these three integrated research directions is given. First provided is an overarching view of the models of boundary-driven open quantum systems, in both the weak- and strong-coupling regimes. This is followed by a review of state-of-the-art analytical and numerical methods that are exact, perturbative, and approximate. Finally, the transport properties of some paradigmatic one-dimensional chains are discussed, with an emphasis on disordered and quasiperiodic systems, the emergence of rectification and negative differential conductance, and the role of phase transitions, and an outlook on further research options is given.

DOI: 10.1103/RevModPhys.94.045006

CONTENTS

*gtlandi@gmail.com
†dario_poletti@sutd.edu.sg
‡g.schaller@hzdr.de

I. INTRODUCTION

A piece of material placed in contact with two baths at different temperatures can reach a nonequilibrium steady state (NESS) characterized by a current of heat from one bath to the other. This corresponds to the simplest scenario of nonequilibrium systems most of us are aware of. The currents are generated by differences in the baths, and the type of current that emerges depends on the properties of the bath, of the system, and of their coupling. The ability to control the transport properties of a system can result in devices such as diodes, transistors, and energy converters, which are at the core of a broad range of applications; cf. Li *et al.* (2012) for a review on "phononics" and Dubi and Di Ventra (2011) and Benenti *et al.* (2017) for reviews on thermoelectricity. A deeper understanding of transport at the quantum scale can lead the way to significant progress in nanotechnology.

Recent years have witnessed significant advances in the study of quantum systems coupled, at their edges, to different baths, as depicted in Fig. 1. We refer to these as *boundary-driven systems*. The possibly different temperatures or chemical potentials of the baths can cause a current, and the basic question to be addressed regards the transport properties of the NESS, such as the properties of the currents generated. This review focuses on this type of scenario in the quantum regime. This is particularly relevant in light of experimental advances, which make setups like the one in Fig. 1 directly accessible in the laboratory. The review is split into three fundamental questions: finding the equations of motion, the development of analytical and numerical tools to study them, and the classification of the phenomenology that emerges, especially for strongly correlated quantum systems.

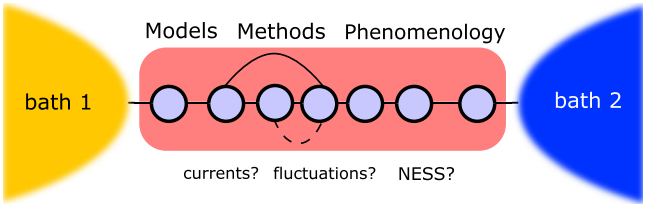

FIG. 1. Boundary-driven systems are composite open systems that are locally coupled to external baths (yellow left and blue right) and internally via a Hamiltonian. This enables nonequilibrium steady states (NESSs) characterized by stationary currents.

To give an idea of the problems that are reviewed here, we consider heat transport between two baths at different temperatures through a bulk material. It was found by Fourier (1822) that the heat current I often reads

$$I = -\kappa_c \frac{\Delta T}{L}, \tag{1}$$

where L is the length of the material in the direction of the current, ΔT is the temperature difference, and κ_c is the thermal conductivity (often considered a constant). One notices that in Eq. (1), known as Fourier's law, the current decays as $I \sim 1/L$, which is referred to as *diffusive transport*.

However, digging deeper one finds that transport can be a much richer field. The conductivity is actually a function of both the temperature T and the system size L. The temperature dependence of the conductivity causes the current to change nonlinearly with temperature. Microscopically, this may result from reservoir modes controlling occupations at the boundaries. A nonlinear response may cause the current to be significantly different in magnitude (and not just in sign) if one flips the temperature gradient ΔT to $-\Delta T$ (Benenti *et al.*, 2016). This means that the system can be used as a diode or rectifier (Terraneo, Peyrard, and Casati, 2002; Li, Wang, and Casati, 2004). For the dependence on the system size, often one finds that the current follows an algebraic dependence

$$I \sim 1/L^{\alpha}. \tag{2}$$

For $\alpha = 0$, the current is independent of the system size, known as *ballistic transport*. As observed with Fourier's law, the case $\alpha = 1$ is called diffusive. For $0 < \alpha < 1$ the transport is called superdiffusive, and for $\alpha > 1$ subdiffusive. In the limit $\alpha \to \infty$ the current goes to zero, which implies that the system is an insulator. In this case the current decays faster than algebraically with the system size, such as $I \sim \exp(-L/L_0)$, where L_0 is referred to as the localization length.[1] For a summary of transport exponents, see Table I in Sec. IV.

[1]In other contexts, the transport scenarios are sometimes defined by focusing on the thermodynamic limit $L \to \infty$ and looking at the conductivity $\kappa_c := -IL/\Delta T$ [Eq. (1)]. Subdiffusiveness would then lead to $\kappa_c \to 0$ (when $L \to \infty$) and hence be referred to as insulating. Similarly, superdiffusiveness would lead to $\kappa_c \to \infty$ and thus be referred to as ballistic. In this review, we focus on finite L, as this allows for deeper insights on the scaling behavior of transport mechanisms (Tritt, 2004).

The techniques to derive the dependence of the conductivity on the system size are also relevant. If one considers transport due to phonons, it is natural to model the system as a chain of coupled harmonic oscillators, which often works well to describe the heat capacity of bulk materials. However, this turns out to result in a ballistic current (Rieder, Lebowitz, and Lieb, 1967; Aoki and Kusnezov, 2001). In classical systems it is found that nonlinearities in the Hamiltonian describing the system are a key ingredient for recovering a size-independent conductivity in Fourier's law in Eq. (1) (Casati *et al.* (1984); see also Dhar, 2008 for a review. It is thus crucial to use the correct models to study the transport properties of a system, as models with different characteristics can result in extremely different dependencies of the currents on the system and bath parameters. This is the essence of boundary-driven systems.

Given the complexity of the systems studied, researchers typically face the following three important questions:

(i) How can one model the dynamics of the system and baths?
(ii) Which analytical or numerical methods could one use?
(iii) What different transport properties can one expect?

Each of these questions could be the focus of a review. However, we aim to give enough breadth and depth of information so that someone starting in the field, or focusing on only some of these questions, can have a more comprehensive perspective. We thus hope to foster more research and advances in the field of boundary-driven systems. We provide answers to the previous questions in Secs. II–IV, respectively.

Given the structure of the review, a reader who is already familiar with some of the questions should be able to fully explore the other issues. The theme of transport is extremely vast and has been studied for more than 200 years. It is thus important that we specify not only what we decided to review but also what we chose not to. Our focus on quantum systems coupled at the their extremities to baths (i.e., dissipative boundary-driven ones) implies that we do not address classical systems; for a review, see Dhar (2008). Regarding the models and methods, we chose not to review linear response theory, Landauer-Büttiker theory, or Green's functions, as they have already been reviewed by Caroli *et al.* (1971), Meir and Wingreen (1992), Prociuk, Phillips, and Dunietz (2010), Aeberhard (2011), Dhar, Saito, and Hänggi (2012), Nikolić *et al.* (2012), and Wang, Agarwalla, and Thingna (2014) or in works given by Economou (2006), Haug and Jauho (2008), and Ryndyk (2016). Similarly, although some of our methods apply to non-Markovian systems, most of our focus will be on Markovian (time-local) quantum dynamics. For reviews specific on non-Markovianity, see Rivas, Huelga, and Plenio (2014), Breuer *et al.* (2016), and de Vega and Alonso (2017). As for recent experimental works, prominent results on strongly interacting systems were reviewed by Bertini *et al.* (2021), and hence we mention only those experiments closer to the phenomenology discussed in Sec. IV. We also focus exclusively on systems without explicit external time dependence, and as such we do not touch on studies of periodically driven systems and their thermodynamic properties (Grifoni and Hänggi, 1998; Kohler, Lehmann, and Hänggi, 2005; Kosloff, 2013; Van den Broeck and Esposito, 2015; Millen and Xuereb, 2016; Vinjanampathy and Anders, 2016; Benenti *et al.*, 2017).

II. MODELS FOR BOUNDARY-DRIVEN OPEN SYSTEMS

A. Paradigms of open quantum system dynamics

We begin by discussing mathematical models of quantum transport. The natural framework for this is the theory of open quantum systems. In standard treatments it is assumed that the global density matrix of the system and its surrounding baths evolves unitarily, according to the Liouville–von Neumann equation (we set $\hbar = 1$ throughout),

$$\frac{d\rho_{\mathrm{SB}}}{dt} = -\mathrm{i}[H_{\mathrm{tot}}, \rho_{\mathrm{SB}}], \tag{3}$$

where $H_{\mathrm{tot}} = H_{\mathrm{S}} + H_{\mathrm{B}} + H_{\mathrm{I}}$ is the total Hamiltonian, encompassing system H_{S}, bath H_{B}, and their interaction H_{I}. This includes the case of multiple baths.

The initial conditions are usually taken such that S and B are uncorrelated; that is, in a product state $\rho_{\mathrm{SB}}(0) = \rho_{\mathrm{S}}(0) \otimes \rho_{\mathrm{B}}(0)$. The global state at time t is then

$$\rho_{\mathrm{SB}}(t) = U(t)\rho_{\mathrm{SB}}(0)U^{\dagger}(t), \qquad U(t) = e^{-\mathrm{i}H_{\mathrm{tot}}t}. \tag{4}$$

The main goal in open quantum systems is to obtain the evolution of the system's reduced density matrix $\rho_{\mathrm{S}}(t) = \mathrm{tr}_{\mathrm{B}}\{\rho_{\mathrm{SB}}(t)\}$, where $\mathrm{tr}_{\mathrm{B}}\{\cdots\}$ stands for the partial trace over the bath. This can be done at the level of the map (4) or the differential equation (3). The former leads to the so-called Kraus maps and the latter to master equations.[2]

Considering first the map (4), it has been shown that the most general open dynamics is given by (Kraus, 1971)

$$\rho_{\mathrm{S}}(t) = \sum_{\alpha} K_{\alpha,t}\rho_{\mathrm{S}}(0)K_{\alpha,t}^{\dagger}, \tag{5}$$

where $K_{\alpha,t}$ are time-dependent operators satisfying $\sum_{\alpha} K_{\alpha,t}^{\dagger}K_{\alpha,t} = \mathbb{1}$. For any choice of such operators K_{α}, the map (5) is said to be completely positive and trace preserving (CPTP). This means that it maps density matrices to density matrices [preserving Hermiticity, normalization, and positivity

[2]The name "master equation" was first coined in a paper about cosmic ray showers (Nordsieck, Lamb, and Uhlenbeck, 1940), where it played the role of a central equation from which all other results could be derived, i.e., a "master key."

even for extensions of the map over ancillas (Nielsen and Chuang, 2000)].[3]

In practice, the Kraus form can be inconvenient, and it is preferable to write the evolution of $\rho_S(t)$ as a differential equation, in general one of the form of (Nakajima, 1958; Zwanzig, 1960)

$$\frac{d\rho_S}{dt} = \int_0^t dt' \mathcal{K}_{t-t'}[\rho_S(t')], \tag{6}$$

where $\mathcal{K}_{t-t'}$ is a linear superoperator called the memory kernel. Equation (6) must be linear in ρ_S since Eq. (5) is also linear. But it will in general be nonlocal in time; i.e., the evolution at time t will depend on the history of the system, a notion of non-Markovianity.

Equation (6) is usually complicated to derive and to solve (de Vega and Alonso, 2017). Instead, we usually search for simpler time-local equations of the form of (Weiss, 1993; Mandel and Wolf, 1995; Breuer and Petruccione, 2002; Schlosshauer, 2007; Rivas and Huelga, 2012)

$$\frac{d\rho_S}{dt} = -i[H_S, \rho_S] + \mathcal{D}(\rho_S), \tag{7}$$

which we refer to as quantum master equations (QMEs). The last term, usually called the *dissipator*, is a linear superoperator that takes into account the effects of the reservoir. Additionally, one may encounter corrections to the Hamiltonian part that are discussed in Sec. II.C. The precise form of $\mathcal{D}(\rho_S)$ depends on the situation at hand. This emphasizes the importance of a microscopic derivation, where $\mathcal{D}(\rho_S)$ is derived from a physical model of system-bath interactions. This will be the main topic of this section.

For example, consider a single spin 1/2 (qubit) with a Hamiltonian $H_S = -h\sigma^z/2$ and a Pauli matrix σ^z. A popular QME for this system describing the contact with a bath at an inverse temperature $\beta = 1/T$ (we also set $k_B = 1$ throughout) is (see Sec. II.C)

$$\frac{d\rho_S}{dt} = -i[H_S, \rho_S] + \gamma(1-f)D[\sigma^-](\rho_S) + \gamma f D[\sigma^+](\rho_S), \tag{8}$$

where the last two terms form the dissipator $\mathcal{D}(\rho_S)$. Here $\gamma > 0$ is the coupling strength to the bath, $f = (e^{\beta h}+1)^{-1}$ is the Fermi-Dirac distribution, and

$$D[L](\rho_S) = L\rho_S L^\dagger - \tfrac{1}{2}\{L^\dagger L, \rho_S\} \tag{9}$$

is called a Lindblad dissipator with jump operators L. The dynamics reflects the interplay between the term $D[\sigma^-]$, which annihilates an excitation with rate $\gamma(1-f)$, and the term $D[\sigma^+]$, which creates an excitation with rate γf. Equation (8) accurately describes many setups, from quantum optics to condensed matter (often with different parametrizations for γ and f). It also has many simple and nice properties: e.g., it relaxes with rate γ to a unique fixed point, which is the thermal state

$$\rho_S^{\rm eq} = \frac{e^{-\beta H_S}}{\mathrm{tr}\{e^{-\beta H_S}\}} = f|1\rangle\langle 1| + (1-f)|-1\rangle\langle -1|, \tag{10}$$

with an average occupation $\langle \sigma^+\sigma^-\rangle_{\rm th} = f$.

One of the most powerful features of the Kraus representation (5) is that it establishes the basic structure that any map should satisfy in order to be CPTP. Similarly, one could ask, given a time-local QME of the form of Eq. (7), what is the most general structure that the dissipator $\mathcal{D}(\rho_S)$ may have to ensure that the dynamics is CPTP? For such a QME and any valid density matrix $\rho_S(0)$, the evolved state $\rho_S(t)$ will continue to be a valid physical state for all times t.

The answer was given independently by Lindblad (1976) and Gorini, Kossakowski, and Sudarshan (1976). Namely, if the master equation has the form

$$\frac{d\rho_S}{dt} = -i[H_S, \rho_S] + \sum_k D[L_k](\rho_S) \tag{11}$$

for any set of operators $\{L_k\}$ and $D[L_k]$ defined in Eq. (9), then it is guaranteed that the dynamics will be CPTP. Equations of this form [such as Eq. (8)] are called Gorini-Kossakowski-Sudarshan-Lindblad (GKSL) QMEs.

The GKSL form ensures only that physical states are mapped to physical states. It says nothing about which kinds of jump operators should be used to model actual thermal baths. To do that, one must derive GKSL equations from models of system-bath reservoirs, for which there is no unique optimal route. Different methods require different approximations and are accurate only in different regimes. A thorough appreciation of the limitations and advantages of each method is therefore crucial to properly tackle boundary-driven systems. This is the overarching theme of this section.

B. Setting the stage through the lens of local master equations

We begin by discussing some prototypical Hamiltonians that we deal with, such as lattices with spins or fermions or bosons. We often consider here 1D lattices containing L sites. This could be a spin chain, where each site i is associated with Pauli operators σ_i^α, $\alpha \in \{x, y, z, +, -\}$. A typical Hamiltonian is the XXZ model in the presence of a magnetic field, which is described by

[3]The specific form of the operators K_α can be obtained from the global map (4) (Stinespring, 1955). We mention two ways to do this. First, if we decompose the bath's initial state as $\rho_B(0) = \sum_n q_n |n\rangle\langle n|$, then one may verify that $K_{nm} = \sqrt{q_n}\langle m|U|n\rangle$ (which is still an operator acting on the system). The index α in K_α is then a collective one $\alpha = (n, m)$. Alternatively, one may decompose the unitary as $U = \sum_j A_j \otimes B_j$, where A_j and B_j are operators acting only on S and B, respectively. Taking the partial trace of Eq. (4) then leads to $\rho_S(t) = \sum_{j,k} C_{jk} A_j \rho_S(0) A_k^\dagger$, where $C_{jk} = \mathrm{tr}_B\{B_k^\dagger B_j \rho_B(0)\}$ is positive semidefinite. Normalization now implies that $\sum_{jk} C_{jk} A_k^\dagger A_j = \mathbb{1}$. This is not yet in Kraus's form (5), but it can be made so by first diagonalizing C_{jk} as $C_{jk} = \sum_\alpha u_{j\alpha}\xi_\alpha u_{k\alpha}^*$, with eigenvalues ξ_α and eigenvectors $u_{j\alpha}$. Defining new operators $K_\alpha = \sqrt{\xi_\alpha}\sum_j u_{j\alpha}^* A_j$ then yields the form (5).

$$H_S = -J\sum_{i=1}^{L-1}(\sigma_i^x\sigma_{i+1}^x + \sigma_i^y\sigma_{i+1}^y + \Delta\sigma_i^z\sigma_{i+1}^z) + \sum_{i=1}^{L} h_i\sigma_i^z, \quad (12)$$

where the first term describes local nearest-neighbor interactions, h_i are local magnetic fields, and Δ is the anisotropy. When $\Delta = 1$ Eq. (12) is called the Heisenberg model and when $\Delta = 0$ it is called the XX model,

$$H_S = -J\sum_{i=1}^{L-1}(\sigma_i^x\sigma_{i+1}^x + \sigma_i^y\sigma_{i+1}^y) + \sum_{i=1}^{L} h_i\sigma_i^z. \quad (13)$$

The XXZ chain is said to be an interacting model, while the XX model is said to be noninteracting. Although the spins interact in both cases, this terminology can be understood through the Jordan-Wigner transformation (Jordan and Wigner, 1928; Lieb, Schultz, and Mattis, 1961), which maps spin operators onto a set of fermionic operators $\{c_i\}$, such as via the mapping

$$c_i = (-\sigma_1^z)(-\sigma_2^z)\cdots(-\sigma_{i-1}^z)\sigma_i^-. \quad (14)$$

Equation (14) is designed to satisfy the canonical algebra $\{c_i, c_j^\dagger\} = \delta_{ij}$ and satisfies $\sigma_i^+\sigma_i^- = c_i^\dagger c_i$ such that $\sigma_i^z = 2c_i^\dagger c_i - \mathbb{1}$. To apply this to the XX chain (13), we note that $\sigma_i^x\sigma_{i+1}^x + \sigma_i^y\sigma_{i+1}^y = 2(\sigma_i^+\sigma_{i+1}^- + \sigma_i^-\sigma_{i+1}^+)$. Up to a constant, this yields the tight-binding model[4]

$$H = -2J\sum_{i=1}^{L-1}(c_i^\dagger c_{i+1} + c_{i+1}^\dagger c_i) + \sum_{i=1}^{L} 2h_i c_i^\dagger c_i. \quad (15)$$

The tight-binding model describes free fermions hopping through a lattice, which is why the XX chain is regarded as noninteracting. Conversely, for the XXZ chain we get an additional term $\Delta(2c_i^\dagger c_i - \mathbb{1})(2c_{i+1}^\dagger c_{i+1} - \mathbb{1})$, which is quartic in the c's.

The typical boundary-driven scenario is to couple this 1D chain to a bath at sites $i = 1$ and $i = L$. The most naive way to do this is to use dissipators like those in Eq. (8), which leads to the local master equation (LME)

$$\frac{d\rho_S}{dt} = -\mathrm{i}[H_S, \rho_S] + \mathcal{D}_1(\rho_S) + \mathcal{D}_L(\rho_S), \quad (16)$$

where

$$\mathcal{D}_i(\rho_S) = \gamma_i(1-f_i)D[\sigma_i^-](\rho_S) + \gamma_i f_i D[\sigma_i^+](\rho_S) \quad (17a)$$

$$= \gamma_i\left(\frac{1-\eta_i}{2}\right)D[\sigma_i^-](\rho_S) + \gamma_i\left(\frac{1+\eta_i}{2}\right)D[\sigma_i^+](\rho_S), \quad (17b)$$

with γ_i describing the coupling strength to each bath $i \in \{1, L\}$. Here η_i and $f_i = (1+\eta_i)/2$ are simply two equivalent parametrizations. If $f_i = \langle\sigma_i^+\sigma_i^-\rangle_{\mathrm{th}}$, then $\eta_i = \langle\sigma_i^z\rangle_{\mathrm{th}}$. For instance, $f_i = 0$ ($\eta_i = -1$) corresponds to a bath that tries to impose the contact site to a spin-down state, $f_i = 1$ ($\eta_i = 1$) imposes spin-up, and $f_i = 1/2$ ($\eta_i = 0$) imposes an infinite-temperature (maximally mixed) state. This would happen, however, only if that site were isolated. Owing to the internal coupling between all sites in the chain, there will be a competition between f_i (η_i) and the Hamiltonian couplings. As a consequence, the steady state will generally differ from what the baths are trying to impose.

Interest is usually in the NESS obtained as the long-time solution of Eq. (16). For different f_1 and f_L, this NESS is characterized by the magnetization current (see Sec. II.D for a discussion)

$$I_M = -2J\langle\sigma_i^x\sigma_{i+1}^y - \sigma_i^y\sigma_{i+1}^x\rangle. \quad (18)$$

In the NESS, I_M is actually independent of the site since the current entering one site is the same as that leaving the other. The question, therefore, is how I_M depends on the system parameters and what kinds of transport regimes emerge.

For instance, the XX model (13) with $h_i = 0$ can be solved analytically (Karevski and Platini, 2009; Žnidarič, 2010b; Asadian *et al.*, 2013), as reviewed in Sec. III.B. Assuming that $\gamma_1 = \gamma_L = \gamma$, one finds that $I_M = [16\gamma J^2/(16J^2+\gamma^2)] \times (f_1 - f_L)$. There will thus be a flow whenever there is a bias between f_1 and f_L. Moreover, the fact that I_M is independent of L shows that transport in the XX chain is ballistic. In addition, the average magnetization in each site will be

$$\langle\sigma_{1,L}^z\rangle = m^* \pm \frac{\gamma}{16J^2}I_M, \qquad \langle\sigma_{2,\ldots,L-1}^z\rangle = m^*, \quad (19)$$

where $m^* = f_1 + f_L - 1$. This constant magnetization profile also indicates that transport is ballistic.

These results illustrate some features of LMEs well. In a nutshell, they correspond to using local dissipators in spatially extended systems and are thus simple to construct. They also have some appealing properties. First, they are GKSL equations by construction, so the dynamics is always guaranteed to be physical, in the sense that it always yields valid density matrices. Second, the dissipators $\mathcal{D}_i$ act only locally on the first and last sites, greatly simplifying numerical and analytical calculations. Third, they provide a straightforward recipe for building other configurations, such as different chain geometries or multiple baths acting on multiple sites. For these reasons, LMEs are often used as the starting point in transport studies with quantum chains.

Even though LMEs produce a CPTP dynamics, they need not reproduce the behavior of standard thermal baths [in the literature, they have been referred to as nonequilibrium or "magnetization" baths (Schuab, Pereira, and Landi, 2016; Žnidarič *et al.*, 2017; Varma and Žnidarič, 2019)]. For instance, Eq. (16) does not properly thermalize the system when the two baths have $f_1 = f_L = f$. Indeed, Eq. (19) predicts that $\langle\sigma_i^z\rangle = m^* = 2f - 1$, while for a thermal state $e^{-\beta H}$ we have $\langle\sigma_i^z\rangle = 0$ since we set $h_i = 0$. Such a discrepancy also appears at the level of the full density matrix. For example, Eq. (16) with $f_1 = f_L$ predicts that all sites should be uncorrelated (Asadian *et al.*, 2013), which is again not the

[4]Instead of fermions, we often work with the bosonic version of the tight-binding model [Eq. (15)]. In this case the Hamiltonian is identical, but the operators satisfy $[c_i, c_j] = 0$ and $[c_i, c_j^\dagger] = \delta_{ij}$.

case for the thermal state $e^{-\beta H}$. These limitations motivate the search for better models for describing the system-bath dynamics, which is the focus of Secs. II.C and II.H.

Notwithstanding these deficiencies, LMEs are still extremely useful in transport studies since they provide a convenient tool for describing the injection and extraction of excitations. Moreover, it is often found that the *transport regime* (ballistic, diffusive, etc.) is independent of the choice of the boundary driving. This cannot be proven in general, but rigorous results for diffusive systems were derived by Žnidarič (2019). This is important because one is often interested in knowing how different ingredients in a Hamiltonian affect the ensuing transport. Quasiperiodic and disordered systems, which are reviewed in Sec. IV.D, are a good example. In this case, different types of disorder lead to dramatically different transport regimes. And while LMEs may not faithfully describe actual heat baths, they may suffice to determine the latter.

C. Weak system-bath coupling

1. Redfield master equation

The usual starting point in the derivation of a master equation for the system density matrix is the partition of the Hamiltonian $H = H_S + H_I + H_B$ into a system part H_S, a bath (reservoir) part H_B, and an interaction part H_I. The first two act on different Hilbert spaces (and thus commute), whereas H_I can generally be decomposed as

$$H_I = \sum_\alpha A_\alpha \otimes B_\alpha, \tag{20}$$

with system and bath coupling operators A_α and B_α, respectively. Such a tensor product decomposition can always be obtained. Additionally, it may prove to be convenient to choose the coupling operators A_α and B_α as individually Hermitian, but we proceed without this assumption. Altogether the system and reservoir constitute the full universe, which evolves unitarily according to the von Neumann equation (3). Since we aim for weak-coupling representations, it is useful to switch to an interaction picture with respect to $H_S + H_B$ by defining $\boldsymbol{\rho}_{SB}(t) \equiv e^{+\mathrm{i}(H_S+H_B)t}\rho_{SB}e^{-\mathrm{i}(H_S+H_B)t}$ (in the following, we use boldface symbols to represent operators in the interaction picture). The von Neumann equation is then changed to

$$\dot{\boldsymbol{\rho}}_{SB} = -\mathrm{i}[\boldsymbol{H}_I(t), \boldsymbol{\rho}_{SB}(t)], \tag{21}$$

where $\boldsymbol{H}_I(t) = \sum_\alpha \boldsymbol{A}_\alpha(t) \otimes \boldsymbol{B}_\alpha(t)$, with $\boldsymbol{A}_\alpha(t) = e^{+\mathrm{i}H_S t}A_\alpha e^{-\mathrm{i}H_S t}$ and $\boldsymbol{B}_\alpha(t) = e^{+\mathrm{i}H_B t}B_\alpha e^{-\mathrm{i}H_B t}$. This equation is still exact but involves all the reservoir degrees of freedom. Integrating both sides in time and solving formally for $\boldsymbol{\rho}_{SB}(t)$, we get $\boldsymbol{\rho}_{SB}(t) = \rho_{SB}(0) - \mathrm{i}\int_0^t [\boldsymbol{H}_I(t'), \boldsymbol{\rho}_{SB}(t')]dt'$, which we can reinsert into Eq. (21). Tracing out the reservoir degrees of freedom, we then obtain the following for the system density matrix in the interaction picture $\boldsymbol{\rho}_S \equiv \mathrm{tr}_B\{\boldsymbol{\rho}_{SB}\}$:

$$\dot{\boldsymbol{\rho}}_S = -\mathrm{i}\,\mathrm{tr}_B\{[\boldsymbol{H}_I(t), \rho_{SB}(0)]\} - \int_0^t dt' \mathrm{tr}_B\{[\boldsymbol{H}_I(t), [\boldsymbol{H}_I(t'), \boldsymbol{\rho}_{SB}(t')]]\}. \tag{22}$$

Equation (22) is still exact but not yet closed, as the rhs still depends on the density matrix $\boldsymbol{\rho}_{SB}(t)$ of the full universe. At the initial time, the system and reservoir are assumed in a product state $\rho_0 = \rho_S^0 \otimes \bar{\rho}_B$. Here $\bar{\rho}_B$ is typically an equilibrium reservoir state (such as a Gibbs state), and we assume that $[H_B, \bar{\rho}_B] = 0$. For many reasonable interaction Hamiltonians and reservoir density matrices, we also have $\mathrm{tr}_B\{B_\alpha \bar{\rho}_B\} = 0$, such that only the second term on the rhs of Eq. (22) remains.[5]

To proceed, we assume the system-reservoir interaction to be small: $H_I = \mathcal{O}\{\lambda\}$, where λ is a dimensionless bookkeeping parameter that is later set to unity. We can thus close Eq. (22) by inserting the Born approximation for all times $\boldsymbol{\rho}_{SB}(t) = \boldsymbol{\rho}_S(t) \otimes \bar{\rho}_B + \mathcal{O}\{\lambda\}$. Owing to the double commutator in Eq. (22), the error in doing this is of $\mathcal{O}\{\lambda^3\}$. The partial trace on the rhs of Eq. (22) can be expressed as follows in terms of the reservoir correlation functions:

$$\begin{aligned} C_{\alpha\beta}(t_1, t_2) &= \mathrm{tr}_B\{\boldsymbol{B}_\alpha(t_1)\boldsymbol{B}_\beta(t_2)\bar{\rho}_B\} \\ &= \mathrm{tr}_B\{\boldsymbol{B}_\alpha(t_1 - t_2)B_\beta\bar{\rho}_B\} \equiv C_{\alpha\beta}(t_1 - t_2), \end{aligned} \tag{23}$$

which depends only on the time difference since $[H_B, \bar{\rho}_B] = 0$. For Gibbs states of the reservoir, at inverse temperature β the correlation functions also obey the Kubo-Martin-Schwinger (KMS) relations

$$C_{\alpha\bar{\alpha}}(\tau) = C_{\bar{\alpha}\alpha}(-\tau - \mathrm{i}\beta), \tag{24}$$

which eventually imprint the thermal properties of the reservoir onto the system (Kubo, 1957; Martin and Schwinger, 1959).

When one makes the correlation functions explicit, the following non-Markovian master equation in integro-differential form results:

$$\begin{aligned} \dot{\rho}_s = -\sum_{\alpha\beta}\int_0^t dt' \{ & C_{\alpha\beta}(t - t')[\boldsymbol{A}_\alpha(t), \boldsymbol{A}_\beta(t')\boldsymbol{\rho}_S(t')] \\ & + C_{\beta\alpha}(t' - t)[\boldsymbol{\rho}_S(t')\boldsymbol{A}_\beta(t'), \boldsymbol{A}_\alpha(t)]\}. \end{aligned} \tag{25}$$

Equation (25) preserves both the trace and the Hermiticity of the system density matrix but can be solved efficiently only for sufficiently simple reservoir correlation functions [such as exponentially decaying ones (Kleinekathöfer, 2004)]. Positivity of ρ_S is also no longer guaranteed, except in special cases (Maniscalco, 2007).

The integrand on the rhs of Eq. (25) is a typically product of rapidly decaying correlation functions with the slowly varying system density matrix. This allows one to perform the Markov approximation in two steps. The first step renders the equation time local by replacing $\boldsymbol{\rho}_S(t') \to \boldsymbol{\rho}_S(t)$, thereby yielding the Redfield-I master equation (Redfield, 1965)

[5]This condition can always be met by the transformation $H_S \to H_S + \sum_\alpha g_\alpha A_\alpha$ and $B_\alpha \to B_\alpha - g_\alpha$ with a suitably chosen $g_\alpha = \mathrm{tr}\{B_\alpha\bar{\rho}_B\} \in \mathbb{C}$ that leaves the total Hamiltonian invariant but redefines the system and interaction Hamiltonians.

$$\dot{\boldsymbol{\rho}}_{\mathrm{s}} = -\sum_{\alpha\beta}\int_0^t dt'\{C_{\alpha\beta}(t-t')[\boldsymbol{A}_\alpha(t),\boldsymbol{A}_\beta(t')\boldsymbol{\rho}_{\mathrm{S}}(t)] + C_{\beta\alpha}(t'-t)[\boldsymbol{\rho}_{\mathrm{S}}(t)\boldsymbol{A}_\beta(t'),\boldsymbol{A}_\alpha(t)]\}. \tag{26}$$

The coefficients still depend on time (even after transforming back to the Schrödinger picture). Therefore, using the same reasoning (fast decay of the correlation functions) the upper integration bounds can, after the substitution $\tau = t - t'$, be sent to infinity. This yields the Redfield-II master equation

$$\dot{\boldsymbol{\rho}}_{\mathrm{s}} = -\sum_{\alpha\beta}\int_0^\infty d\tau\{C_{\alpha\beta}(\tau)[\boldsymbol{A}_\alpha(t),\boldsymbol{A}_\beta(t-\tau)\boldsymbol{\rho}_{\mathrm{S}}(t)] + C_{\beta\alpha}(-\tau)[\boldsymbol{\rho}_{\mathrm{S}}(t)\boldsymbol{A}_\beta(t-\tau),\boldsymbol{A}_\alpha(t)]\}. \tag{27}$$

Back in the Schrödinger picture, this has the advantage of not only being time local but also having constant coefficients:

$$\begin{aligned}\dot{\rho}_{\mathrm{S}} = {}& -\mathrm{i}[H_{\mathrm{S}},\rho_{\mathrm{S}}(t)] \\ & -\sum_{\alpha\beta}\int_0^\infty C_{\alpha\beta}(+\tau)[A_\alpha, e^{-\mathrm{i}H_{\mathrm{S}}\tau}A_\beta e^{+\mathrm{i}H_{\mathrm{S}}\tau}\rho_{\mathrm{S}}(t)]d\tau \\ & -\sum_{\alpha\beta}\int_0^\infty C_{\beta\alpha}(-\tau)[\rho_{\mathrm{S}}(t)e^{-\mathrm{i}H_{\mathrm{S}}\tau}A_\beta e^{+\mathrm{i}H_{\mathrm{S}}\tau}, A_\alpha]d\tau.\end{aligned} \tag{28}$$

The remaining integrals can be explicitly computed by inserting Fourier transforms of the reservoir correlation functions, as done in Eq. (34), and invoking the Sokhotski-Plemelj theorem

$$\frac{1}{2\pi}\int_0^\infty e^{+\mathrm{i}\omega\tau}d\tau = \frac{1}{2}\delta(\omega) + \frac{\mathrm{i}}{2\pi}\mathcal{P}\frac{1}{\omega}, \tag{29}$$

where $\mathcal{P}$ denotes the Cauchy principal value. It is straightforward to show that Redfield versions I and II both unconditionally preserve the trace and Hermiticity of the system density matrix. But they do not necessarily preserve the positivity, which has led to extensive efforts to correct for this shortcoming (Gaspard and Nagaoka, 1999; Kiršanskas, Franckié, and Wacker, 2018; Farina and Giovannetti, 2019; Ptaszyński and Esposito, 2019). Additionally, they may not exactly thermalize the system with the reservoir temperature, but when the perturbative assumptions employed in the derivation are valid, one may show that violations of both the positivity and the thermodynamic consistency of $\mathcal{O}\{\lambda^3\}$ will also be small (Thingna, Wang, and Hänggi, 2012). One also finds that the so-called fluctuation relations (Esposito and Mukamel, 2006) are not necessarily obeyed by the Redfield master equation (Hussein and Kohler, 2014).

2. Global GKSL master equation

The Redfield-II QME is not in GKSL form [Eq. (11)] and generally does not relax the system to its local equilibrium state. To arrive at a GKSL generator, an additional approximation is necessary. We return to Eq. (27) and make the interaction-picture time dependence of the coupling operators explicit,

$$\boldsymbol{A}_\alpha(t) = \sum_{ab}\langle a|A_\alpha|b\rangle e^{+\mathrm{i}(E_a-E_b)t}|a\rangle\langle b|, \tag{30}$$

with the system energy eigenbasis defined by

$$H_{\mathrm{S}}|a\rangle = E_a|a\rangle. \tag{31}$$

Neglecting all terms that oscillate in t amounts to applying the secular approximation, which generally yields a dissipator of GKSL form (even in the presence of degeneracies). This approximation generally differs from the similar rotating wave approximation that is performed on the level of the initial Hamiltonian instead (Mäkelä and Möttönen, 2013). After some algebra, the result is, in terms of $L_{ab} \equiv |a\rangle\langle b|$,

$$\dot{\boldsymbol{\rho}}_{\mathrm{S}} = -\mathrm{i}\sum_{ab}\sigma_{ab}[L_{ab},\boldsymbol{\rho}_{\mathrm{S}}] + \sum_{abcd}\gamma_{ab,cd}\left[L_{ab}\boldsymbol{\rho}_{\mathrm{S}}L_{cd}^\dagger - \frac{1}{2}\{L_{cd}^\dagger L_{ab},\boldsymbol{\rho}_{\mathrm{S}}\}\right] \equiv \mathcal{L}(\boldsymbol{\rho}_{\mathrm{S}}), \tag{32}$$

which is usually referred to as a global master equation (GME), as it leads to dissipators that act globally on the system. An alternative term is Born-Markov-secular master equation. We have also used the calligraphic notation for the *superoperator* $\mathcal{L}$ and defined the coefficients[6]

$$\begin{aligned}\gamma_{ab,cd} &= \delta_{E_b-E_a,E_d-E_c}\sum_{\alpha\beta}\gamma_{\alpha\beta}(E_b-E_a)\langle a|A_\beta|b\rangle\langle c|A_\alpha^\dagger|d\rangle^*, \\ \sigma_{ab} &= \delta_{E_a,E_b}\sum_{\alpha\beta}\sum_c\frac{\sigma_{\alpha\beta}(E_a-E_c)}{2\mathrm{i}}\langle c|A_\beta|b\rangle\langle c|A_\alpha^\dagger|a\rangle^*.\end{aligned} \tag{33}$$

In Eq. (33) $\gamma_{ab,cd}$ and the Lamb-shift Hamiltonian elements σ_{ab} are defined in terms of the even and odd Fourier transforms of the reservoir correlation functions in Eq. (23),

$$\begin{aligned}\gamma_{\alpha\beta}(\omega) &= \int C_{\alpha\beta}(\tau)e^{+\mathrm{i}\omega\tau}d\tau, \\ \sigma_{\alpha\beta}(\omega) &= \int C_{\alpha\beta}(\tau)\mathrm{sgn}(\tau)e^{+\mathrm{i}\omega\tau}d\tau = \frac{\mathrm{i}}{\pi}\mathcal{P}\int\frac{\gamma_{\alpha\beta}(\omega')}{\omega-\omega'}d\omega',\end{aligned} \tag{34}$$

where the relation between the two follows from Eq. (29). The secular approximation leads to the Kronecker-δ functions in Eqs. (33). Transforming back to the Schrödinger picture simply amounts to the system Hamiltonian H_{S} reappearing in the commutator term. The proof that Eq. (32) is in GKSL form relies only on proving the positive definiteness of the dampening matrix $\gamma_{ab,cd}$ and the Hermiticity of the Lamb-shift Hamiltonian.

Since $\sigma_{ab} \propto \delta_{E_a,E_b}$, the Lamb shift in Eq. (32) commutes with the system Hamiltonian $[H_{\mathrm{S}}, \sum_{ab}\sigma_{ab}L_{ab}] = 0$. For

[6]Note that when one demands the coupling operators A_α in Eq. (20) to be individually Hermitian (Breuer and Petruccione, 2002), which can always be achieved, Eq. (32) falls back to the known results.

nondegenerate H_S, this term will merely affect the dynamics of the coherences in the energy eigenbasis. Beyond the secular approximation, however, it may become important for near or exact degeneracies of H_S, where it can select a preferred pointer basis (Schultz and von Oppen, 2009; Trushechkin, 2021). For thermal reservoirs, the KMS relations (24) can be used to show that the thermal state $\rho_{ss} \propto e^{-\beta H_S}$ is a stationary state of the GME (32).

This becomes even more apparent in the case when not only is the spectrum of H_S nondegenerate ($\delta_{E_a,E_b} = \delta_{ab}$), the set of Bohr (transition) frequencies $\{\omega_{ab} = E_a - E_b\}$ is also. Then, Eq. (32) completely decouples populations and coherences in the system energy eigenbasis. The coherences $\rho_{ij} \equiv \langle i|\rho_S|j\rangle$ with $i \neq j$ simply decay ($\gamma_{ai,ai} \geq 0$) according to

$$\dot{\rho}_{ij} = \left[-\frac{1}{2}\left(\sum_a \gamma_{ai,ai} + \sum_a \gamma_{aj,aj}\right) - \mathrm{i}(\sigma_{ii} - \sigma_{jj})\right]\rho_{ij}, \tag{35}$$

while the populations obey the classical Pauli master equation

$$\dot{\rho}_{aa} = \sum_b \{W_{ab}\rho_{bb} - W_{ba}\rho_{aa}\}, \tag{36}$$

with transition rates from eigenstate $|b\rangle$ to eigenstate $|a\rangle$ given by $W_{ab} = \gamma_{ab,ab} \geq 0$. Thermalization then follows from the fact that the transition rates obey detailed balance, $W_{ab}/W_{ba} = e^{-\beta(E_a - E_b)}$, which is a consequence of the KMS condition (24). Thermalization is also found for grand-canonical bath states (Cuetara, Esposito, and Schaller, 2016).

Despite this, we stress that a GKSL form ensures only positivity, not that the dynamics is in fact physically accurate (Strasberg, 2022). Moreover, having the thermal state as a fixed point grants compliance with thermodynamics only in the parameter regime that allows one to perform the necessary approximations (Spohn, 1978; Dümcke and Spohn, 1979). It may fail, e.g., beyond weak coupling or when the system energy splittings are small in comparison to the system-reservoir coupling, which can happen when the system consists of many components; see the discussion around Eq. (41). Beyond GKSL generators, exact thermalization is a feature expected only for vanishing coupling strength (Mori and Miyashita, 2008; Fleming and Cummings, 2011; Thingna, Wang, and Hänggi, 2012; Xu, Thingna, and Wang, 2017). Higher-order perturbative expansions (Laird, 1991; Jang, Cao, and Silbey, 2002; Schröder, Schreiber, and Kleinekathöfer, 2007; Thingna, Zhou, and Wang, 2014) are required to see the effects of the system-reservoir coupling strength in a steady-state solution.

3. Additivity for multiple reservoirs

The previous derivation considered only one reservoir at equilibrium. When multiple reservoirs (labeled with the index ν) are present, the bath Hamiltonian may be decomposed as $H_B = \sum_\nu H_B^{(\nu)}$, with the individual contributions acting on different Hilbert spaces. Usually it is assumed that each bath is held in a local equilibrium state $\bar{\rho}_B = \otimes_\nu \bar{\rho}_B{}^{(\nu)}$, with $\bar{\rho}_B{}^{(\nu)} = e^{-\beta_\nu(H_B^{(\nu)} - \mu_\nu N_B^{(\nu)})}/Z_B^{(\nu)}$ characterized by local inverse temperatures β_ν and chemical potentials μ_ν. The system-bath coupling in Eq. (20) can now be written as $H_I = \sum_\alpha A_\alpha \otimes \sum_\nu B_\alpha^{(\nu)}$, where A_α may be a complete set of operators for the system and the possibility $B_\alpha^{(\nu)} \to 0$ allows one to consider reservoir-specific couplings. With this, one can follow the same steps in the derivation of a master equation for weak couplings.

Since we are working in a frame where the first-order correlation function vanishes ($\mathrm{tr}\{B_\alpha^{(\nu)}\bar{\rho}_B{}^{(\nu)}\} = 0$), this also applies to product terms between different reservoirs, such that $\mathrm{tr}_B\{\boldsymbol{B}_\alpha^{(\nu)}(t_1)\boldsymbol{B}_\beta^{(\nu')}(t_2)\bar{\rho}_B\} = \delta_{\nu\nu'}C_{\alpha\beta}^{(\nu)}(t_1,t_2)$. Consequently, a weak-coupling treatment yields an additive decomposition of the dissipators $\dot{\rho}_S = -\mathrm{i}[H_S,\rho_S] + \sum_\nu \mathcal{D}_\nu\rho_S$, with one dissipator for each reservoir ν. Notice that to define *additivity* strictly, each dissipator $\mathcal{D}_\nu$ should also depend only on the parameters of the reservoir ν, as is the case here. For instance, in the case of thermal reservoirs, each GME dissipator will thermalize the system with its associated reservoir $\mathcal{D}_\nu e^{-\beta_\nu(H_S - \mu_\nu N_S)} = 0$.

The additivity property has important consequences: First, from a practical point of view it enables one to split the problem into smaller pieces, i.e., to derive the dissipator by treating the system as if it were coupled to only one reservoir. Second, it allows one to properly define the currents entering or leaving the system (Sec. II.D.1). Additivity is not preserved for stronger system-reservoir coupling (see Sec. II.H) and the definition of currents may require microscopic approaches, as explained in Sec. II.I.2.

4. Local GKSL master equation

For multiple reservoirs, the interaction Hamiltonian typically couples the reservoirs only to finite portions of the system. In regimes where the system–internal coupling strengths are smaller than the system-reservoir coupling strengths, the LME approach is often more applicable than the GME; see also Sec. II.G. We therefore now turn to the more detailed look at how to derive LMEs that is introduced in Sec. II.B. We first show how they can be derived from *collisional models* (also called repeated interactions) (Rau, 1963; Englert and Morigi, 2002; Scarani *et al.*, 2002), where the open dynamics is replaced by a series of sequential collisions with small bath units. We proceed to show how the methods put forth in Sec. II.C.1 can be adapted to yield LMEs instead.

a. Derivation based on collisional models

The basic idea of a collisional model is to describe the open dynamics as a series of unitary collisions, which involve only the system and a small piece of the bath (often called *ancillas*). The ancillas are independent and identically prepared, usually in thermal states. Each interaction lasts for a short period of time, after which the ancilla is discarded and never participates again in the dynamics. In the next step a fresh new ancilla is introduced and the process starts anew. This therefore generates a stroboscopic dynamics whose continuous-time limit can be shown to be a LME. The refreshing of the ancillas is consistent with the idea of a Markovian bath. And the sequential nature of the collisions fits with Boltzmann's molecular chaos hypothesis (*Stosszahlansatz*), where at any given time the system interacts with only a fraction of the

environment (which is subsequently reset due to the bath's inherent complexity).

This connection, within the context of boundary-driven systems, was first established by Karevski and Platini (2009). Since then collisional models have experienced a revival of interest. This is partially because they allow one to construct thermodynamically consistent models (Barra, 2015; Strasberg *et al.*, 2017; De Chiara *et al.*, 2018; Pereira, 2018; Strasberg, 2019).

For illustration, following Landi *et al.* (2014) we consider the derivation of Eq. (16) with a system spin Hamiltonian H_S containing L sites, as in Eq. (12). We start by focusing on a single collision. In addition to the L sites of the chain, we use two extra spins as ancillas, labeled 0 and $L+1$, such that the total Hamiltonian becomes

$$H_T = H_S + h_0\sigma_0^z + h_{L+1}\sigma_{L+1}^z + \sqrt{\gamma}(V_{0,1} + V_{L,L+1}), \tag{37}$$

where $V_{i,j} = \sigma_i^-\sigma_j^+ + \sigma_i^+\sigma_j^-$. The system starts in an arbitrary state ρ_S, whereas the two new spins are prepared in the thermal states ρ_0 and ρ_{L+1} as in Eq. (10), but with Fermi-Dirac occupations f_0 and f_{L+1} given by $f_i = (e^{\beta_i h_i}+1)^{-1}$ and $i = 0, L+1$. The joint system then evolves for a time τ, resulting in $e^{-iH_T\tau}(\rho_0 \otimes \rho_S \otimes \rho_{L+1})e^{iH_T\tau}$. We are interested only in the reduced state of the system, which is found by tracing out 0 and $L+1$, that is,

$$\rho_S' = \mathrm{tr}_{0,L+1}\{e^{-iH_T\tau}(\rho_0 \otimes \rho_S \otimes \rho_{L+1})e^{iH_T\tau}\}. \tag{38}$$

This can be viewed as the basic building block of a collisional model since after this interaction the ancillas are discarded and fresh new ones are introduced. One then simply reapplies the same map of Eq. (38), but with ρ_S' as the input. Repeating the procedure leads to a set of states $\rho_S^0, \rho_S^1, \rho_S^2, \ldots$ that describe the stroboscopic open evolution of the system in steps of τ.

The previous construction applies to collisions of arbitrary duration. To obtain the LME, we now consider the continuous-time limit $\tau \to 0$ such that the unitaries $e^{\pm iH_T\tau}$ can be expanded in a Taylor series. Owing to the partial trace in Eq. (38), many terms vanish and, to leading order in τ, we are left with

$$\rho_S' = \rho_S - i\tau[H_S, \rho_S] + \tau^2[\mathcal{D}_1(\rho_S) + \mathcal{D}_L(\rho_S)], \tag{39}$$

where $\mathcal{D}_1(\rho_S) = -(\gamma/2)\mathrm{tr}_{0,L+1}\{[V_{01}, [V_{01}, \rho_0 \otimes \rho_S \otimes \rho_{L+1}]]\}$ and a similar approach is followed for $\mathcal{D}_L$. Using the specific form of $V_{i,j}$, together with the fact that the initial states of sites 0 and $L+1$ are thermal, one finds for $i \in \{1, L\}$ the dissipators

$$\mathcal{D}_i = \gamma(1-f_i)D[\sigma_i^-] + \gamma f_i D[\sigma_i^+], \tag{40}$$

where $f_1 \coloneqq f_0$ and $f_L \coloneqq f_{L+1}$. These are the exact GKSL dissipators appearing in the LME (17a).

As the last step, we now rewrite Eq. (39) to form the time derivative $d\rho_S/dt \simeq (\rho_S' - \rho_S)/\tau$. Upon taking the limit $\tau \to 0$, however, we encounter a problem. The dissipative term is of the order of τ^2 and would thus vanish if this limit were taken naively. The continuous-time limit corresponds to a small τ, but the limit $\tau \equiv 0$ would mean no interaction at all. One should therefore interpret the continuous-time limit as a physical limit where $(\rho_S' - \rho_S)/\tau$ is sufficiently smooth to be interpreted as a derivative, but the last term in Eq. (39) is nonetheless finite. One way to implement this mathematically is to rescale the interaction strengths $\sqrt{\gamma}$ in Eq. (37) to $\sqrt{\gamma/\tau}$. That is, the interaction is taken to be short, but also strong. This idea is also used in classical Brownian motion to introduce the δ-correlated noise in the Langevin equation (Coffey, Kalmykov, and Waldron, 2004). With this proviso, we precisely obtain Eq. (16). Thus, LMEs can indeed be viewed as the continuous-time limit of collisional models.

In the literature, LMEs of the form of Eq. (16) are often said to represent *magnetization baths* (Schuab, Pereira, and Landi, 2016; Žnidarič *et al.*, 2017; Varma and Žnidarič, 2019). This is used to emphasize that they are not describing actual thermal baths, but instead act so as to force the magnetization of the boundary sites to point in certain directions. The previously mentioned collisional model derivation provides a clear interpretation of this idea. At each collision, the spins 0 and $L+1$ tend to polarize the magnetization of the boundary sites (1 and L). But since the interaction time τ is short, this effect cannot propagate deeply within the chain after just one collision, and thus remains confined to the first and last sites. This is ultimately the reason why collisional models with local ancillas yield local jump operators. In principle, the same idea can be used to derive GMEs, but then the ancillas have to interact with multiple parts of the chain. Recently it was shown (Cattaneo *et al.*, 2021) that one may algorithmically reproduce any Markovian evolution through a suitably chosen collisional model.

b. Derivation based on weak internal couplings

It is tempting to ask whether LMEs can somehow be viewed as a special limit of GMEs. Indeed, Eq. (32) is formulated in terms of the global system energy eigenbasis equation (31). Consider what happens if the system is composed of different subsystems (for now we consider only two, but this will be straightforwardly generalized)

$$H_S = H_S^1 + H_S^2 + \xi H_S^{12}, \tag{41}$$

with the local Hamiltonians H_S^μ and the intrasystem interaction $H_S^{\mu\nu}$, quantified by the dimensionless bookkeeping parameter ξ. In the limit $\xi \to 0$, the system energy eigenbasis equation (31) factorizes as $|a\rangle \to |a_1\rangle \otimes |a_2\rangle$ while $E_a \to E_{a_1} + E_{a_2}$, where $H_S^\mu|a_\mu\rangle = E_{a_\mu}|a_\mu\rangle$. With this limit, one may often retrieve a LME from the GME (provided that the coupling operators A_α in the Hamiltonian are local).

However, this does not always work. In particular, when the subsystems are identical, H_S becomes degenerate when $\xi \to 0$. Whereas superpositions of global eigenstates with the same eigenvalue are still global eigenstates, they need not be given by tensor products of local eigenstates if global symmetries are conserved. An example for this is the master equation for superradiant decay (Gross and Haroche, 1982). Although here one has a cloud of noninteracting atoms (i.e., $\xi = 0$ from the beginning), the jump operators remain global due to a globally conserved symmetry (the collective coupling induces angular momentum conservation), and hence do not

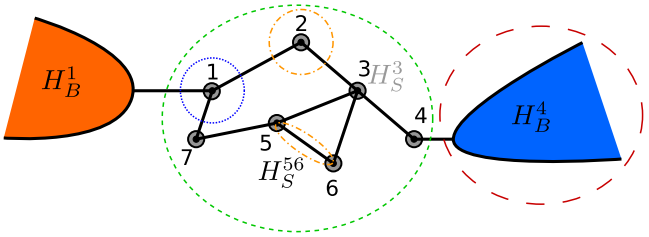

FIG. 2. Sketch of the considered setup. Small gray spheres correspond to sites with Hamiltonians H_{S}^{ν}, and connecting black lines correspond to couplings (either bonds $H_{\mathrm{S}}^{\mu\nu}$ or system-reservoir couplings H_{I}^{ν}). GMEs are obtained by treating only system-reservoir couplings (traversing the green short-dashed sphere) perturbatively. Conversely, LMEs result from treating both system-reservoir couplings and system-internal couplings (such as traversing the blue dotted sphere) perturbatively. Currents through various interfaces (dashed and/or dotted curves) can be meaningfully defined by balance equations of locally conserved observables (Sec. II.D). For instance, we discuss the global energy balance of the system (green short-dashed sphere) in Eq. (50) and the local energy current entering a boundary site (blue dotted circle) from the reservoir in Eq. (68). Local balances of internal sites and internal bonds (orange dash-dotted spheres) are discussed in Eqs. (56) and (62), respectively. The energy balances of the reservoir (red long-dashed sphere) are treated using the full counting statistics discussed in Sec. II.I.

reduce to local jump operators.[7] It is therefore advisable to retrieve the LME from the Redfield master equation (27) by performing the limit $\xi \to 0$ on it.

Alternatively, one may also derive the LME by treating the system-bath interactions H_{I} and the internal system interactions $H_{\mathrm{S}}^{\mu\nu}$ on equal footing, as we now outline. We start with the usual decomposition of the universe Hamiltonian $H_{\mathrm{tot}} = H_{\mathrm{S}} + H_{\mathrm{B}} + H_{\mathrm{I}}$. The system is assumed to have an internal structure such that H_{S} can be written as

$$H_{\mathrm{S}} = H_{\mathrm{S}}^{0} + H_{\mathrm{S}}^{1} = \sum_{\nu} H_{\mathrm{S}}^{\nu} + \sum_{\mu<\nu} H_{\mathrm{S}}^{\mu\nu}, \tag{42}$$

where the free parts of the system H_{S}^{ν} act on different Hilbert spaces, such that $[H_{\mathrm{S}}^{\nu}, H_{\mathrm{S}}^{\mu}] = 0$, and $H_{\mathrm{S}}^{\mu\nu}$ represents pair interactions between these parts. In addition, we assume multiple reservoirs $H_{\mathrm{B}} = \sum_{\nu} H_{\mathrm{B}}^{\nu}$, with each bath H_{B}^{ν} coupled only locally to subsystem ν according to the interaction [cf. Eq. (20)]

$$H_{\mathrm{I}} = \sum_{\nu} H_{\mathrm{I}}^{\nu} = \sum_{\nu} \sum_{\alpha} A_{\alpha}^{\nu} \otimes B_{\alpha}^{\nu}. \tag{43}$$

[7]In this model, one has for N two-level atoms in total 2^N energy eigenstates, but due to the globally conserved angular momentum only at most $N+1$ of them couple to each other. If one performs the secular approximation in the local energy eigenbasis, couplings to coherences between degenerate energy eigenstates must be kept in the global master equation. By contrast, choosing the angular momentum eigenstates as the eigenbasis (which also diagonalizes the Hamiltonian), one obtains a simple rate equation in each angular momentum subspace.

We can choose some of the $H_{\mathrm{I}}^{\nu} = 0$, allowing for boundary-driven setups with internal parts not directly coupled to any reservoir, as in Fig. 2. By construction, the system coupling operators A_{α}^{ν} act only on their respective sites, such that $[H_{\mathrm{S}}^{\nu}, A_{\alpha}^{\mu\neq\nu}] = 0$, and similarly for the reservoir couplings.

The problem now involves the interplay between two small couplings $H_{\mathrm{I}} = \mathcal{O}\{\lambda\}$ and $H_{\mathrm{S}}^{\mu\nu} = \mathcal{O}\{\xi\}$, with small dimensionless bookkeeping parameters λ and ξ. These terms may be of similar strength, but they are both small in comparison to the other parts of the Hamiltonian. We therefore use an interaction picture with respect to the free part of the system Hamiltonian and the reservoirs

$$H_0 = \sum_{\nu} H_{\mathrm{S}}^{\nu} + \sum_{\nu} H_{\mathrm{B}}^{\nu}. \tag{44}$$

In this picture (marked as bold symbols in the following), the exact von Neumann equation for the full universe reads

$$\dot{\boldsymbol{\rho}} = -\mathrm{i}[\boldsymbol{H}_{\mathrm{S}}^{1}(t), \boldsymbol{\rho}(t)] - \mathrm{i}[\boldsymbol{H}_{\mathrm{I}}(t), \boldsymbol{\rho}(t)], \tag{45}$$

which is analogous to Eq. (22). The rhs is small ($\mathcal{O}\{\xi\} + \mathcal{O}\{\lambda\}$) and we can use an equivalent perturbative treatment as for the derivation of the global master equation in Secs. II.C.1 and II.C.2, with only small modifications. We formally integrate Eq. (45), but in contrast to the treatment there we insert the solution only in the second commutator term. Performing the partial trace over the reservoir degrees of freedom then yields the exact equation

$$\begin{aligned}\dot{\rho}_{\mathrm{S}} = {} & -\mathrm{i}[\boldsymbol{H}_{\mathrm{S}}^{1}(t), \mathrm{tr}_{\mathrm{B}}\{\boldsymbol{\rho}(t)\}] - \mathrm{i}\,\mathrm{tr}_{\mathrm{B}}\{[\boldsymbol{H}_{\mathrm{I}}(t'), \rho_0]\} \\ & - \int_0^t \mathrm{tr}_{\mathrm{B}}\{[\boldsymbol{H}_{\mathrm{I}}(t), [\boldsymbol{H}_{\mathrm{S}}^{1}(t') + \boldsymbol{H}_{\mathrm{I}}(t'), \boldsymbol{\rho}(t')]]\} dt'. \end{aligned} \tag{46}$$

First, when a factorizing initial condition $\rho(0) = \rho_{\mathrm{S}}^{0} \otimes_{\nu} \bar{\rho}_{\mathrm{B}}{}^{\nu}$ and the assumption that $\mathrm{tr}_{\mathrm{B}}\{\boldsymbol{H}_{\mathrm{I}}(t)\bar{\rho}_{\mathrm{B}}\} = 0$ is used, the second commutator term on the first line in Eq. (46) vanishes identically. Second, we extend this assumption to all times with the Born approximation $\boldsymbol{\rho}(t) = \boldsymbol{\rho}_{\mathrm{S}}(t) \otimes_{\nu} \bar{\rho}_{\mathrm{B}}{}^{\nu} + \mathcal{O}\{\lambda\} + \mathcal{O}\{\xi\}$. Considering that $\boldsymbol{\rho}_{\mathrm{S}}(t)$ is only an approximation of the exact reduced density matrix $\mathrm{tr}_{\mathrm{B}}\{\boldsymbol{\rho}(t)\}$, neglecting the remainder terms in the first commutator and in the nested double commutator leads to

$$\begin{aligned}\dot{\boldsymbol{\rho}}_{\mathrm{S}} = {} & -\mathrm{i}[\boldsymbol{H}_{\mathrm{S}}^{1}(t), \boldsymbol{\rho}_{\mathrm{S}}(t)] \\ & - \sum_{\nu} \int_0^t \mathrm{tr}_{\nu}\{[\boldsymbol{H}_{\mathrm{I}}^{\nu}(t), [\boldsymbol{H}_{\mathrm{I}}^{\nu}(t'), \boldsymbol{\rho}_{\mathrm{S}}(t') \otimes \bar{\rho}_{\mathrm{B}}{}^{\nu}]]\} dt' \\ & + \mathcal{O}\{\lambda\xi\} + \mathcal{O}\{\xi^2\} + \mathcal{O}\{\lambda^2\xi\} + \mathcal{O}\{\lambda\xi^2\} + \mathcal{O}\{\lambda^3\}, \end{aligned} \tag{47}$$

where we have neglected the mixed terms between system and reservoir and also between different reservoirs. Furthermore, we have already performed all the trivial partial traces. The step in going from Eq. (46) to Eq. (47) highlights the terms that are discarded in a local approach. The first line contains the intrasystem interactions. Upon transforming back to the Schrödinger picture, it restores together with H_{S}^{0} the full system Hamiltonian. In addition, the double commutator term involves only system operators acting on the specific

subsystem ν since, due to a different interaction picture, we have $\boldsymbol{H}_{\mathrm{I}}^{\nu}(t)=\sum_{\alpha}e^{+\mathrm{i}H_{\mathrm{S}}^{\nu}t}A_{\alpha}^{\nu}e^{-\mathrm{i}H_{\mathrm{S}}^{\nu}t}\otimes e^{+\mathrm{i}H_{\mathrm{B}}^{\nu}t}\boldsymbol{B}_{\alpha}^{\nu}e^{-\mathrm{i}H_{\mathrm{B}}^{\nu}t}$. It in fact yields the same (LME) dissipator that one would obtain if subsystem ν were exclusively coupled to its adjacent reservoir; see Schaller *et al.* (2022) for an application in the Fermi-Hubbard model. Hence, the previous equation generates a local non-Markovian master equation, and following the standard Markov approximations discussed in Sec. II.C.1 one can also derive local versions of the Redfield-I and Redfield-II equations (26) and (27). Accordingly, the final secular approximation only requires the splittings of the local system parts H_{S}^{ν} to be large, and it is not invalidated by possibly many degeneracies of $\sum_{\nu}H_{\mathrm{S}}^{\nu}$. Eventually, one obtains the sum of local dissipators, but the commutator from the first line of Eq. (47) will mediate an interaction between distant system sites (and reservoirs). Upon transforming back to the Schrödinger picture, the full system Hamiltonian (anything inside the green short-dashed circle in Fig. 2) is restored, but dissipative contributions (also Lamb-shift terms) are the same as if one had derived the master equation from Sec. II.C.2 for the coupled parts only. It hence always generates LMEs; see Wichterich *et al.* (2007) for specific applications. Here the term "local" refers to the chosen partition of the system, for which a suitable choice is dictated by the relation between coupling strengths. Often H_{S}^{ν} are thought of as individual bosonic or fermionic modes, but they can also be complicated interacting systems themselves, and in this sense there may be varying degrees of locality depending on the context. We also point out approaches that effectively provide interpolations between LMEs and GMEs, such as those followed by Lidar, Bihary, and Whaley (2001) and Seah, Nimmrichter, and Scarani (2018).

c. Derivation for a negligible system Hamiltonian

Yet another derivation, the *singular coupling limit* that leads to LMEs, arises in the limit where the system Hamiltonian is small in comparison to the system-reservoir coupling. The Born and Markov approximations are applied as before, with the only difference being that, due to the small system Hamiltonian, one can neglect the time dependence of the system coupling operators in the interaction picture, rendering a secular approximation unnecessary. The simple outcome of this procedure is an equation of GKSL form that can technically also be obtained from Eq. (32) by setting all system energies zero (Palmer, 1977). In the Schrödinger picture it reads (assuming Hermitian coupling operators $A_{\alpha}=A_{\alpha}^{\dagger}$)

$$\dot{\rho_{\mathrm{S}}}=-\mathrm{i}[H_{\mathrm{S}},\rho_{\mathrm{S}}]-\mathrm{i}\sum_{\alpha\beta}\frac{\sigma_{\alpha\beta}(0)}{2\mathrm{i}}[A_{\alpha}A_{\beta},\rho_{\mathrm{S}}]+\sum_{\alpha\beta}\gamma_{\alpha\beta}(0)\left[A_{\beta}\rho_{\mathrm{S}}A_{\alpha}-\frac{1}{2}\{A_{\alpha}A_{\beta},\rho_{\mathrm{S}}\}\right],\tag{48}$$

where the Fourier transforms of the reservoir correlation functions of Eq. (34) are evaluated at vanishing arguments. Since it follows from the KMS relation (24) that $\gamma_{\alpha\bar{\alpha}}(0)=\gamma_{\bar{\alpha}\alpha}(0)$, one finds that the completely mixed (infinite-temperature) state $\rho_{\mathrm{S}}\propto\mathbb{1}$ is one (not necessarily unique) stationary solution of the previous master equation. As the Lindblad operators coincide with those in the coupling Hamiltonian (20), phenomenological approaches to boundary-driven systems like Eq. (17a) may actually be microscopically motivated in the singular coupling limit. The interaction with further (nonsingular) reservoirs may nevertheless introduce interesting stationary nonequilibrium properties as may also be obtained by combining the singular coupling limit with conventional GME treatments (Schultz and von Oppen, 2009).

D. Transport properties and currents

The usual boundary-driven scenario consists of a system coupled to multiple baths, which is left to evolve until it reaches a steady state. The latter, being out of equilibrium, is characterized by stationary currents from one bath to another (Dhar, Saito, and Hänggi, 2012). It is therefore essential to correctly determine these currents for each model. This includes not only the currents of energy but also other observables like particle number or magnetization and spin.

The crucial aspect when dealing with transport is to correctly account for all possible sources and sinks of the quantity in question. Take energy, for instance. It makes sense to talk about energy transport only if the amount of energy leaving one region is the same as the amount entering the other. If in between energy is spontaneously created (such as by an external work agent) or if some energy is trapped in the interaction potential, this must be properly taken into account. This introduces the idea of *continuity equations*. That is, equations that identify how the changes in a given quantity are linked to fluxes of that quantity to other regions of space. There are two types of continuity equations that one may consider: *system resolved*, which look only at net currents from the bath to the system, and *site resolved*, which analyze the flows within the system.

1. System-resolved continuity equations

Consider a master equation of the form

$$\frac{d\rho_{\mathrm{S}}}{dt}=-\mathrm{i}[H_{\mathrm{S}},\rho_{\mathrm{S}}]+\sum_{\nu}\mathcal{D}_{\nu}(\rho_{\mathrm{S}}),\tag{49}$$

where H_{S} describes all internal energies of the system and $\mathcal{D}_{\nu}$ summarizes the net effect of bath ν (which may also contain Lamb-shift contributions). In the case of Redfield equations or GMEs, $\mathcal{D}_{\nu}$ has support over the entire system, while for LMEs it acts only on specific sites.

The following system-resolved continuity equation for $\langle H_{\mathrm{S}}\rangle$ is readily found using Eq. (49):

$$\frac{d\langle H_{\mathrm{S}}\rangle}{dt}=\sum_{\nu}\mathrm{tr}\{H_{\mathrm{S}}\mathcal{D}_{\nu}(\rho_{\mathrm{S}})\}\coloneqq\sum_{\nu}I_{\mathrm{E}}^{\nu}.\tag{50}$$

Each term on the rhs of Eq. (50) can be identified by the flow of energy entering the system (inside the short-dashed green circle in Fig. 2) from reservoir ν. Changes in energy of the system are thus entirely due to the fluxes arriving from each bath. At steady state, $d\langle H_{\mathrm{S}}\rangle/dt=0$ and all fluxes balance out: $\sum_{\nu}I_{E,\mathrm{ss}}^{\nu}=0$. For just two baths, this becomes $I_{E,\mathrm{ss}}^{1}=-I_{E,\mathrm{ss}}^{2}$, meaning that all energy entering from bath 1 leaves for bath 2.

Next we consider another operator $\mathcal{O}$ of the system. From Eq. (49), we determine that its rate of change will be given by

$$\frac{d\langle\mathcal{O}\rangle}{dt} = \mathrm{i}\langle[H_\mathrm{S},\mathcal{O}]\rangle + \sum_\nu \mathrm{tr}\{\mathcal{O}\mathcal{D}_\nu(\rho_\mathrm{S})\}. \tag{51}$$

The last term in Eq. (51) is associated with the "flow of $\mathcal{O}$" to each bath, but now we also have the term $[H_\mathrm{S},\mathcal{O}]$. When this is nonzero, $\mathcal{O}$ can be spontaneously created or destroyed even if the system is isolated. We therefore typically speak of transport of $\mathcal{O}$ only when $[H_\mathrm{S},\mathcal{O}]=0$, in which case we get

$$\frac{d\langle\mathcal{O}\rangle}{dt} = \sum_\nu \mathrm{tr}\{\mathcal{O}\mathcal{D}_\nu(\rho_\mathrm{S})\} = \sum_\nu I^\nu_\mathcal{O}. \tag{52}$$

For example, if the Hamiltonian H_S conserves the total particle number $[H_\mathrm{S},N_\mathrm{S}]=0$, we can define the particle current via

$$\frac{d\langle N_\mathrm{S}\rangle}{dt} = \sum_\nu \mathrm{tr}\{N_\mathrm{S}\mathcal{D}_\nu(\rho)\} = \sum_\nu I^\nu_\mathrm{N}. \tag{53}$$

Similarly, we can consider the transport of magnetization $\mathcal{M}=\sum_i \sigma^i_z$ in spin chains. However, some Hamiltonians may not conserve $\mathcal{M}$. One such example is the following XYZ chain:

$$H_\mathrm{S} = -\sum_{i=1}^{L-1}(J_x\sigma^x_i\sigma^x_{i+1} + J_y\sigma^y_i\sigma^y_{i+1} + J_z\sigma^z_i\sigma^z_{i+1}) + \sum_{i=1}^{L} h_i\sigma^z_i. \tag{54}$$

One may verify that $\mathcal{M}$ is only conserved in the XXZ limit [$J_x=J_y$; Eq. (12)]. Thus, one may study magnetization transport in XXZ or XX chains, but not in the full XYZ model.

2. Site-resolved continuity equations: Unitary components

Equation (51) can also be employed in the case where $\mathcal{O}$ is a local operator, associated with either a site or a bond. This will give rise to *site-resolved continuity equations*. In this case, the unitary term $\mathrm{i}[H_\mathrm{S},\mathcal{O}]$ is crucial. And since it is independent of the type of QME used, we treat it separately in this section. For concreteness we assume that the system has a 1D nearest-neighbor Hamiltonian

$$H_\mathrm{S} = \sum_{k=1}^{L} H^k_\mathrm{S} + \sum_{k=1}^{L-1} H^{k,k+1}_\mathrm{S}. \tag{55}$$

The indices for each term clarify in which Hilbert space it has support. For instance, $H^{2,3}_\mathrm{S}$ acts only on sites 2 and 3, and thus commutes with any operator that does not pertain to these two sites. Let $\mathcal{O}^k$ denote a generic local operator with support only over site k. Therefore, $[H_\mathrm{S},\mathcal{O}^k] = [H^k_\mathrm{S},\mathcal{O}^k] + [H^{k-1,k}_\mathrm{S},\mathcal{O}^k] + [H^{k,k+1}_\mathrm{S},\mathcal{O}^k]$. This helps one to identify what is required for a proper site-resolved continuity equation for $\mathcal{O}^k$. One must first assume that $\mathcal{O}^k$ is "locally conserved," in the sense that $[H^k_\mathrm{S},\mathcal{O}^k]=0$. Equation (51) then gives (without the dissipative part)

$$\frac{d\langle\mathcal{O}^k\rangle}{dt} = \mathrm{i}\langle[H^{k-1,k}_\mathrm{S},\mathcal{O}^k]\rangle + \mathrm{i}\langle[H^{k,k+1}_\mathrm{S},\mathcal{O}^k]\rangle. \tag{56}$$

It is tempting to associate $\mathrm{i}\langle[H^{k-1,k}_\mathrm{S},\mathcal{O}^k]\rangle$ with the flow from site $k-1$ to k, and $-\mathrm{i}\langle[H^{k,k+1}_\mathrm{S},\mathcal{O}^k]\rangle$ with the flow leaving k for $k+1$. But this makes sense only if it agrees with the flow entering $k+1$ from k, which is obtained by looking at $\mathcal{O}^{k+1}$:

$$\frac{d\langle\mathcal{O}^{k+1}\rangle}{dt} = \mathrm{i}\langle[H^{k,k+1}_\mathrm{S},\mathcal{O}^{k+1}]\rangle + \mathrm{i}\langle[H^{k+1,k+2}_\mathrm{S},\mathcal{O}^{k+1}]\rangle.$$

The term that we are looking for is $\mathrm{i}\langle[H^{k+1,k}_\mathrm{S},\mathcal{O}^{k+1}]\rangle$. However, in general $-\mathrm{i}\langle[H^{k,k+1}_\mathrm{S},\mathcal{O}^k]\rangle \neq \mathrm{i}\langle[H^{k,k+1}_\mathrm{S},\mathcal{O}^{k+1}]\rangle$. That is, the quantity leaving k for $k+1$ is not necessarily the same as that entering $k+1$ from k. From this, we conclude that a site-resolved continuity equation for a set of local operators $\mathcal{O}^k$ is possible only when

$$[H^{k,k+1}_\mathrm{S},\mathcal{O}^k+\mathcal{O}^{k+1}] = 0. \tag{57}$$

Together with $[H^k_\mathrm{S},\mathcal{O}^k]=0$, Eq. (57) implies that

$$[H_\mathrm{S},\sum_k \mathcal{O}^k] = 0. \tag{58}$$

Hence, the condition (58) is seen as equivalent to the one we used in going from Eq. (51) to Eq. (52), namely, that $[H_\mathrm{S},\mathcal{O}]=0$, with $\mathcal{O}=\sum_k\mathcal{O}^k$. Consequently, both the system- and the site-resolved approaches are founded on similar assumptions. The latter, however, generally provides an additional level of detail.

When Eq. (57) is satisfied, we may unambiguously define the current of a given observable $\mathcal{O}^k$ leaving k for $k+1$ as

$$I^{k,k+1}_\mathcal{O} = -\mathrm{i}\langle[H^{k,k+1}_\mathrm{S},\mathcal{O}^k]\rangle, \tag{59}$$

such that Eq. (56) becomes

$$\frac{d\langle\mathcal{O}^k\rangle}{dt} = I^{k-1,k}_\mathcal{O} - I^{k,k+1}_\mathcal{O}. \tag{60}$$

These definitions hold for all sites, provided that we define $I^{0,1}_\mathcal{O} = I^{L,L+1}_\mathcal{O} = 0$. For instance, in the XXZ chain Eq. (59) yields $I^{k,k+1}_\mathrm{M} = -2J\langle\sigma^x_k\sigma^y_{k+1} - \sigma^y_k\sigma^x_{k+1}\rangle$, which is Eq. (18). The structure of Eq. (59) also naturally invites one to define a corresponding current operator

$$\mathcal{I}^{k,k+1}_\mathcal{O} = -\mathrm{i}[H^{k,k+1}_\mathrm{S},\mathcal{O}^k], \tag{61}$$

such that $\langle\mathcal{I}^{k,k+1}_\mathcal{O}\rangle = I^{k,k+1}_\mathcal{O}$. Current operators find many uses, especially in unitary dynamics, such as in Kubo's formula.

For energy, the situation is a bit more delicate since H_S has contributions from both sites and bonds [Eq. (55)]. In some cases, such as when $H^{k,k+1}_\mathrm{S}$ are small, it may be reasonable to analyze a site-resolved continuity equation for the local energies H^k_S. However, for this to exist, one must satisfy Eq. (57); that is, $[H^{k,k+1}_\mathrm{S}, H^k_\mathrm{S}+H^{k+1}_\mathrm{S}]=0$. For example, take

$H_S^{k,k+1} = a_k^\dagger a_{k+1} + a_{k+1}^\dagger a_k$ and suppose that $H_S^k = \epsilon_k a_k^\dagger a_k$, with different energies ϵ_k for each site. This interaction preserves the number of quanta, so Eq. (57) is satisfied for $\mathcal{O}^k = a_k^\dagger a_k$. However, it will not preserve the local energies when the ϵ_k are different.

Instead, we can construct a local energy current via a *bond-resolved continuity equation* (Wu and Segal, 2009a). We first rewrite Eq. (55) as a sum over bonds $H_S = \sum_{i=1}^{L-1} \tilde{H}_S^{i,i+1}$ for some new operators $\tilde{H}_S^{i,i+1}$. A continuity equation for $\tilde{H}_S^{i,i+1}$ will then read

$$\frac{d\langle \tilde{H}_S^{i,i+1}\rangle}{dt} = \mathrm{i}\langle[\tilde{H}_S^{i-1,i}, \tilde{H}_S^{i,i+1}]\rangle + \mathrm{i}\langle[\tilde{H}_S^{i+1,i+2}, \tilde{H}_S^{i,i+1}]\rangle. \tag{62}$$

The first term in Eq. (62) is the current entering bond $(i, i+1)$ from bond $(i-1, i)$, and the second term is the current going from bond $(i, i+1)$ to $(i+1, i+2)$. The latter will always coincide with the current entering $(i+1, i+2)$ from $(i, i+1)$, as one may explicitly verify by constructing an analogous equation for $d\langle \tilde{H}_S^{i+1,i+2}\rangle/dt$. With the proper boundary conditions, one also finds that the total Hamiltonian is a constant of motion.

3. Site-resolved continuity equations

We now include the effects of dissipation through Eq. (49). We first consider the LME case, where each dissipator $\mathcal{D}_\nu$ acts only on a specific site (such that ν can be linked to k). For a set of local observables $\mathcal{O}^k$ satisfying Eq. (57), Eq. (60) becomes

$$\frac{d\langle \mathcal{O}^k\rangle}{dt} = I_{\mathcal{O}}^{k-1,k} - I_{\mathcal{O}}^{k,k+1} + I_{\mathcal{O},\mathrm{diss}}^k, \tag{63}$$

where $I_{\mathcal{O},\mathrm{diss}}^k = \mathrm{tr}\{\mathcal{O}^k \mathcal{D}_k(\rho_S)\}$. In the noteworthy case where the baths couple to the first and last sites, we get

$$\frac{d\langle \mathcal{O}^1\rangle}{dt} = -I_{\mathcal{O}}^{1,2} + I_{\mathcal{O},\mathrm{diss}}^1, \tag{64}$$

$$\frac{d\langle \mathcal{O}^k\rangle}{dt} = I_{\mathcal{O}}^{k-1,k} - I_{\mathcal{O}}^{k,k+1}, \qquad k = 2, \ldots, L-1, \tag{65}$$

$$\frac{d\langle \mathcal{O}^1\rangle}{dt} = I_{\mathcal{O}}^{L-1,L} + I_{\mathcal{O},\mathrm{diss}}^L. \tag{66}$$

In the steady state, $d\langle \mathcal{O}^k\rangle/dt = 0$ and all currents coincide,

$$I_{\mathcal{O},\mathrm{diss}}^1 = I_{\mathcal{O}}^{1,2} = I_{\mathcal{O}}^{2,3} = \cdots = I_{\mathcal{O}}^{L-1,L} = -I_{\mathcal{O},\mathrm{diss}}^L \equiv I_{\mathcal{O}}, \tag{67}$$

yielding a unique current $I_{\mathcal{O}}$ through the system. For instance, with $\mathcal{O}^k = \sigma_z^i$ and LME baths [Eq. (17b)] we get $I_{\mathrm{M},\mathrm{diss}}^i = \gamma_i(\eta_i - \langle\sigma_i^z\rangle)$.

A similar analysis can also be done for the energy. Once again, one must distinguish between a bond- or site-resolved description. For bonds Eq. (62) is appended with dissipative currents $\mathrm{tr}\{\tilde{H}_S^{k,k+1}(\mathcal{D}_k + \mathcal{D}_{k+1})\rho_S\}$. For LMEs, however, site-resolved equations for the local energies H_S^k are in a sense more natural. The reason is that, as reviewed in Sec. II.C.4, LMEs can be microscopically derived, assuming that the system-system interactions $H_S^{k,k+1}$ are small. In this case, provided that Eq. (57) is satisfied, the site-resolved continuity equation will have the form $d\langle H_S^k\rangle/dt = I_E^{k-1,k} - I_E^{k,k+1} + I_{E,\mathrm{diss}}^k$, where $I_E^{k,k+1} = -\mathrm{i}\langle[H_S^{k,k+1}, H_S^k]\rangle$. The last term is thus interpreted as the local energy current entering site k via the adjacent reservoir

$$I_{E,\mathrm{diss}}^k = \mathrm{tr}\{H_S^k \mathcal{D}_k(\rho_S)\}, \tag{68}$$

and analogous considerations for the particle current lead to

$$I_{N,\mathrm{diss}}^k = \mathrm{tr}\{N_S^k \mathcal{D}_k(\rho_S)\}, \tag{69}$$

with particle number operator N_S^k of site k. Explicit formulas for $I_{E,\mathrm{diss}}^k$ for the XXZ chain in the presence of magnetic fields were provided by Mendoza-Arenas, Al-Assam *et al.* (2013). The local energy current $I_{E,\mathrm{diss}}^k$ from bath k to site k is generally different than $\mathrm{tr}\{H_S \mathcal{D}_k(\rho_S)\}$ since the latter has additional contributions $\mathrm{tr}\{H_S^{k,k\pm1}\mathcal{D}_k(\rho_S)\}$; cf. Eq. (55). However, using the same bookkeeping notation as in Sec. II.C.4, where the system-bath couplings are of the order of λ and the system-system couplings are of the order of ξ, we see that these extra contributions will be of the order of $\lambda^2\xi$, so

$$\mathrm{tr}\{H_S \mathcal{D}_k(\rho_S)\} = I_{E,\mathrm{diss}}^k + O(\lambda^2\xi). \tag{70}$$

For Redfield equations or GMEs, each dissipator $\mathcal{D}_\nu$ in Eq. (49) will act on the entire chain, even if the coupling is to a specific site. Thus, instead of Eq. (63) one will have

$$\frac{d\langle \mathcal{O}^k\rangle}{dt} = I_{\mathcal{O}}^{k-1,k} - I_{\mathcal{O}}^{k,k+1} + \sum_\nu \mathrm{tr}\{\mathcal{O}^k \mathcal{D}_\nu(\rho_S)\}, \tag{71}$$

where each term in the sum represents the action of bath ν on site k. This reflects the nonlocal character of the dissipators. For this reason, one often does not assess site-resolved equations for global dissipators, focusing instead only on system-resolved equations such as Eqs. (50) and (52). In fact, as pointed out by Wichterich *et al.* (2007), the local currents can even be unphysical in GMEs due to the secular approximation [a workaround was put forth by Kamiya (2015)].

E. Thermodynamics of LMEs and GMEs

Section II.D illustrated how to write consistent expressions for the first law of thermodynamics in the form of continuity equations for the energy. Here we show that a similar argument can also be made concerning the second law. The key quantity of interest, in this case, is the irreversible entropy production (Landi and Paternostro, 2021). Unlike energy, entropy does not satisfy a continuity equation. Part of the change in the von Neumann entropy of the system $S[\rho_S] = -\mathrm{tr}\{\rho_S \ln \rho_S\}$ can be associated with a flow of entropy to the reservoirs. But there is also another part (the entropy production rate $\dot{\Sigma}$) associated with the irreversible nature of the process. From the usual thermodynamic arguments, it follows that the entropy flux to a thermal reservoir at temperature T_ν is I_Q^ν/T_ν, where I_Q^ν is the heat current entering the reservoir. The

entropy balance equation for the system should therefore read $dS/dt = \dot{\Sigma} + \sum_\nu I^\nu_{\rm Q}/T_\nu$. While dS/dt may in general have any sign, the entropy production rate is by construction always non-negative ($\dot{\Sigma} \geq 0$), which is a mathematical statement of the second law.

Determining $\dot{\Sigma}$ is thus a relevant task for any open quantum process. The difficulty is that since the baths are traced out in a microscopic derivation, the value of $I^\nu_{\rm Q}$ (which is a bath quantity) can be wrongly assessed from the reduced description of the master equation. In fact, as discussed later, this might even lead to apparent violations of the second law. Landi and Paternostro (2021) showed that this is fully resolved only if one has access to the full system-bath dynamics. Here we instead discuss how the latter might be approximated in different types of master equations of the form of Eq. (49) to arrive at thermodynamically consistent expressions.

We start with GMEs. From the global energy and particle currents [Eqs. (50) and (53)], we define the *heat current* for each bath $I^\nu_{\rm Q,GME} = I^\nu_{\rm E} - \mu_\nu I^\nu_{\rm N}$. Additionally, we assume as in Sec. II.C.2 that each dissipator targets a thermal state at temperature β_ν and chemical potential μ_ν; that is, $\mathcal{D}_\nu(\rho^\nu_{\rm ss,GME}) = 0$, where $\rho^\nu_{\rm ss,GME} = e^{-\beta_\nu(H_{\rm S}-\mu_\nu N_{\rm S})}/Z_\nu$. From classical thermodynamic considerations, the change in entropy of reservoir ν is related to its energy and particle change via $dU_\nu = T_\nu dS_\nu + \mu_\nu dN_\nu$, so $\dot{S}_\nu = \beta_\nu(dU_\nu/dt - \mu_\nu dN_\nu/dt)$. Assuming that there is energy and particle conservation between system and reservoir, which is generally true under weak-coupling conditions, this can be given as $\dot{S}_\nu = -\beta_\nu I_{Q,\rm GME} = -\beta_\nu(I^\nu_{\rm E} - \mu_\nu I^\nu_{\rm N})$. The entropy production, computed as the rate of change of the entropy of the full universe, is thus (Alicki, 1979)

$$\begin{aligned}\dot{\Sigma}_{\rm GME} &\approx -\frac{d}{dt}{\rm tr}\{\rho_{\rm S}\ln\rho_{\rm S}\} - \sum_\nu \beta_\nu[I^\nu_{\rm E} - \mu_\nu I^\nu_{\rm N}] \\ &= -{\rm tr}\{\dot{\rho_{\rm S}}\ln\rho_{\rm S}\} - \sum_\nu \beta_\nu {\rm tr}\{(H_{\rm S} - \mu_\nu N_{\rm S})(\mathcal{D}_\nu\rho_{\rm S})\} \\ &= -\sum_\nu {\rm tr}\{(\mathcal{D}_\nu\rho_{\rm S})\ln\rho_{\rm S}\} + \sum_\nu {\rm tr}\{(\mathcal{D}_\nu\rho_{\rm S})\ln\rho^\nu_{\rm ss,GME}\} \\ &= -\sum_\nu {\rm tr}\{(\mathcal{D}_\nu\rho_{\rm S})[\ln\rho_{\rm S} - \ln\rho^\nu_{\rm ss,GME}]\} \geq 0. \end{aligned} \tag{72}$$

On the third line of Eq. (72), we substituted Eq. (49) for $\dot{\rho_{\rm S}}$ in the first term and represented the second term as a logarithm (the partition function does not contribute since $\mathcal{D}_\nu$ is traceless). The inequality on the last line follows from Spohn's inequality (Spohn, 1978) applied to each term in the sum.

Similar considerations can be made for LMEs. In this case the second law must be formulated in terms of the local energy and particle currents $I^k_{\rm E,diss}$ and $I^k_{\rm N,diss}$ [Eqs. (68) and (69)], defined in terms of the local Hamiltonians $H^k_{\rm S}$ for each site k; cf. Eq. (55). The local heat currents are then $I^k_{\rm Q,LME} = I^k_{\rm E,diss} - \mu_k I^k_{\rm N,diss}$. With this proviso, we find a similar inequality

$$\dot{\Sigma}_{\rm LME} = -\frac{d}{dt}{\rm tr}\{\rho_{\rm S}\ln\rho_{\rm S}\} - \sum_k \beta_k I^k_{Q,\rm LME} \geq 0, \tag{73}$$

now defined in terms of local currents. The derivation is similar to Eq. (72) but exploits the fact that the local dissipators $\mathcal{D}^{\rm LME}_k$ thermalize only the local states $\rho^k_{\rm ss,LME} = e^{-\beta_k(H^k_{\rm S}-\mu_k N^k_{\rm S})}/Z_k$. This allows us to write[8] $\dot{\Sigma}_{\rm LME} = \sum_k {\rm tr}\{\mathcal{D}_k\rho_{\rm S}[\ln\rho_{\rm S} - \ln\rho^k_{\rm ss,LME}]\} \geq 0$.

There are at least two physical arguments explaining why for LMEs Eq. (73) must be formulated in terms of local heat currents $I^k_{\rm Q,LME}$. First, in a microscopic derivation the LME is a good approximation only when $H^{k,k+1}_{\rm S}$ are small, in which case the local and global currents are approximately the same [Eq. (70)]. Second, if the LME stems from a collisional model (Sec. II.C.4), it was shown by Barra (2015) and De Chiara *et al.* (2018) that $I^k_{\rm Q,LME}$ is the actual heat current flowing to the ancillas, while the terms associated with $H^{k,k+1}_{\rm S}$ are related to the work cost of turning the bath interactions on and off. This is consistent with the fact that the last term in Eq. (73) should be the change in entropy of the environments.

To summarize, in formulating the second law one should use global currents for GMEs and local currents for LMEs. Otherwise, one may arrive at apparent violations of the second law. An example was discussed by Levy and Kosloff (2014), who considered two bosonic modes with frequencies $\omega_{1(2)}$ coupled to baths at $\beta_{1(2)}$. They used LMEs but employed global currents to compute the entropy production rate, leading to $\dot{\Sigma} \propto (\omega_1 + \omega_2)(\beta_2 - \beta_1)(n_1 - n_2)$, where $n_k = (e^{\beta_k\omega_k} - 1)^{-1}$. As one may verify, it is possible to tune $\omega_{1(2)}$ so as to always induce $\dot{\Sigma} < 0$, which suggests an inadequacy of LMEs in describing the second law. This was reconciled by Barra (2015), De Chiara *et al.* (2018), and Pereira (2018) with the help of a collision model. The resulting entropy production rate, derived in terms of local currents, now has the form $\dot{\Sigma} \propto (\beta_2\omega_2 - \beta_1\omega_1)(n_1 - n_2)$, which depends only on the products $\beta_i\omega_i$, which are strictly non-negative and zero if and only if $\beta_1\omega_1 = \beta_2\omega_2$.

F. Local versus global versus Redfield master equations

As illustrated in Sec. II.C, even within the weak-coupling paradigm there are still many QMEs that one can derive, each based on different (and sometimes opaque) approximations. This may lead one to ask which is the best QME to use in a given situation. In this section, we provide a rough guideline. LMEs (Secs. II.B and II.C.4) work well if both internal system-system coupling and system-reservoir couplings are weak. They do not exactly thermalize the system when the baths are at the same temperature, but they are easy to use. GMEs (Sec. II.C.2) rely heavily on the secular approximation, and thus tend to work better if the internal system-system interactions are strong, since large energy splittings better justify the secular approximation. They may also produce unphysical internal currents (Wichterich *et al.*, 2007), but global currents are reliable. Finally, Redfield equations (Sec. II.C.1) often capture the best of both worlds, in that

[8]This does not require all sites to be connected to a bath. Since the $\mathcal{D}_k$ act locally, the sum is only over those sites that are actually connected to a bath.

they compare well with the exact solutions (Sec. II.G). But they can produce unphysical states, since they are not CPTP.

QMEs are benchmarked by comparing them to models that allow for exact solutions. Section II.G provides a detailed example. Rivas *et al.* (2010) studied LMEs and GMEs in bosonic systems. They first considered a single harmonic oscillator coupled to a bath (where LMEs and GMEs coincide) and found that QMEs work well, except at short times. Afterward they considered two bosonic modes with operators a_1 and a_2 coupled to two baths with operators $\{b_k\}$ and $\{c_k\}$. The dynamics was modeled with a Hamiltonian of the form

$$H = \Omega(a_1^\dagger a_1 + a_2^\dagger a_2) + \sum_k (\omega_{1k} b_k^\dagger b_k + \omega_{2k} c_k^\dagger c_k) + \xi \vartheta(a_1, a_2) + \lambda \sum_k [g_{1k}\vartheta(a_1, b_k) + g_{2k}\vartheta(a_2, c_k)], \tag{74}$$

where $\vartheta(a,b) = a^\dagger b + b^\dagger a$ is a shorthand notation and [as in our discussion near Eq. (41)] ξ gauges the internal system coupling, while λ gauges the overall system-environment interaction (with g_{ik} an additional, dimensionless parameter).

Comparing the LME and GME resulting from this Hamiltonian with the exact solution, Karrlein and Grabert (1997) and Serafini (2017) found that for small ξ the LME works better than the GME. Conversely, for large ξ the GME tends to be the better choice. Qualitatively similar results were found for fermions (Ribeiro and Vieira, 2015; Mitchison and Plenio, 2018); see also Sec. II.G. Purkayastha, Dhar, and Kulkarni (2016b) extended these results to Redfield equations and found that, over a large parameter regime, it yielded dramatically better results than the LME and GME. The Hamiltonian (74) assumes a hopping interaction that conserves the number of quasiparticles. In contrast, a "position-position" interaction $(a + a^\dagger)(b + b^\dagger)$ was studied by González *et al.* (2017). The conclusions were similar but spanned a much wider range of parameter space. Recently Potts, Kalaee, and Wacker (2021) compared the LME and GME approaches with a specific emphasis on the first law of thermodynamics, i.e., on the proper identification of thermal currents. Mitchison and Plenio (2018) also addressed the additivity of multiple reservoirs. As discussed in Sec. II.C.3, LMEs and GMEs have the convenient property that reservoirs combine additively. Comparing them to the exact solutions, Mitchison and Plenio found that in general this is not a good assumption, as also revealed by strong-coupling methods (Sec. II.H). The previously mentioned studies focused on the NESS. Transient behavior was studied by Scali, Anders, and Correa (2021), who showed that LMEs generally perform better. This is due to the fact that the secular approximation tends to destroy key dynamical features of GMEs.

All these analyzes address what is the "best QME" by comparing them to the exact solutions. However, these are available only for special classes of systems (usually non-interacting ones). Little is known about interacting systems. Hartmann and Strunz (2020) studied spin-boson models and benchmarked the Redfield master equation with a pseudo-mode approach (Imamoğlu, 1994; Garraway, 1997a, 1997b; Tamascelli *et al.*, 2018); these were found to agree better than GKSL equations. These findings can be contrasted with the results given by McCauley *et al.* (2020), which showed that, for systems weakly coupled via a constant spectral density, one may find GKSL master equations that are superior to the Redfield approach. Xu, Thingna *et al.* (2019) compared LMEs and Redfield master equations with exact solutions for large spin chains of up to 21 sites (simulated using tensor networks). They found that Redfield equations performed significantly better than LMEs in the presence of strong interactions within the system. A comparison with GMEs was not possible, owing to the computational cost.

G. Connection with exactly solvable systems

Despite the complexity of open quantum systems, there are some cases where the dynamics is exactly solvable. This includes the pure-dephasing limit of the spin-boson model (Leggett *et al.*, 1987; Lidar, Bihary, and Whaley, 2001), where the dynamics is simple since the interaction commutes with the system Hamiltonian and thus cannot change the system energy. Additionally, quadratic models also allow for an exact solution, which can be obtained through various methods. In the bosonic case, for example, exact non-Markovian master equations for systems of coupled oscillators have been studied (Karrlein and Grabert, 1997). Noninteracting models can also be treated with nonequilibrium Green's functions (Caroli *et al.*, 1971; Meir and Wingreen, 1992; Economou, 2006; Haug and Jauho, 2008; Prociuk, Phillips, and Dunietz, 2010; Aeberhard, 2011; Zimbovskaya and Pederson, 2011; Dhar, Saito, and Hänggi, 2012; Nikolić *et al.*, 2012; Wang, Agarwalla, and Thingna, 2014), including slowly driven systems (Bhandari *et al.*, 2021). Complications arise, though, when interactions are considered (Meir and Wingreen, 1992; Meir, Wingreen, and Lee, 1993).

In this section we expose a simpler approach, that fully suffices to treat models with quadratic Hamiltonians. Although we exemplify the model for fermions, a similar derivation works for bosons. We focus on reservoirs modeled by 1D tight-binding chains, but this is not a restriction, since any chain can be mapped onto a set of noninteracting modes, and vice versa; see Sec. II.H. The advantage of the homogeneous tight-binding chain is that it can be analytically diagonalized even for finite chain lengths.

We consider two chain reservoirs $\alpha \in \{L, R\}$, described by N_α fermionic operators $d_{i,\alpha}$ each and modeled by a tight-binding Hamiltonian [Eq. (15)] $H_{\mathrm{B}}^{(\alpha)} = \epsilon \sum_{i=1}^{L_\alpha} d_{i,\alpha}^\dagger d_{i,\alpha} + \tau \sum_{i=1}^{L_\alpha - 1} [d_{i,\alpha}^\dagger d_{i+1,\alpha} + d_{i+1,\alpha}^\dagger d_{i,\alpha}]$, where $\epsilon \in \mathbb{R}$ and $\tau > 0$. The system, in turn, is described by N noninteracting sites, with operators d_i and Hamiltonian $H_{\mathrm{S}} = \sum_{i,j=1}^{N} h_{ij} d_i^\dagger d_j$. The coupling to the baths occurs at sites 1 and N, and has the form $H_{\mathrm{I}} = \tau_L (d_{1,L}^\dagger d_1 + d_1^\dagger d_{1,L}) + \tau_R (d_{1,R}^\dagger d_N + d_N^\dagger d_{1,R})$, with tunnel amplitudes $\tau_\alpha > 0$. The reservoirs are diagonalized with the transformation

$$d_{i,\alpha} = \sqrt{\frac{2}{L_\alpha + 1}} \sum_{k=1}^{L_\alpha} \sin\left(\frac{\pi i k}{L_\alpha + 1}\right) c_{k,\alpha}$$

to a new set of operators $c_{k,\alpha}$, leading to

$$H_{\mathrm{B}}^{(\alpha)}=\sum_{k=1}^{L_\alpha}\epsilon_{k\alpha}c_{k,\alpha}^{\dagger}c_{k,\alpha},\qquad \epsilon_{k\alpha}=\epsilon-2\tau\cos\left(\frac{\pi k}{L_\alpha+1}\right). \tag{75}$$

In turn, the system-bath interactions change to

$$H_{\mathrm{I}}=\sum_{k=1}^{N_L}t_{kL}[c_{kL}^{\dagger}d_1+\mathrm{H.c.}]+\sum_{k=1}^{N_R}t_{kR}[c_{kR}^{\dagger}d_N+\mathrm{H.c.}], \tag{76}$$

with

$$t_{k\alpha}=\tau_\alpha\sqrt{\frac{2}{L_\alpha+1}}\sin\left(\frac{\pi k}{L_\alpha+1}\right).$$

Diagonalizing $H_{\mathrm{B}}^{(\alpha)}$ has the advantage that we can explicitly eliminate the reservoir operators from the Heisenberg equations of motion: $\dot{\boldsymbol{d}}_1=-\mathrm{i}\sum_j h_{1j}\boldsymbol{d}_j-\mathrm{i}\sum_k t_{kL}\boldsymbol{c}_{kL}$ for the first site, $\dot{\boldsymbol{d}}_a=-\mathrm{i}\sum_j h_{aj}\boldsymbol{d}_j$ for $2\le a\le N-1$, $\dot{\boldsymbol{d}}_N=-\mathrm{i}\sum_j h_{Nj}\boldsymbol{d}_j-\mathrm{i}\sum_k t_{kR}\boldsymbol{c}_{kR}$ for the last site, and $\dot{\boldsymbol{c}}_{kL}=-\mathrm{i}\epsilon_{kL}\boldsymbol{c}_{kL}-\mathrm{i}t_{kL}\boldsymbol{d}_1$ and $\dot{c}_{kR}=-\mathrm{i}\epsilon_{kR}\boldsymbol{c}_{kR}-\mathrm{i}t_{kR}\boldsymbol{d}_N$ for the left and right reservoir operators, respectively.

An exact solution is possible using nonequilibrium Green's functions (Haug and Jauho, 2008). In the Appendix we provide a more direct exact approach based on Laplace transforms. It applies to reservoirs in the star representation (Schaller, 2014) and explicitly incorporates the initial conditions, which complies with generalized formulations of nonequilibrium thermodynamics (Esposito, Lindenberg, and den Broeck, 2010). The baths are characterized by the spectral coupling density $\Gamma_\alpha(\omega)=2\pi\sum_k|t_{k\alpha}|^2\delta(\omega-\epsilon_{k\alpha})$ (also termed the bare tunneling rate in this context), which in our case becomes

$$\Gamma_\alpha(\omega)=\frac{2\tau_\alpha^2}{\tau}\sqrt{1-\frac{(\omega-\epsilon)^2}{4\tau^2}}\Theta\left(4\tau^2-(\omega-\epsilon)^2\right), \tag{77}$$

which has strict finite support. This is known as the semi-elliptical, or Newns, spectral density (Newns, 1969; Mitchison and Plenio, 2018). Nonconstant spectral densities (Schaller, Zedler, and Brandes, 2009; Topp, Brandes, and Schaller, 2015) can be used to model non-Markovian effects (Zedler *et al.*, 2009), and finite support can even lead to phenomena like *bound states* (Longhi, 2007; Jussiau, Hasegawa, and Whitney, 2019).

Considering first the simplified case of a single dot coupled to only one reservoir, we can compare the exact solution for the dot occupation $\langle d_1^{\dagger}d_1\rangle$, for various bath sizes, to the solution arising from a GKSL treatment, as shown in Fig. 3. One can see that finite-size baths (system and reservoir) lead to backflows of information (here a fermionic particle tunneling back to the system), which one can use as a non-Markovianity measure (Breuer, 2012). If the dot energy is significantly outside the support of $\Gamma_\alpha(\omega)$, a bound state may emerge (Longhi, 2007; Jussiau, Hasegawa, and Whitney, 2019), which is not captured by a Markovian master equation (not shown).

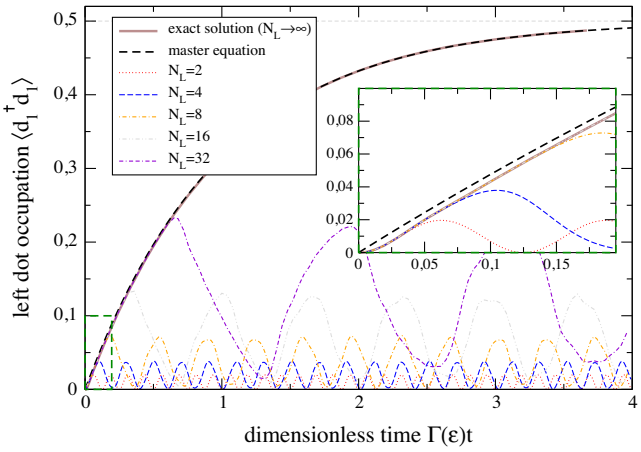

FIG. 3. Time-dependent occupation of a single dot of energy ϵ coupled to a tight-binding chain of different lengths N_L. As $N_L\to\infty$, the reservoir drags the system toward a stationary occupation, but for finite chain lengths recurrences occur. For the chosen parameters (weak system-reservoir coupling), the QME (dashed lines) captures the dynamics well, except at small times (inset). The horizontal dashed line at 0.5 is the long-time steady-state occupation. The other parameters are $h_{11}=h_{22}=\epsilon\equiv\varepsilon$, $h_{12}=0$, $\mu_\nu=\varepsilon$, $\tau=\varepsilon$, $\tau_\nu=0.1\varepsilon$, and $\Gamma_\nu(\varepsilon)\beta_\nu=2\tau_\nu^2\beta_\nu/\tau=0.02$.

Next we go back to the original two-bath configuration and consider the steady state. We assume for simplicity the *wideband limit*, where $\Gamma_\alpha(\omega)\to\Gamma_\alpha$. Formally, this can be achieved by taking $\tau,\tau_\alpha\to\infty$ such that $2\tau_\alpha^2/\tau\equiv\Gamma_\alpha=\mathrm{const}$. In this limit, the Green's function $G_{ij}(z)$ [defined in the Appendix following Eq. (A4)] has only isolated poles with a negative real part. We may thus drop the initial-state dependence and all poles with a negative real part in the inverse Laplace transform such that the stationary limit eventually simplifies to

$$\begin{aligned}\langle d_i^{\dagger}d_j\rangle_t\overset{t\to\infty}{\longrightarrow}&\int\Gamma_L(\omega)G_{i1}^{*}(0^+-\mathrm{i}\omega)G_{j1}(0^+-\mathrm{i}\omega)f_L(\omega)\frac{d\omega}{2\pi}\\&+\int\Gamma_R(\omega)G_{i2}^{*}(0^+-\mathrm{i}\omega)G_{j2}(0^+-\mathrm{i}\omega)f_R(\omega)\frac{d\omega}{2\pi},\end{aligned} \tag{78}$$

which coincides with Green's function approaches (Caroli *et al.*, 1971; Meir and Wingreen, 1992; Economou, 2006; Haug and Jauho, 2008; Prociuk, Phillips, and Dunietz, 2010; Aeberhard, 2011; Zimbovskaya and Pederson, 2011; Dhar, Saito, and Hänggi, 2012; Nikolić *et al.*, 2012; Wang, Agarwalla, and Thingna, 2014).

We compare this with the LME, GME, and Redfield equations (Levy and Kosloff, 2014; González *et al.*, 2017; Hofer *et al.*, 2017; Farina *et al.*, 2020) by considering a two-site system (double quantum dot), with $d_{1(2)}\equiv d_{L(R)}$, $h_{11}=h_L$, $h_{22}=h_R$, and $h_{12}=h_{21}=h$. The LME from Sec. II.C.4 becomes in this case

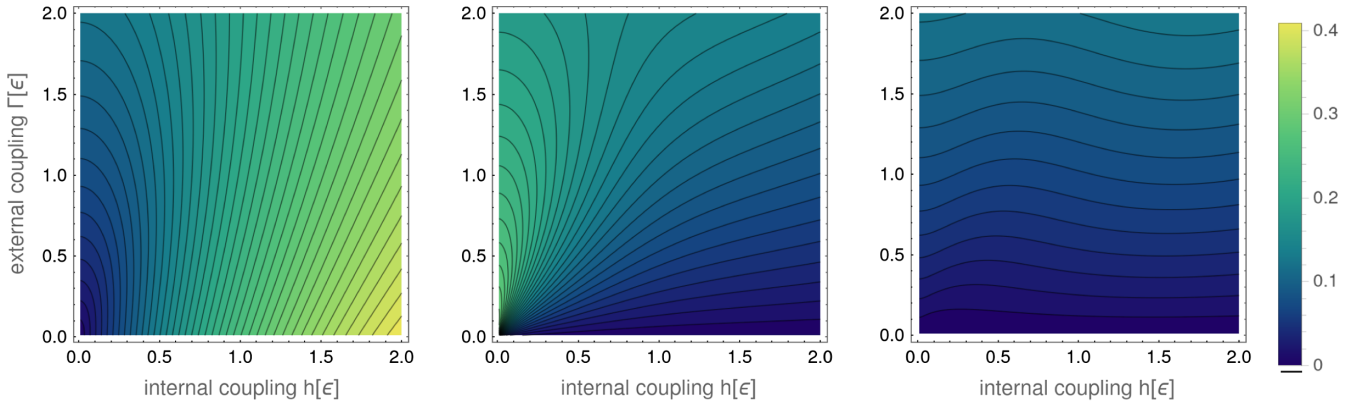

FIG. 4. Contour plot of the trace distance between the NESS single-particle density matrix [Eq. (83)] of the exact solution and the perturbative solutions for the LME $D(\rho_1^{\mathrm{EX}}, \rho_1^{\mathrm{LME}})$ (left panel), GME $D(\rho_1^{\mathrm{EX}}, \rho_1^{\mathrm{GME}})$ (middle panel), and Redfield equations $D(\rho_1^{\mathrm{EX}}, \rho_1^{\mathrm{RED}})$ (right panel). Dark (blue) indicates agreement of solutions. The plots are done as a function of the dimensionless internal coupling $h_{12}/\epsilon = h_{21}/\epsilon \equiv h/\epsilon$ (horizontal axes) and the dimensionless external coupling $\Gamma_L/\epsilon = \Gamma_R/\epsilon = \Gamma/\epsilon$ (vertical axes) with contours in steps of 0.01, assuming different chemical potentials and a wideband limit. The parameters are $h_L = h_{11} = h_{22} = h_R \equiv \epsilon$, $\beta_\nu \epsilon = 1$, and $\mu_L = \epsilon = -\mu_R$.

$$\dot{\rho_{\mathrm{S}}} = -\mathrm{i}[H_{\mathrm{S}}, \rho_{\mathrm{S}}] + \sum_{\alpha=L,R} \Gamma_\alpha \{[1 - f_\alpha(h_\alpha)] D[d_\alpha](\rho_{\mathrm{S}}) + f_\alpha(h_\alpha) D[d_\alpha^\dagger](\rho_{\mathrm{S}})\}. \tag{79}$$

For the GME (32), we must first diagonalize H_{S}:

$$H_{\mathrm{S}} = (d_L^\dagger, d_R^\dagger) \begin{pmatrix} h_L & h \\ h & h_R \end{pmatrix} \begin{pmatrix} d_L \\ d_R \end{pmatrix} = \epsilon_- c_-^\dagger c_- + \epsilon_+ c_+^\dagger c_+. \tag{80}$$

Finally, the Redfield equation (28), assuming that $h_L = h_R = \epsilon$ and dropping the principal values in Eq. (29), becomes

$$\begin{aligned} \dot{\rho_{\mathrm{S}}} = & -\mathrm{i}[H_{\mathrm{S}}, \rho_{\mathrm{S}}] \\ & - \frac{\Gamma_L}{4} f_L(\epsilon + h)\{[d_L, (d_L^\dagger + d_R^\dagger)\rho_{\mathrm{S}}] + [\rho_{\mathrm{S}}(d_L + d_R), d_L^\dagger]\} \\ & - \frac{\Gamma_L}{4} f_L(\epsilon - h)\{[d_L, (d_L^\dagger - d_R^\dagger)\rho_{\mathrm{S}}] + [\rho_{\mathrm{S}}(d_L - d_R), d_L^\dagger]\} \\ & - \frac{\Gamma_L}{4} f_L^-(\epsilon + h)\{[d_L^\dagger, (d_L + d_R)\rho_{\mathrm{S}}] + [\rho_{\mathrm{S}}(d_L^\dagger + d_R^\dagger), d_L]\} \\ & - \frac{\Gamma_L}{4} f_L^-(\epsilon - h)\{[d_L^\dagger, (d_L - d_R)\rho_{\mathrm{S}}] + [\rho_{\mathrm{S}}(d_L^\dagger - d_R^\dagger), d_L]\} \\ & + (L \leftrightarrow R), \end{aligned} \tag{81}$$

where $f_L^-(\omega) \equiv 1 - f_L(\omega)$. For small internal couplings $h \to 0$, this falls back to the LME (79).

In Fig. 4 we compare the trace distance

$$D(\rho, \sigma) = \mathrm{tr}\{|\rho - \sigma|\}/2, \tag{82}$$

between the single-particle density matrix

$$\rho_1 = \begin{pmatrix} \langle d_1^\dagger d_1 \rangle & \langle d_1^\dagger d_2 \rangle \\ \langle d_2^\dagger d_1 \rangle & \langle d_2^\dagger d_2 \rangle \end{pmatrix} \frac{1}{\langle d_1^\dagger d_1 \rangle + \langle d_2^\dagger d_2 \rangle}, \tag{83}$$

of the stationary exact solution (EX) to those from the LME, GME, and Redfield (RED) equations (left, middle, and right panels of Fig. 4, respectively). The horizontal and vertical axes are the internal system coupling h and the system bath coupling Γ (in units of $\epsilon = 1$). We see that the QMEs complement each other and have their own region of validity (González *et al.*, 2017; Hofer *et al.*, 2017; De Chiara *et al.*, 2018). For large h and small Γ, the GME performs well, while for small h the LME is better. One can also see that the Redfield equation yields good results throughout, despite not being in GKSL form. In fact, the superiority of the Redfield equation has been observed for a number of models where an exact solution exists. The development of GKSL equations reaching Redfield accuracy at steady state is therefore currently an interesting route of research (Kiršanskas, Franckié, and Wacker, 2018; Kleinherbers *et al.*, 2020; McCauley *et al.*, 2020; Trushechkin, 2021).

A qualitatively similar picture arises for the currents. For noninteracting electronic transport, the exact stationary particle current can be computed using Landauer's formula (Landauer, 1957; Büttiker, 1986; Nazarov and Blanter, 2009),

$$I_{\mathrm{N}}^{\mathrm{EX}} = \frac{1}{2\pi} \int T(\omega)[f_L(\omega) - f_R(\omega)] d\omega, \tag{84}$$

where $0 \le T(\omega) \le 1$ is the transmission function (Haug and Jauho, 2008). The comparison to the LME, GME, and RED (not shown) is qualitatively similar to Fig. 4. There are regimes, however, where although the steady state is poorly approximated both LME and GME happen to give acceptable results for the currents.

H. Strong system-bath coupling

The physics of strong system-bath coupling has been an intense research topic in both classical and quantum systems (Campisi, Hänggi, and Talkner, 2011; Talkner and Hänggi, 2020). In strong coupling, the QMEs of Sec. II.C are not applicable, the influence of multiple reservoirs no longer simply adds up (compare to Sec. II.C.3), the currents may need to be computed using full counting statistics (Sec. II.I)

since multiple particles may be emitted or absorbed at once (Schaller *et al.*, 2013), and reservoirs may crosstalk (Talarico, Maniscalco, and Gullo, 2020). However, strong coupling also offers possibilities. For example, with nonadditive reservoirs one may build an autonomous refrigerator with just two levels (Mu *et al.*, 2017), whereas for additive reservoirs this requires at least three levels (Linden, Popescu, and Skrzypczyk, 2010).

In this section we review techniques for describing boundary-driven systems in the strong-coupling regime. There are two main strategies: The first is to extend the system with a portion of the bath that, after careful transformations, can be weakly coupled to a residual bath. This includes the *reaction-coordinate* (Sec. II.H.1) and *polaron* approaches (Sec. II.H.3). The other strategy is to unitarily evolve system and baths together, which can be done using the star-to-chain and thermofield transformations (Sec. II.H.2), as well as other methods reviewed in Sec. II.H.4. The problem can also be approached with Green's function (Sec. II.G), higher-order calculations (Schröder, Schreiber, and Kleinekathöfer, 2007; Kast and Ankerhold, 2013), generalized thermodynamic arguments (Aurell, 2018; Perarnau-Llobet *et al.*, 2018), surrogate Hamiltonians (Katz and Kosloff, 2016), phenomenological collective modes (Cabot, Galve, and Zambrini, 2017), Feynman-Vernon influence functionals (Jin *et al.*, 2010; Yang *et al.*, 2020), etc.

1. Reaction coordinates

The approximations used in the derivation of QMEs can be easily violated when the system-reservoir coupling strength is not small, if short timescales are considered or when the system has near-degenerate levels. Some of these restrictions can be overcome if the framework is applied in a different frame, where the boundaries between system and reservoir are shifted. Transitions between different frames can be realized by Bogoliubov transforms (Woods *et al.*, 2014). To properly address the strong-coupling limit, one should make sure to start from a Hamiltonian that maintains a lower spectral bound. For example, considering a single bosonic reservoir with dimensionless system coupling operator S, this would be guaranteed when

$$H_{\mathrm{tot}} = H_{\mathrm{S}} + \sum_k \omega_k \left(b_k^\dagger + \frac{h_k}{\omega_k} S^\dagger\right)\left(b_k + \frac{h_k^*}{\omega_k} S\right), \tag{85}$$

where ω_k and h_k are constants. Upon expanding the second term, we get the usual system and reservoir Hamiltonian, together with a renormalization

$$\Delta H_{\mathrm{S}} = \sum_k \frac{|h_k|^2}{\omega_k} S^2 = \frac{1}{2\pi}\int_0^\infty \frac{\Gamma^{(0)}(\omega)}{\omega} S^2 d\omega, \tag{86}$$

where

$$\Gamma^{(0)}(\omega) = 2\pi \sum_k |h_k|^2 \delta(\omega - \omega_k) \tag{87}$$

is the spectral coupling density (Leggett *et al.*, 1987; Xu, Shen *et al.*, 2019; Mascherpa *et al.*, 2020).

Beyond weak coupling, a perturbative treatment of the system-reservoir interaction h_k is not applicable. Instead, we apply a Bogoliubov transform $b_k = \sum_q (u_{kq} B_q + v_{kq} B_q^\dagger)$ to new bosonic annihilation operators B_q, where $u_{kq} \in \mathbb{C}$ and $v_{kq} \in \mathbb{C}$ are coefficients that have to ensure proper commutation relations for the B_q. The idea is to choose them so as to recast H_{tot} in the form

$$H_{\mathrm{tot}} = H_{\mathrm{S}} + \Omega_1 \left(B_1^\dagger + \frac{\lambda_1}{\Omega_1} S\right)\left(B_1 + \frac{\lambda_1}{\Omega_1} S\right) + \sum_{q>1} \Omega_q \left(B_q^\dagger + \frac{H_q}{\Omega_q}(B_1 + B_1^\dagger)\right)\left(B_q + \frac{H_q^*}{\Omega_q}(B_1 + B_1^\dagger)\right), \tag{88}$$

such that S couples only to a single mode B_1 (called the reaction coordinate) with coupling strength λ_1 and energy Ω_1. In turn, B_1 couples to the residual reservoir modes $B_{q>1}$ via new coupling constants H_q, which parametrize a residual spectral density

$$\Gamma^{(1)}(\omega) = 2\pi \sum_{k>1} |H_k|^2 \delta(\omega - \Omega_k). \tag{89}$$

Finding the Bogoliubov coefficients is generally tedious, but for an infinitely large reservoir with dense level spacing, the following explicit formulas for λ_1, Ω_1, and $\Gamma^{(1)}(\omega)$ can be derived (Strasberg *et al.*, 2016; Nazir and Schaller, 2019):

$$\Omega_1^2 = \frac{\int_0^\infty \omega \Gamma^{(0)}(\omega) d\omega}{\int_0^\infty [\Gamma^{(0)}(\omega)/\omega] d\omega}, \tag{90}$$

$$\lambda_1^2 = \frac{1}{2\pi\Omega_1}\int_0^\infty \omega \Gamma^{(0)}(\omega) d\omega, \tag{91}$$

$$\Gamma^{(1)}(\omega) = \frac{4\lambda_1^2 \Gamma^{(0)}(\omega)}{\{(1/\pi)\mathcal{P}\int_{-\infty}^{+\infty} [\Gamma^{(0)}(\omega')/(\omega' - \omega)] d\omega'\}^2 + [\Gamma^{(0)}(\omega)]^2}, \tag{92}$$

where on the last line an analytic continuation as an odd function $\Gamma^{(n)}(\omega') = -\Gamma^{(n)}(-\omega')$ is understood under the integral. Multiple variants of such mapping exist; cf. Woods *et al.* (2014) and Nazir and Schaller (2019).

The usefulness of this approach lies in the fact that, even though the original couplings h_k are strong, the new couplings H_k to the residual bath can be weak. To see this, notice that Eq. (87) is $\mathcal{O}(h_k^2)$, while the new spectral density $\Gamma^{(1)}$ is $\mathcal{O}(1)$. Hence, although S and B_1 couple strongly, B_1 and its residual bath do not (Martinazzo *et al.*, 2011; Strasberg *et al.*, 2016), which was benchmarked by Iles-Smith, Lambert, and Nazir (2014) and Iles-Smith *et al.* (2016). This has been observed to hold for even stronger residual couplings (Correa, Xu, and Adesso, 2019). The effects of system-reservoir correlations (Iles-Smith, Lambert, and Nazir, 2014) or non-Markovian dynamics (Iles-Smith *et al.*, 2016) within the original system also come within reach. The price one has to pay is that the reaction coordinate needs to be treated explicitly, which for two bosonic reservoirs can already be challenging (Anto-Sztrikacs and Segal, 2021).

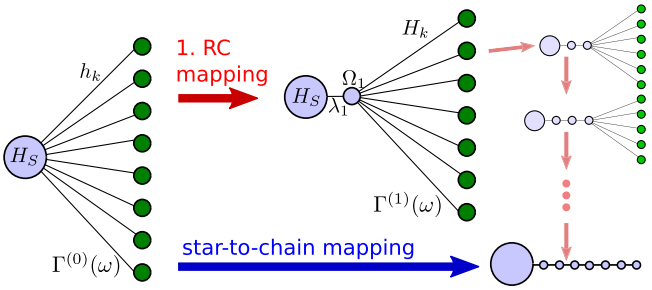

FIG. 5. Sketch of a single reaction-coordinate (RC) mapping (top left arrow) that effectively transfers 1 degree of freedom from the reservoir (dark green circles) to the system (light blue circles) generating an enlarged supersystem that requires an explicit treatment. Recursive applications (on the right in faint colors) generate a chain configuration, effectively implementing the star-to-chain mapping (bottom long arrow) described in Sec. II.H.2.

The reaction-coordinate mappings can, with slight modifications, be applied to fermionic systems as well, where the explicit treatment of a fermionic reaction coordinate is computationally not as costly as for bosonic ones. This was used by Schaller *et al.* (2018), Strasberg *et al.* (2018), and Restrepo *et al.* (2019) to discuss quantum nonequilibrium thermodynamics of fermionic systems.

The previous mapping is independent of H_S such that one can use these approaches to study interacting systems (Strasberg, 2019; Tamascelli *et al.*, 2019; Brenes *et al.*, 2020). In addition, the transformed Hamiltonian is equivalent to the original upon identifying $S \to B_1 + B_1^\dagger$ and $H_S \to H_S + \Omega_1[B_1^\dagger + (\lambda_1/\Omega_1)S^\dagger][B_1 + (\lambda_1/\Omega_1)S]$. The procedure can thus be applied recursively, which would eventually map the "starlike" system-reservoir interaction, where the system is coupled to each bath mode, into a chain, where the system and each bath site are coupled only to nearest neighbors (Fig. 5). The typical intention of the reaction-coordinate formalism is to stop after a few iterations. As a rule of thumb, the transformed spectral densities tend to become more and more structureless with each iteration, which at some point enables a Markovian description (Martinazzo *et al.*, 2011; Woods *et al.*, 2014). For methods requiring a chain representation, however, it is possible to perform the star-to-chain mapping directly; see Sec. II.H.2. Alternatively, since Bogoliubov transforms are invertible, one may also exploit reverse reaction-coordinate mappings to map long chains with structureless reservoirs into a single quantum dot with highly structured reservoirs, which can be treated with nonequilibrium Green's functions (Martensen and Schaller, 2019; Ehrlich and Schaller, 2021).

If the system is coupled to multiple reservoirs, the reaction-coordinate mapping is applied individually to each bath. Hence, the resulting QME will still add up. However, a dissipator for reservoir ν now depends on the system plus reaction-coordinate Hamiltonian, and hence on the parameters of the original reservoirs. As such, the original reservoirs no longer enter additively in the sense of Sec. II.C.3.

We can also generalize the formalism to multiple reaction coordinates. For example, at each step of the mapping one may split the support of $\Gamma^{(n)}(\omega)$ into intervals and introduce a reaction coordinate for each interval. This will lead to tree-type network topologies that can be more efficient than a chain mapping (Huh *et al.*, 2014; Mascherpa *et al.*, 2020; Pleasance, Garraway, and Petruccione, 2020). Alternatively, one may represent $\Gamma^{(0)}(\omega)$ by a sum of simpler (e.g., Lorentzian) functions, which also introduces multiple collective coordinates at once. This is often called the pseudomode approach (Imamoğlu, 1994; Garraway, 1997a, 1997b; Pleasance, Garraway, and Petruccione, 2020) and has been used to describe strong coupling and non-Markovianity. Brenes *et al.* (2020) combined this with multisite GKSL baths (Sec. II.K.2) and tensor networks (Sec. III.E), with a specific focus on applications in many-body thermal machines.

2. Star-to-chain and Thermofield transformations

Recursively applying the reaction-coordinate method takes the star configuration [Eq. (85)] into a chain configuration for the bath (Fig. 5). Since they can be interpreted as successive Bogoliubov transforms, their joint application is also a Bogoliubov transform. The star-to-chain mapping can thus be performed on a single step. In this section, we describe this idea in more detail. In addition, we show how to combine it with the thermofield transformation, which ensures that the resulting chain reservoirs are empty, thus providing simple initial conditions for simulations.

a. Star-to-chain transformation

Consider for simplicity a continuous bath with Hamiltonian $H_B = \int \omega(k) b^\dagger(k) b(k) dk$ and coupling

$$H_I = S \int h(k)[b(k) + b^\dagger(k)]dk, \tag{93}$$

where S acts only on the system and $h(k)$ is the coupling density. The spectral function analogous to Eq. (87) is thus $J(\omega) = \pi h^2[k(\omega)]dk(\omega)/d\omega$ (Leggett *et al.*, 1987; Bulla *et al.*, 2005).

To apply the star-to-chain mapping directly, one may discretize the spectrum [as in the numerical renormalization group (Wilson, 1975; Bulla, Costi, and Pruschke, 2008)], use orthogonal polynomials (Chin, Rivas *et al.*, 2010; Prior *et al.*, 2010), or perform numerical optimization via a cost function (Caffarel and Krauth, 1994; Dorda *et al.*, 2014). In *direct discretization*, we split the range of frequencies of the bath in different intervals and use a set of basis functions to describe the bath operators within each range, thus recovering a discrete bath. A strategy that properly weights different energy scales is the logarithmic discretization, which considers intervals at frequencies $\omega_n = \omega_{\max}\Lambda^{-n}$ where $\Lambda > 1$ (Bulla, Costi, and Pruschke, 2008). In each interval, one can choose basis functions that are plain waves in that interval and 0 elsewhere such that $\int_0^{\omega_{\max}} d\omega = \sum_n \int_{\omega_{n+1}}^{\omega_n} d\omega$.

Conversely, with orthogonal polynomials one introduces a new set of bosonic operators $B_n = \int U_n(k) b(k) dk$, with $n = 0, 1, \ldots$ and $U_n(k) = h(k)\rho_n^{-1}\pi_n(k)$. Here ρ_n is a normalization factor and $\pi_n(k)$ are orthogonal polynomials with inner product $\int h^2(k)\pi_n(k)\pi_m(k)dk = \rho_n \delta_{n,m}$. Since all information

about the environment is contained in $J(\omega)$ (Leggett *et al.*, 1987), one may choose $\omega(k)$ and $h^2(k)$ freely, as long as $J(\omega)$ is preserved. A useful choice is $\omega(k)=\omega_c k$ and $h^2(k)=\omega_c J(\omega(k))/\pi$. This transforms the bath and the interaction into

$$H_{\mathrm{B}}=\omega_c\left[\sum_n \alpha_n B_n^\dagger B_n+\left(\sqrt{\beta_{n+1}}B_{n+1}^\dagger B_n+\mathrm{H.c.}\right)\right], \tag{94}$$

$$H_{\mathrm{I}}=S\sqrt{\frac{\eta_J}{\pi}}(B_0+B_0^\dagger), \qquad \eta_J=\int J(\omega)d\omega, \tag{95}$$

which follow from the recursion relation $k\pi_n(k)=\alpha_n\pi_n(k)+\beta_n\pi_{n-1}(k)+\pi_{n+1}(k)$ [which holds when $\omega(k)=\omega_c k$]. Choosing $\pi_{-1}(k)=0$ and $\pi_1(k)=1$, the coefficients α_n and β_n in H_{B} are then given by $\beta_0=0$, $\beta_n=\gamma_n/\gamma_{n-1}$, $\gamma_n=\int h^2(k)\pi_n(k)^2dk$, and $\alpha_n=\gamma_n^{-1}\int kh^2(k)\pi_n(k)^2dk$, which are amenable to numerical evaluation (Gautschi, 2005). These coefficients are bounded if the spectrum is finite. And if the measure $h^2(k)dk$ belongs to the Szegő class (Szegő, 1939), they converge to a value independent of n. Hence, deep within the chain the couplings will be uniform, as is the case in reaction coordinates (Woods *et al.*, 2014). Additional details were given by Chin, Rivas *et al.* (2010).

If the bath is already discrete, a Lanczos or Householder transform will turn the originally diagonal bath Hamiltonian tridiagonal, i.e., a chain. The important step is to choose as the first vector the sum of all modes weighted by their coupling with the system (de Vega, Schollwöck, and Wolf, 2015).

Converting the original problem to a chain configuration allows it to be more readily tackled with tensor networks (Sec. III.E). However, this is not always advantageous. For instance, for fermionic baths (Wolf, McCulloch, and Schollwöck, 2014; Lu *et al.*, 2019; Rams and Zwolak, 2020) the star configuration may lead to a slower growth of entanglement limited by the large number of fully occupied states in the Fermi sea that do not participate in the evolution.

b. Thermofield transformation

The star-to-chain mapping allows one to study the evolution of the system plus baths together as a single system. A difficulty of bosonic chains, however, is that they may have large local occupations at high temperatures. Using the thermofield transformation (Bargmann, 1961; Araki and Woods, 1963; Takahashi and Umezawa, 1996; Blasone, Jizba, and Vitiello, 2011; de Vega and Bañuls, 2015), we can map the chain, at least at initial times, to two empty chains. This can be particularly useful in tensor network algorithms (Sec. III.E). The thermofield transformation is employed in bosonic baths modeled with bilinear couplings to the system. It applies to arbitrary coupling strengths and could also be extended to considering initial correlations between system and bath. Extensions to fermionic systems were discussed by Blasone, Jizba, and Vitiello (2011), de Vega and Bañuls (2015), Schwarz *et al.* (2018), and Nüßeler *et al.* (2020).

Given a bath defined by modes b_k, the idea is to introduce another bath, with modes c_k, that is identical to the physical one, such that for thermal density matrices ρ_{B} the expectation value can be written as $\mathrm{tr}(\cdot\rho_{\mathrm{B}})=\langle\Omega|\cdot|\Omega\rangle$, with

$$|\Omega\rangle=\bigotimes_k\left(\sum_{n_k=0}^{\infty}\frac{e^{-\beta\omega_k n_k/2}}{\sqrt{1+\bar{n}_k}}|n_k\rangle_{b_k}|n_k\rangle_{c_k}\right), \tag{96}$$

where $\bar{n}_k=1/(e^{\beta\omega_k}-1)$ and $|n\rangle_{b_k}$ and $|n\rangle_{c_k}$ are Fock states of b_k and c_k. The state $|\Omega\rangle$ is called the thermal vacuum. It satisfies $\exp(-\beta H_{\mathrm{B}})/Z_{\mathrm{B}}=\mathrm{tr}_C\{|\Omega\rangle\langle\Omega|\}$ and can be obtained from the global vacuum $|\mathbf{0}\rangle$ of b_k and c_k via a thermal Bogoliubov transformation $|\Omega\rangle=e^{-\mathrm{i}G}|\mathbf{0}\rangle$, with $G=\mathrm{i}\sum\theta_k(b^\dagger{}_k c^\dagger{}_k-b_k c_k)$ and $\tanh(\theta_k)=\exp(-\beta\omega_k/2)$. This implies that $|\Omega\rangle$ is the vacuum of a new set of bosonic modes $a_{1,k}=e^{-\mathrm{i}G}b_k e^{\mathrm{i}G}$ and $a_{2,k}=e^{-\mathrm{i}G}c_k e^{\mathrm{i}G}$.

We can now simulate the evolution of a system, initially prepared in the pure state $|\psi\rangle$ and coupled to a thermal bath of harmonic oscillators, as the evolution of the pure state $|\psi\rangle\otimes_k|0\rangle_{a1,k}|0\rangle_{a2,k}$. However, to do so we must transform the Hamiltonian from the b_k, c_k to the $a_{1,k}$, $a_{2,k}$ representation. It is much more convenient to use a slightly different Hamiltonian $H_{\mathrm{tot}}^{\mathrm{TF}}=H_{\mathrm{tot}}-\sum_k\omega_k c_k^\dagger c_k$. Adding such a decoupled term, one that depends only on the c_k modes, has no physical consequences. Using $H_{\mathrm{tot}}^{\mathrm{TF}}$ uncouples the modes $a_{1,k}$ and $a_{2,k}$ in the equations of motion, resulting in a much simpler treatment. A similar idea also leads to better numerical performance of tensor network methods when studying finite temperatures (Karrasch, Bardarson, and Moore, 2012).

As an example, consider the Hamiltonian

$$H_{\mathrm{tot}}=H_{\mathrm{S}}+\sum_k\omega_k b_k^\dagger b_k+\sum_k h_k(a_{\mathrm{S}}^\dagger b_k+a_{\mathrm{S}}b_k^\dagger), \tag{97}$$

where a_{S} and $a_{\mathrm{S}}^\dagger$ act on the system only. After a thermal Bogoliubov transformation, the thermofield Hamiltonian $H_{\mathrm{tot}}^{\mathrm{TF}}$ becomes

$$\begin{aligned}H_{\mathrm{tot}}^{\mathrm{TF}}=H_{\mathrm{S}}&+\sum_k\omega_k(a_{1,k}^\dagger a_{1,k}-a_{2,k}^\dagger a_{2,k})\\&+\sum_{i\in\{1,2\}}\sum_k h_{i,k}(a_{\mathrm{S}}^\dagger a_{i,k}+a_{\mathrm{S}}a_{i,k}^\dagger),\end{aligned} \tag{98}$$

with new couplings $h_{1,k}=h_k\cosh(\theta_k)$ and $h_{2,k}=h_k\sinh(\theta_k)$. This can then be used together with the star-to-chain mapping, thereby transforming a single thermal bath into two empty semi-infinite chains (Guo *et al.*, 2018; Schwarz *et al.*, 2018; Chen *et al.*, 2020).

3. Polaron treatments

A convenient tool for studying the strong-coupling regime with bosonic environments is the *polaron master equation*. The starting point is a system-environment Hamiltonian parametrized as in Eq. (85). The polaron or Lang-Firsov transform (Lang and Firsov, 1963) amounts to a global unitary transformation of the system and reservoir

$$U_{\mathrm{p}}=\exp\left\{S\sum_k\left(\frac{h_k^*}{\omega_k}b_k^\dagger-\frac{h_k}{\omega_k}b_k\right)\right\}, \tag{99}$$

where h_k and ω_k are as defined in Eq. (85). As one may verify, this yields $U_{\mathrm{p}}SU_{\mathrm{p}}^\dagger=S$ and $U_{\mathrm{p}}b_kU_{\mathrm{p}}^\dagger=b_k-(h_k^*/\omega_k)S$. Hence, under this transform Eq. (85) becomes

$$H'_{\mathrm{tot}} = \underbrace{\mathrm{tr}_{\mathrm{B}}\left\{U_{\mathrm{p}} H_{\mathrm{S}} U_{\mathrm{p}}^{\dagger} \frac{e^{-\beta\sum_k \omega_k b_k^{\dagger} b_k}}{Z}\right\} \otimes \mathbb{1}_{\mathrm{B}}}_{H'_{\mathrm{S}}} + \sum_k \omega_k b_k^{\dagger} b_k + \underbrace{\left[U_{\mathrm{p}} H_{\mathrm{S}} U_{\mathrm{p}}^{\dagger} - \mathrm{tr}_{\mathrm{B}}\left\{U_{\mathrm{p}} H_{\mathrm{S}} U_{\mathrm{p}}^{\dagger} \frac{e^{-\beta\sum_k \omega_k b_k^{\dagger} b_k}}{Z}\right\} \otimes \mathbb{1}_{\mathrm{B}}\right]}_{H'_{\mathrm{I}}},$$

where we added and subtracted the same term to make the renormalized interaction H'_{I} obey $\mathrm{tr}_{\mathrm{B}}\{H'_{\mathrm{I}}\bar{\rho}_{\mathrm{B}}\} = 0$, such that the standard derivation of a GME or LME from Sec. II.C can be followed. To apply a perturbative treatment, it is not necessary for h_k to be small, but rather that H'_{I} is. In fact, since the polaron transform is unitary, none of these terms diverge when $h_k \to \infty$. In the weak-coupling limit the standard QME is reproduced, and for pure-dephasing models ($[H_{\mathrm{S}}, S] = 0$) the system is untouched ($H'_{\mathrm{S}} = H_{\mathrm{S}}$). More involved statements on the thermodynamic consistency of the polaron approach are possible, including fluctuation theorems (Schaller *et al.*, 2013; Krause *et al.*, 2015).

Such favorable properties have been used to advocate for the polaron approach as being capable of interpolating between the weak- and strong-coupling regimes (Wang, Ren, and Cao, 2015; Wang and Sun, 2015). Furthermore, it has been found to yield consistent thermodynamic results even for driven systems (Gelbwaser-Klimovsky and Aspuru-Guzik, 2015). Various improvements have been suggested, including variational polaron transforms (McCutcheon *et al.*, 2011) and mixtures of polaron transforms and reaction-coordinate mappings (Wächtler and Schaller, 2020). Finally, we remark that for multiple reservoirs a polaron transform designed to modify the coupling to one bath will dress the couplings to others (Brandes, 2005; Schaller *et al.*, 2013), making the nonadditivity explicit.

4. Evolution of the system and large finite baths

The previously mentioned methods rely on quadratic interactions and the harmonicity of the bath Hamiltonian. However, baths composed of interacting particles are often more realistic. Hence, depending on the model it may not be possible to use the previously mentioned methods, requiring one to treat the system and bath almost on the same footing. The bath does not have to be infinite in size, but as long as the system does not feel any finite-size effects and the dynamics has reached an approximate steady state, one can still learn about its transport properties.

For instance, Karrasch, Ilan, and Moore (2013) studied the dynamics of an XXZ chain with different types of perturbations and within a quantum Ising chain when each half was prepared at a different temperature, as depicted in Fig. 6. They showed that the system relaxes quickly to a steady current value in the presence of a nonzero Drude weight (Sec. IV.B). Mascarenhas, Giudice, and Savona (2017) considered a spin chain in the center, coupled at the edges to two chains prepared in different (nonthermal) states. Ljubotina, Znidaric, and Prosen (2017) and Žnidarič and Ljubotina (2018) considered a similar setup and studied the evolution of the time-integrated current $\int_0^t I dt' \propto t^{\phi}$, with ϕ characterizing the transport regime according to Table I. One

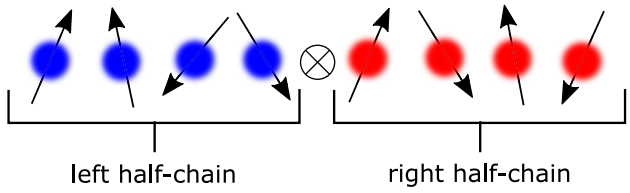

FIG. 6. Unitary (Hamiltonian) dynamics can be simulated for two long but finite spin chains prepared in an initial product state, with each chain in a different pure or mixed state (differing colors).

can also consider the unitary evolution of two different integrable chains, each prepared in a different thermal state (Biella *et al.*, 2016, 2019). The contact interaction between the two chains was chosen to break the integrability and induce the formation of a growing region supporting steady transport until finite-size effects came into play. This idea was previously suggested by Ponomarev, Denisov, and Hänggi (2011), who studied thermalization in bosonic systems.

In a recent study by Xu, Guo, and Poletti (2022) on a setup analogous to Fig. 6, they considered pure state preparations of each half chain. They showed that, in the regime of weak coupling between the two halves, the emergence of a steady current is typical. This means that for any initial condition formed of energy eigenstates within an energy window the resulting long-lasting current converges, in the thermodynamic limit, to the expected current from microcanonical preparations of each half.

A slightly different approach was taken by Mascarenhas *et al.* (2019), where additional dissipation at the edges of the baths was used to extend the time for which the system could be studied. More recently a different way of periodically refreshing the baths was put forward (Purkayastha *et al.*, 2021), and a hierarchy of master equations for the description of finite-size baths was introduced by Riera-Campeny, Sanpera, and Strasberg (2022). For noninteracting systems, works along these lines with fermionic-mesoscopic baths were introduced by Ajisaka *et al.* (2012) and Ajisaka and Barra (2013).

I. Full counting statistics and generalized master equations

Full counting statistics (FCS) asks for the number of jump processes during a given timespan. If the jumps are net particle transfers, the time derivative of that number yields the particle current. Similarly, if they come with net energy changes, one can construct energy currents. FCS goes beyond the average, however, and also accounts for fluctuations. We begin with a phenomenological introduction in Sec. II.I.1, followed by a microscopic derivation in Sec. II.I.2. Tools on how to actually extract the results are discussed in Sec. II.I.3.

1. Phenomenological introduction

When studying the dynamics of GKSL QMEs [Eq. (11)], one may wonder about the statistics of the *quantum jumps* described by the terms $L_\alpha \rho_{\mathrm{S}} L_\alpha^{\dagger}$ (Wiseman and Milburn, 2010). To track it, we can decompose the full Liouvillian into a no-jump evolution $\mathcal{L}_0$ and a jump term of interest (Brandes, 2008), i.e.,

$$\mathcal{L} = \mathcal{L}_0 + \mathcal{L}_1, \qquad \mathcal{L}_1\rho_S \equiv \gamma_{\bar{\alpha}} L_{\bar{\alpha}} \rho_S L_{\bar{\alpha}}^\dagger, \tag{100}$$

for a single chosen process[9] $\bar{\alpha}$. When a Dyson series is used, the full propagator $\mathcal{P}(t,t_0) = e^{\mathcal{L}(t-t_0)}$ can be expressed as a sequence of jump-free evolutions $\mathcal{P}_0(t) = e^{\mathcal{L}_0 t}$ interrupted by a variable number of quantum jumps:

$$\begin{aligned}\mathcal{P}(t,t_0) = \mathcal{P}_0(t-t_0) &+ \int_0^t dt_1 \mathcal{P}_0(t-t_1)\mathcal{L}_1\mathcal{P}_0(t_1-t_0) \\ &+ \int_0^t dt_2 \int_0^{t_2} dt_1 \mathcal{P}_0(t-t_2)\mathcal{L}_1\mathcal{P}_0(t_2-t_1) \\ &\times \mathcal{L}_1\mathcal{P}_0(t_1-t_0) + \cdots. \end{aligned} \tag{101}$$

The first term in Eq. (101) describes a trajectory without jumps, the second term a trajectory with a single quantum jump at $0 < t_1 < t$, the third one a trajectory with two quantum jumps at $0 < t_1 < t_2 < t$, etc.

To select trajectories with a specific number of jumps, one introduces a counting field χ (Levitov, Lee, and Lesovik, 1996; Esposito, Harbola, and Mukamel, 2007), tilting the Liouvillian according to $\mathcal{L}(\chi) = \mathcal{L}_0 + \mathcal{L}_1 e^{+i\chi}$. In the Dyson series of $\mathcal{P}(\chi,t) = e^{\mathcal{L}(\chi)t}$ terms containing n jumps then go with $e^{in\chi}$. Using the orthogonality relation $\int_{-\pi}^{\pi}(d\chi/2\pi)e^{i(n-m)\chi} = \delta_{n,m}$, we can then select the propagator associated with a dynamics with specifically n jumps up to time t:

$$\mathcal{P}^{(n)}(t) = \frac{1}{2\pi}\int_{-\pi}^{+\pi} \mathcal{P}(\chi,t)e^{-in\chi}d\chi. \tag{102}$$

The associated probability $p_n(t)$ of obtaining n quantum jumps during the time interval $[t_0,t]$ is then simply the following trace of the conditional dynamics $\mathcal{P}^{(n)}(t)\rho_S(t_0)$:

$$p_n(t) = \frac{1}{2\pi}\int_{-\pi}^{+\pi} \mathrm{tr}\{e^{\mathcal{L}(\chi)(t-t_0)}\rho_S(t_0)\}e^{-in\chi}d\chi. \tag{103}$$

The explicit evaluation is numerically tedious and is analytically possible only in special cases (Schaller, Kießlich, and Brandes, 2010). It is more convenient to look at the moment-generating function

$$M(\chi,t) = \mathrm{tr}\{\rho(\chi,t)\}, \qquad \rho(\chi,t) \coloneqq e^{\mathcal{L}(\chi)(t-t_0)}\rho_S(t_0), \tag{104}$$

where $\rho(\chi,t)$ is the solution of the generalized master equation, $\dot{\rho}(\chi,t) = \mathcal{L}(\chi)\rho(\chi,t)$. From $M(\chi,t)$, we obtain the cumulant-generating function $C(\chi,t) = \ln M(\chi,t)$, which is the QME equivalent of the Levitov-Lesovik formula for noninteracting electrons (Levitov and Lesovik, 1993; Klich, 2003; Schönhammer, 2007). Specific techniques to extract the lowest cumulants are discussed in Sec. II.I.3.

The questions raised in FCS are universal: They have been rigorously treated in both GMEs (Schaller, 2014) and LMEs (Garrahan and Lesanovsky, 2010; Žnidarič, 2014a, 2014b), where approximate methods have been developed for large and interacting 1D systems (Carollo *et al.*, 2017; Carollo, Garrahan, and Lesanovsky, 2018). Some GKSL extensions include feedback interventions (Brandes, 2010; Wiseman and Milburn, 2010) and the analysis of factorial cumulants (Stegmann *et al.*, 2015; Stegmann, König, and Sothmann, 2020). Beyond the GKSL framework, FCS was used in the Redfield equation (Hussein and Kohler, 2014; Jin, Filippone, and Giamarchi, 2020) and non-Markovian QMEs (Flindt, Braggio, and Novotný, 2007; Flindt *et al.*, 2008; Braggio, Flindt, and Novotný, 2009). Electronic transport setups also allow one to test these concepts experimentally (Fujisawa *et al.*, 2006; Gustavsson *et al.*, 2006; Flindt *et al.*, 2009; Utsumi *et al.*, 2010; Wagner *et al.*, 2017; Kurzmann *et al.*, 2019). Alternatively, one may also ask for the waiting-time distribution $\Omega(t)$ (Cohen-Tannoudji and Dalibar, 1986) between jumps, which is related to the probability of no jump by $\Omega(t) = -(d/dt)p_0(t)$. This can also be extended to the waiting times between different jumps (Brandes, 2008).

As an example, consider the QME (32). If we want only the total number of jumps (termed *dynamical activity*), we can tilt all jump operators identically $L_{ab}\rho_S L_{cd}^\dagger \to L_{ab}\rho_S L_{cd}^\dagger e^{+i\chi}$. Conversely, to count the particle current we use $L_{ab}\rho_S L_{cd}^\dagger \to L_{ab}\rho_S L_{cd}^\dagger e^{+i\chi(N_a-N_b)}$ (the coefficients $\gamma_{ab,cd}$ require that $N_d - N_c = N_b - N_a$). Similarly, the energy current can be counted with $L_{ab}\rho_S L_{cd}^\dagger \to L_{ab}\rho_S L_{cd}^\dagger e^{+i\chi(E_a-E_b)}$. For multiple reservoirs, specific counting fields can track the exchanges with each individual bath. Sometimes, however, a phenomenological identification of jump terms is not obvious. In these cases, one must instead resort to a microscopic derivation, as now discussed.

2. Microscopic derivation

Esposito, Harbola, and Mukamel (2009) provided a microscopic approach to connect changes in the bath with quantum jumps in the system. The assumption is that the reservoir observable of interest $\hat{O}$ (such as the particle number or energy) commutes with the reservoir Hamiltonian $[\hat{O}, H_B] = 0$. For a typical reservoir, the absolute value of such observables may assume infinite values. However, one needs only to track their changes during the time interval $[0,t]$. These can be obtained from a *two-point measurement* scheme, where we measure $\hat{O}$ at time 0 and again at time t. If we let $\hat{O} = \sum_\ell O_\ell |\ell\rangle\langle\ell|$ in the first measurement, the outcome O_ℓ occurs with a probability $p_\ell = \mathrm{tr}\{|\ell\rangle\langle\ell|\bar{\rho}_B\}$ and projects $\bar{\rho}_B$ to $\bar{\rho}_B{}^{(\ell)}/p_\ell$, where $\bar{\rho}_B{}^{(\ell)} = |\ell\rangle\langle\ell|\bar{\rho}_B|\ell\rangle\langle\ell|$. Since we measure only the reservoir, this does not affect the system. When averaged over all outcomes of the first measurement, the moment-generating function is

$$M(\chi,t) = \sum_\ell \mathrm{tr}_{SB}\{e^{i\chi(\hat{O}-O_\ell)}\boldsymbol{U}(t)\rho_S^0 \otimes \bar{\rho}_B{}^{(\ell)}\boldsymbol{U}^\dagger(t)\}, \tag{105}$$

where $U(t)$ is the full evolution operator in the interaction picture. This is similar to Eq. (104) but from the perspective of the system plus bath unitary dynamics. Analogously, derivatives with respect to χ generate the moments of the distribution of changes in $\hat{O}$.

We can also rewrite Eq. (105) as $M(\chi,t) = \mathrm{tr}_{SB}\rho_{SB}(\chi,t)$, where $\rho_{SB}(\chi,t) = U_{+\chi/2}(t)(\rho_0 \otimes \bar{\rho}_B)U_{-\chi/2}^\dagger(t)$

[9]One may generalize to many different jumps.

and $U_{+\chi/2}(t) = e^{+i\hat{O}\chi/2}U(t)e^{-i\hat{O}\chi/2}$. As a consequence, $\rho_{SB}(\chi,t)$ will evolve according to

$$\frac{d\boldsymbol{\rho}_{SB}(\chi,t)}{dt} = -i[\boldsymbol{H}_{\chi/2}(t)\boldsymbol{\rho}_{SB}(\chi,t) - \boldsymbol{\rho}_{SB}(\chi,t)\boldsymbol{H}_{-\chi/2}(t)], \quad (106)$$

with the tilted Hamiltonian

$$\begin{aligned}\boldsymbol{H}_{\chi/2}(t) &= e^{+i\hat{O}\chi/2}\boldsymbol{H}_{\mathbf{I}}(t)e^{-i\hat{O}\chi/2} \\ &= \sum_{\alpha}\boldsymbol{A}_{\boldsymbol{\alpha}}(t)\otimes e^{+i\hat{O}\chi/2}\boldsymbol{B}_{\boldsymbol{\alpha}}(t)e^{-i\hat{O}\chi/2}. \end{aligned} \quad (107)$$

The tools of Sec. II.C can now be employed to trace out the bath and derive a generalized QME for $\rho_S = \mathrm{tr}_B\{\cdots\}(\rho_{SB})$ that will have the form $\dot{\rho}_S = \mathcal{L}(\chi)\rho_S$. The moment-generating function will then be given by Eq. (104). Formally, $\mathcal{L}(\chi)$ looks similar to the GKSL generator derived in Sec. II.C, with the exception that the jump terms will now be given by

$$C^{\chi}_{\alpha\beta}(t_1,t_2) \equiv \mathrm{tr}\{e^{-i\hat{O}\chi/2}\boldsymbol{B}_{\alpha}(t_1)e^{+i\hat{O}\chi/2}e^{+i\hat{O}\chi/2}\boldsymbol{B}_{\beta}(t_2)e^{-i\hat{O}\chi/2}\bar{\bar{\rho}}_B\}. \quad (108)$$

In the other terms of Eq. (104) [where ρ_S appears on either the left or the right; cf. Eq. (32)], the standard correlation function (23) applies. For energy, in particular, $\hat{O} = H_B$, Eq. (108) simplifies to $C^{\chi}_{\alpha\beta}(\tau) = C_{\alpha\beta}(\tau - \chi)$.

The FCS formalism counts net transfers from the reservoir, i.e., those crossing the red long-dashed circle in Fig. 2. For the particle current, this typically coincides with the previously mentioned phenomenological replacements since typical system-reservoir couplings do not create particles. Those leaving the reservoir must enter the system, and are thus tracked using either approach. The secular approximation (which neglects the energy in the system-reservoir interaction Hamiltonian) enforces an analogous property for the energy. However, for nonsecular QMEs, the phenomenological introduction of energy counting fields is usually not obvious. In the Redfield equation (81), for instance, a microscopic derivation would yield tilted jump terms of the form $f_L(\epsilon \pm h)\hat{A}\rho_S\hat{B} \to f_L(\epsilon \pm h)\hat{A}\rho_S\hat{B}e^{-i\chi_L(\epsilon\pm h)}$ and $[1 - f_L(\epsilon \pm h)]\hat{A}\rho_S\hat{B} \to [1 - f_L(\epsilon \pm h)]\hat{A}\rho_S\hat{B}e^{+i\chi_L(\epsilon\pm h)}$, counting energies positively when they enter the left reservoir.

Finally, although we focused on QMEs, the FCS is defined via Eq. (107), and can thus be extracted from other (perturbative and nonperturbative) methods; see Schönhammer (2007), Saito and Utsumi (2008), Simine and Segal (2012), Friedman, Agarwalla, and Segal (2018), and Kilgour, Agarwalla, and Segal (2019).

3. Extracting full counting statistics

The computation of moments or cumulants is generally simpler than obtaining the full distribution (103). The kth moment $\langle n^k\rangle$ or the kth cumulant $\langle\langle n^k\rangle\rangle$ is found by differentiating the moment (cumulant) generating function $M(\chi)$ [$C(\chi)$] defined in Eq. (104), that is, $\langle n^k\rangle \equiv (-i\partial_\chi)^k M(\chi,t)|_{\chi=0}$ and $\langle\langle n^k\rangle\rangle \equiv (-i\partial_\chi)^k C(\chi,t)|_{\chi=0}$. If the steady state is unique, one may show that the long-time cumulant-generating function is given by the dominant eigenvalue of $\mathcal{L}(\chi)$ (Touchette, 2009),

$$C(\chi,t) = \ln M(\chi,t) \xrightarrow{t\to\infty} \lambda_{\mathrm{dom}}(\chi)t, \quad (109)$$

which is the eigenvalue with the largest real part. This eigenvalue obeys $\lambda_{\mathrm{dom}}(0) = 0$ and corresponds to the stationary state as $\chi \to 0$; see Sec. III.A for a discussion on the spectrum of $\mathcal{L}$. For simple systems, the eigenvalues of $\mathcal{L}(\chi)$ may be directly accessible. If not, one may perform a series expansion on the leading coefficients of the characteristic polynomial (Bruderer *et al.*, 2014; Friedman and Segal, 2019), which allows the lowest cumulants to be extracted analytically.

Often one is interested only in the first two cumulants, i.e., the average current and its fluctuations. These can be extracted without computing $C(\chi,t)$. Differentiating $M(\chi,t)$ with respect to χ and using the fact that $\mathcal{L}(0)$ is traceless, we find that the average current is

$$\begin{aligned} I(t) \equiv \frac{d}{dt}\langle\langle n\rangle\rangle_t &= -i\partial_\chi \mathrm{tr}\{\mathcal{L}(\chi)\rho(\chi,t)\}|_{\chi=0} \\ &= -i\,\mathrm{tr}\{\mathcal{L}'(0)\rho(t)\}, \end{aligned}$$

which depends only on $\rho(t)$. Similarly, the current fluctuations can be written as

$$\frac{d}{dt}\langle\langle n^2\rangle\rangle_t = -\mathrm{tr}\{\mathcal{L}''(0)\rho(t)\} - 2i\,\mathrm{tr}\{\mathcal{L}'(0)\sigma(t)\}, \quad (110)$$

where $\sigma(t) \equiv -i\partial_\chi\rho(\chi,t)/\mathrm{tr}\{\rho(\chi,t)\}|_{\chi=0}$ is an auxiliary quantity. It need not be computed via $\rho(\chi,t)$ but can be obtained by solving the differential equation

$$\dot{\sigma} = -i\mathcal{L}'(0)\rho(t) - I(t)\rho(t) + \mathcal{L}(0)\sigma(t), \quad (111)$$

with $\sigma(0) = 0$ [which implies that $\mathrm{tr}\{\sigma(t)\} = 0$]. These results can be generalized to driven systems (Benito, Niklas, and Kohler, 2016; Restrepo *et al.*, 2019). In the steady state, Eq. (111) reduces to the algebraic equation $\mathcal{L}\sigma_{ss} = i\mathcal{L}'(0)\rho_{ss} + I_{ss}\rho_{ss}$, which can be solved using standard linear algebra routines.[10]

J. Dephasing and bulk noises

Bulk noises refer to a series of methods designed to induce diffusive transport, even in noninteracting chains. In the classical literature they are usually termed self-consistent baths (Bolsterli, Rich, and Visscher, 1970), whereas in mesoscopics they are called Büttiker probes (Büttiker, 1986). The boundary-driven community usually employs the quantum information name *dephasing*. The idea is illustrated in Fig. 7: one introduces virtual reservoirs acting on all sites that are designed to inject noise without currents. The interesting physics emerging from this is reviewed in Sec. IV.E.

[10]Since $\mathcal{L}$ is not invertible, this has an infinite number of solutions, and one must pick the one satisfying $\mathrm{tr}\{\sigma(t)\} = 0$.

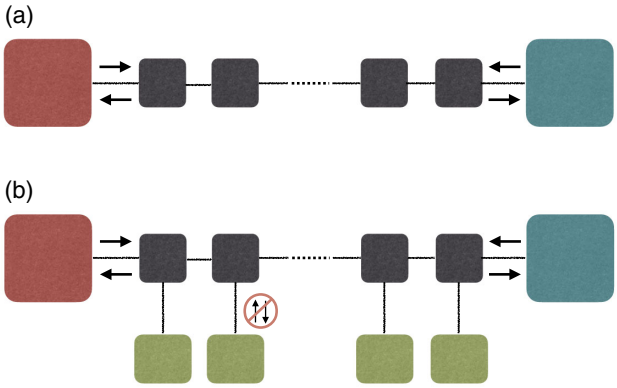

FIG. 7. Comparison between (a) a standard boundary-driven model and (b) a model involving bulk noises. In the latter, additional baths act on all sites and are adjusted so that no current flows between the bulk baths and the system.

For concreteness, consider a 1D tight-binding Hamiltonian (15) with L sites. Dephasing can be described using a dissipator of the form[11]

$$D_i^{\mathrm{deph}}(\rho_{\mathrm{S}}) = \Gamma\big(c_i^\dagger c_i \rho_{\mathrm{S}} c_i^\dagger c_i - \tfrac{1}{2}\{(c_i^\dagger c_i)^2, \rho_{\mathrm{S}}\}\big), \tag{112}$$

with rate Γ. In spin systems, the dephasing might instead be written as

$$D_i^{\mathrm{deph}}(\rho_{\mathrm{S}}) = \Gamma(\sigma_i^z \rho \sigma_i^z - \rho), \tag{113}$$

where we used $(\sigma_i^z)^2 = \mathbb{1}$. The dissipator (112) induces no particle current at the operator level, although there may still be an energy current (Mendoza-Arenas, Al-Assam *et al.*, 2013; Werlang and Valente, 2015).

The full QME for a system subject to dephasing will have the form

$$\frac{d\rho_{\mathrm{S}}}{dt} = -\mathrm{i}[H_{\mathrm{S}}, \rho_{\mathrm{S}}] + \mathcal{D}_{\mathrm{b}}(\rho_{\mathrm{S}}) + \sum_{i=1}^{L} D_i^{\mathrm{deph}}(\rho_{\mathrm{S}}), \tag{114}$$

where $\mathcal{D}_{\mathrm{b}}(\rho_{\mathrm{S}})$ refers generically to the boundary dissipators. As discussed in Sec. III.B, the effects of dephasing on the steady state are dramatic (Karevski and Platini, 2009; Asadian *et al.*, 2013; Žnidarič, 2010a). For any $\Gamma > 0$, dephasing will always lead to diffusive transport for sufficiently large chains.

Self-consistent reservoirs are an alternative to dephasing (Bolsterli, Rich, and Visscher, 1970). Instead of Eq. (112), one adds local dissipators $D_i^{\mathrm{sc}}(\rho_{\mathrm{S}}) = \Gamma(1 \pm N_i^{\mathrm{sc}})D[c_i] + \Gamma N_i^{\mathrm{sc}} D[c_i^\dagger]$, where the plus sign (the minus sign) refers to bosons (fermions). The parameters N_i^{sc} are then chosen to match the local occupation of the system $N_i^{\mathrm{sc}} = \langle c_i^\dagger c_i \rangle$ (hence the name self-consistent). This enforces zero particle current since $I_{\mathrm{i}}^{\mathrm{sc}} = \mathrm{tr}\{c_i^\dagger c_i D_i^{\mathrm{sc}}(\rho)\} = \Gamma(N_i^{\mathrm{sc}} - \langle c_i^\dagger c_i \rangle) = 0$. Although similar in spirit, the two methods are different: self-consistent baths only enforce zero current on average, while dephasing does so at the operator level. Thus, while they may predict the same steady-state currents, the steady-state density matrices will be different. For instance, in noninteracting Hamiltonians, self-consistent baths lead to Gaussian steady states, while dephasing does not (Malouf *et al.*, 2020).

K. Other heuristic methods

We discuss here two additional approaches that are employed in the literature to deal with strong-coupling, quasistatic equilibrium reservoirs (Sec. II.K.1) and multisite baths (Sec. II.K.2). Other approaches such as surrogate Hamiltonians (Baer and Kosloff, 1997; Torrontegui and Kosloff, 2016) are not discussed, as they have not yet been applied, to our knowledge, in boundary-driven systems.

1. Quasistatic equilibrium reservoirs

In most QMEs, the reservoirs are typically kept at constant equilibrium states $\bar{\rho}_{\mathrm{B}} \propto e^{-\beta(H_{\mathrm{B}} - \mu N_{\mathrm{B}})}$. We can also model *mesoreservoirs* (i.e., reservoirs of finite size that always remain close to local equilibrium) by fixing its dynamics to be of the form (Schaller, Nietner, and Brandes, 2014; Amato *et al.*, 2020)

$$\bar{\rho}_{\mathrm{B}}(t) = \frac{e^{-\beta(t)[H_{\mathrm{B}} - \mu(t) N_{\mathrm{B}}]}}{\mathrm{tr}\{e^{-\beta(t)[H_{\mathrm{B}} - \mu(t) N_{\mathrm{B}}]}\}}, \tag{115}$$

with the time-dependent parameters $\beta(t)$ and $\mu(t)$ determined from the energy and particle currents. To find these, we write the currents to the bath as $I_{\mathrm{E}}^{\mathrm{res}} \equiv (d/dt)\int \rho_{\mathrm{d}}(\omega)\omega n_{\pm}(\omega, t)d\omega$ and $I_{\mathrm{N}}^{\mathrm{res}} \equiv (d/dt)\int \rho_{\mathrm{d}}(\omega) n_{\pm}(\omega, t)d\omega$, where $\rho_{\mathrm{d}}(\omega)$ denotes the density of states of the fermionic or bosonic mesoreservoir and $n_{\pm}(\omega, t) \equiv [e^{\beta(t)[\omega - \mu(t)]} \pm 1]^{-1}$ are Fermi-Dirac or Bose-Einstein distributions, respectively. Following the chain rule, the time derivative will generate terms proportional to $\dot{\mu}$ and $\dot{\beta}$, with the prefactors interpreted as a heat capacitance and charge capacitance. Imposing energy and matter conservation, we can then equate $I_{\mathrm{E(N)}}^{\mathrm{res}}$ with minus the currents entering the system [Eq. (50)], resulting in nonlinear first-order differential equations for $\beta(t)$ and $\mu(t)$. For N mesoreservoirs this will yield $2N$ coupled equations. Solving these equations numerically thus allows one to track the evolution of quasistatic equilibrium reservoirs.

2. Multisite GKSL baths for nonintegrable spin chains

LME dissipators lack information on interactions within the system. Motivated by this, Prosen and Žnidarič (2009) considered nonintegrable spin chains where entire chunks (instead of single sites) were coupled to the baths (Fig. 8). The jump operators were chosen so as to push these chunks to specific thermal states. This cooperates with the nonintegrability of the chain, yielding an accurate model of heat transport.

[11] More generally, the term dephasing stands for a GKSL dissipator $\mathcal{D}[L]$ with a Hermitian jump operator L. Any state satisfying $[\rho_{\mathrm{S}}, L]$ will be a fixed point; states tend to destroy coherences in the eigenbasis of L while leaving the diagonal entries unchanged, thus increasing the system's entropy (Polkovnikov, 2011). Equation (112), for example, tends to destroy coherences between different positions. Using the logarithmic sum inequality, one can show that the entropy increase is monotonic.

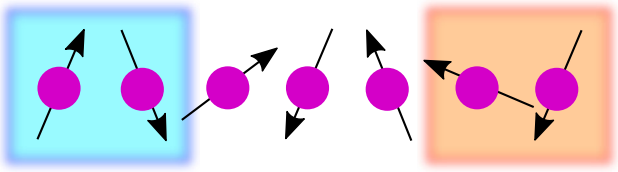

FIG. 8. Depiction of the multisite GKSL thermal baths model described in Sec. II.K.2. The last two sites at each edge are in contact with a bath that drives them toward different target states.

To better understand the idea, we focus on two-site dissipators. They can be parametrized as $\mathcal{D}(\rho)=\sum_{i,j}\gamma_{ij}[\Gamma_i\rho\Gamma_j^\dagger-(1/2)\{\Gamma_j^\dagger\Gamma_i,\rho\}]$, with jump operators Γ_j acting only on the two sites involved. For spin $1/2$ systems, the indices i and j take 16 values since, in each site, we can act with $\sigma^\pm=(\sigma^x\pm i\sigma^y)/2$, $\sigma^u=(\mathbb{1}+\sigma^z)/2$, and $\sigma^d=(\mathbb{1}-\sigma^z)/2$. The matrix γ_{ij} thus has 256 entries, which can be adjusted to impose that the fixed point of $D(\rho)$ is a thermal state ρ_T on the two sites (due to the other Hamiltonian terms, the steady state of the entire chain will generally differ). Since ρ_T only has 16 entries, there is significant freedom in choosing γ_{ij}. Prosen and Žnidarič (2009) chose them so that all excited modes decayed at the same rate. Palmero *et al.* (2019) chose rates satisfying detailed balance, which improves the performance by producing states closer to the thermal one at lower temperatures. An extension to baths coupling to more than two sites was studied by Guimarães, de Oliveira, and Landi (2016).

The target state $\rho_T\propto e^{-\beta_T H_\mathrm{T}}$ is determined by β_T and the target Hamiltonian H_T, for which two choices have been considered. Mendoza-Arenas, Clark, and Jaksch (2015) took H_T as the reduced Hamiltonian of the two sites, including their interactions, but neglected any couplings to other sites. Alternatively, Žnidarič *et al.* (2010), Žnidarič (2011c), and Mendoza-Arenas *et al.* (2019) took ρ_T as the reduced density matrix of the two sites if the entire chain was in equilibrium: $\rho_T\propto \mathrm{tr}_{3,\ldots,L}\{\exp[-\beta(H_\mathrm{S}-\mu M)]\}$, where μ is the chemical potential and M is the total magnetization.

To evaluate the consistency of the method, one may couple the chain to only one dissipator, or to two at the same temperature, and check to see whether the steady state behaves like a thermal state The first thing to point out is that ρ_{ss} does not typically approach a thermal state at β_T, but rather at some other $\beta_\mathrm{S}<\beta_T$. If β_T is small enough, the system will thus approach the thermal state $\propto\exp(-\beta_\mathrm{S}H_\mathrm{S})$. One can then compute expectation values $\langle O\rangle_S$ of different observables and determine whether they are consistent with those at the corresponding thermal state $\langle O\rangle_{\beta_\mathrm{S}}$. This defines an effective temperature β_O for each O. If ρ_S indeed approaches a thermal state, then β_O will be the same for all observables. Using this criterion, Žnidarič (2011c) and Palmero *et al.* (2019) found that the dispersion in β_O's was smaller at high temperatures, and when they had smaller support (such as one-site observables rather than two-site ones).

One may also consider the trace distance [Eq. (82)] between the reduced density matrix of a portion of ρ_{ss} and that of the same portion in a thermal state (Mendoza-Arenas, Clark, and Jaksch, 2015; Zanoci and Swingle, 2021). This measure is meaningful since it bounds the differences between expectation values of any operator with finite eigenvalues (Mendoza-Arenas, Clark, and Jaksch, 2015).

This methodology can be implemented with tensor networks (Prosen and Žnidarič, 2009; Žnidarič *et al.*, 2010; Žnidarič, 2011c; Mendoza-Arenas, Clark, and Jaksch, 2015; Mendoza-Arenas *et al.*, 2019; Palmero *et al.*, 2019) (Sec. III.E), resulting in an effective approach for studying heat transport in a strongly interacting quantum system. This has been used to study transport in chains, with and without disorder, which we review in Sec. IV. For instance, Fig. 12(b) was obtained with this tool. The method is accurate only at relatively large temperatures. However, in this regime and for large strongly correlated systems, it is more efficient than other methods like GMEs or LMEs. The former requires H_S to be diagonalized and the latter does not faithfully represent thermal baths at strong coupling. Multisite baths also require a smaller number of sites than a thermofield plus star-to-chain mapping (Sec. II.H.2).

III. METHODS FOR BOUNDARY-DRIVEN OPEN SYSTEMS

This section provides methods specifically designed for boundary-driven problems. We do not review methods designed for open quantum systems but which have not been applied to boundary-driven problems. These include variational and cluster mean-field methods (Weimer, 2015; Jin *et al.*, 2016), quantum Monte Carlo methods (Nagy and Savona, 2018), corner-space renormalization (Finazzi *et al.*, 2015), and neural-network *Ansätze* (Hartmann and Carleo, 2019; Nagy and Savona, 2019; Vicentini *et al.*, 2019; Yoshioka and Hamazaki, 2019; Luo *et al.*, 2020). We also do not discuss microscopically exact approaches like nonequilibrium Green's functions (Caroli *et al.*, 1971; Meir and Wingreen, 1992; Economou, 2006; Haug and Jauho, 2008; Prociuk, Phillips, and Dunietz, 2010; Aeberhard, 2011; Zimbovskaya and Pederson, 2011; Dhar, Saito, and Hänggi, 2012; Nikolić *et al.*, 2012; Wang, Agarwalla, and Thingna, 2014), hierarchies of equations of motion (Tanimura and Kubo, 1989; Tanimura, 1990), or path integrals (Aleiner, Brouwer, and Glazman, 2002; Mühlbacher and Rabani, 2008; Segal, Millis, and Reichman, 2010; Hützen *et al.*, 2012).

A. Vectorization

Irrespective of the type of system-bath interaction, many boundary-driven problems are described by linear time-local evolution equations of the form

$$\frac{d\rho}{dt}=\mathcal{L}(\rho), \tag{116}$$

where $\mathcal{L}$, called the Liouvillian, is a linear superoperator. Since ρ is an operator, $\mathcal{L}(\rho)$ will involve left and right multiplication. Notwithstanding, Eq. (116) is in the exact same spirit as a linear matrix-vector equation like $dx/dt=Ax$.

Since matrix-vector equations are standard in scientific computing, it is often convenient to recast Eq. (116) in this

form. This can be done by introducing a *vectorization* operation that maps a matrix M onto a vector $\mathrm{vec}(M) \equiv \vec{M}$ (the two notations are used interchangeably) by stacking the columns (Turkington, 2013), e.g.,

$$\mathrm{vec}\begin{pmatrix} a & b \\ c & d \end{pmatrix} = \begin{pmatrix} a \\ c \\ b \\ d \end{pmatrix}. \tag{117}$$

The most important property of vectorization is the following: Given arbitrary matrices A, B, and C, one obtains[12]

$$\mathrm{vec}(ABC) = (C^{\mathrm{T}} \otimes A)\mathrm{vec}(B). \tag{118}$$

Equation (118) allows us to write the superoperator $\mathcal{L}$ as a matrix $\hat{\mathcal{L}}$, and hence recast Eq. (116) as

$$\frac{d\vec{\rho}}{dt} = \hat{\mathcal{L}}\,\vec{\rho}\,. \tag{119}$$

For example, take $\mathcal{L}(\rho) = -\mathrm{i}[H,\rho] + \sum_k D[L_k](\rho)$. Terms such as $H\rho$ can be written as $H\rho\mathbb{1}$ so that $\mathrm{vec}(H\rho) = (\mathbb{1} \otimes H)\vec{\rho}$. Proceeding similarly with the other terms yields the vectorized Liouvillian

$$\hat{\mathcal{L}} = -\mathrm{i}(\mathbb{1} \otimes H - H^{\mathrm{T}} \otimes \mathbb{1}) + \sum_k \left[L_k^* \otimes L_k - \frac{1}{2}\mathbb{1} \otimes L_k^\dagger L_k - \frac{1}{2}(L_k^\dagger L_k)^{\mathrm{T}} \otimes \mathbb{1} \right], \tag{120}$$

which is now a matrix of dimension $d^2 \times d^2$ instead of a superoperator.

Vectorization can also be viewed as the operation taking

$$|i\rangle\langle j| \to |j\rangle \otimes |i\rangle, \tag{121}$$

which is known as the Choi-Jamiolkowski isomorphism (Jamiolkowski, 1972; Choi, 1975). As a consequence, a d-dimensional density matrix $\rho = \sum_{ij}\rho_{ij}|i\rangle\langle j|$ is vectorized to $\mathrm{vec}(\rho) = \sum_{ij}\rho_{ij}|j\rangle \otimes |i\rangle$, with length d^2. The inner product between two vectorized operators is related to the Hilbert-Schmidt inner product

$$\mathrm{vec}(A)^\dagger \mathrm{vec}(B) = \mathrm{tr}(A^\dagger B). \tag{122}$$

Accordingly, the normalization condition $\mathrm{tr}(\rho) = 1$ is mapped onto $\mathrm{vec}(\mathbb{1})^\dagger \mathrm{vec}(\rho) = 1$, where $\mathrm{vec}(\mathbb{1}) = \sum_i |i\rangle \otimes |i\rangle$ is the vectorized identity.

1. Spectral properties of the Liouvillian

Vectorization converts the master equation (116) into the standard matrix-vector equation (119) for $\vec{\rho}$. The formal solution is then simply

$$\vec{\rho}(t) = e^{\hat{\mathcal{L}}t}\vec{\rho}(0), \tag{123}$$

which leads to the problem of computing the exponential of the non-Hermitian matrix $\hat{\mathcal{L}}$. To gain some intuition, we first assume that $\hat{\mathcal{L}}$ is diagonalizable. Being non-Hermitian, however, it will have different right and left eigenvectors $\vec{x}_\alpha$ and $\vec{y}_\alpha$,

$$\hat{\mathcal{L}}\vec{x}_\alpha = \lambda_\alpha \vec{x}_\alpha, \qquad \vec{y}_\alpha^\dagger \hat{\mathcal{L}} = \lambda_\alpha \vec{y}_\alpha^\dagger, \tag{124}$$

associated with the eigenvalue λ_α [sometimes called *rapidities* (Kimura, Ajisaka, and Watanabe, 2017)]. If S is a matrix with columns $\vec{x}_\alpha$, then $\vec{y}_\alpha^\dagger$ are the rows of S^{-1}. Hence, $\vec{y}_\alpha^\dagger \vec{x}_{\alpha'} = \delta_{\alpha,\alpha'}$ and

$$\hat{\mathcal{L}} = \sum_\alpha \lambda_\alpha \vec{x}_\alpha \vec{y}_\alpha^\dagger = S\Lambda S^{-1}, \tag{125}$$

where $\Lambda = \mathrm{diag}(\lambda_1, \lambda_2, \ldots)$. The rapidities λ_α are in general complex. In particular, for GKSL generators $\hat{\mathcal{L}}$ one finds that they have nonpositive real parts (indicating a decay toward the steady state) and come in complex conjugate pairs (if λ_α is an eigenvalue, then so is λ_α^*) (Albert and Jiang, 2014). In fact, the pairing is a necessary condition for $\vec{\rho}(t)$ to be Hermitian at all t.

The steady state ρ_{ss} is the fixed point of Eq. (119):

$$\hat{\mathcal{L}}\vec{\rho}_{\mathrm{ss}} = 0. \tag{126}$$

As Evans (1977), Frigerio (1978), Evans and Hanche-Olsen (1979), and Baumgartner and Narnhofer (2008) showed, GKSL equations always have at least one fixed point ρ_{ss}. However, if some rapidity is purely imaginary, the system may never relax toward it, but will instead oscillate indefinitely in a dark subspace (D'Abbruzzo and Rossini, 2021; Buča, Booker, and Jaksch, 2022). Moreover, ρ_{ss} may not be unique (Schaller, Kießlich, and Brandes, 2010; Buča and Prosen, 2012; Manzano and Hurtado, 2014; Buča, Tindall, and Jaksch, 2019; Thingna and Manzano, 2021), although this is often the case (Evans, 1977; Nigro, 2019).

For concreteness, we henceforth assume that ρ_{ss} is unique. Equation (126) then shows that $\vec{\rho}_{\mathrm{ss}} = \vec{x}_0$ is the right eigenvector of $\hat{\mathcal{L}}$ with eigenvalue $\lambda_0 = 0$. In addition, since the dynamics is trace preserving, it must also follow that $\mathrm{vec}(\mathbb{1})^\dagger \hat{\mathcal{L}} = 0$. Thus, $\mathrm{vec}(\mathbb{1}) = \vec{y}_0$ is the left eigenvector of $\hat{\mathcal{L}}$ with eigenvalue $\lambda_0 = 0$. Assuming that Eq. (125) holds, one may write[13] $e^{\hat{\mathcal{L}}t} = \sum_\alpha e^{\lambda_\alpha t}\vec{x}_\alpha \vec{y}_\alpha^\dagger$, so Eq. (123) becomes

$$\vec{\rho}_t = \sum_\alpha c_\alpha e^{\lambda_\alpha t}\vec{x}_\alpha, \tag{127}$$

[12] If one defines vectorization by stacking rows instead of columns, then one should use instead $\mathrm{vec}(ABC) = (A \otimes C^{\mathrm{T}})\mathrm{vec}(B)$.

[13] If $\hat{\mathcal{L}}$ is not diagonalizable, we instead get $e^{\hat{\mathcal{L}}t} = \sum_\alpha e^{\lambda_\alpha t} \times (\sum_{k=0}^{N_\alpha - 1} t^k \mathcal{A}_{\alpha k})$, where N_α denotes the multiplicity of eigenvalue λ_α and $\mathcal{A}_{\alpha k}$ are unknown matrices that follow from the Jordan-block decomposition of $\hat{\mathcal{L}}$. They can be determined by differentiating both sides of this equation, which generates a set of equations for jointly determining λ_α and $\mathcal{A}_{\alpha k}$.

where $c_\alpha = \vec{y}_\alpha^\dagger \vec{\rho}_0$ is determined by the initial conditions. The evolution will thus be a linear combination of the right eigenvectors $\vec{x}_\alpha$, each with weight c_α and evolving in time with an exponential dependence $e^{\lambda_\alpha t}$. The spectral properties thus allow us to classify the decay modes α into oscillatory [$\mathrm{Re}(\lambda_\alpha) = 0$], purely decaying [$\mathrm{Im}(\lambda_\alpha) = 0$], decaying spirals [$\mathrm{Re}(\lambda_\alpha) < 0$ and $\mathrm{Im}(\lambda_\alpha) \neq 0$], and steady states ($\lambda_\alpha = 0$) (Albert and Jiang, 2014).

We can single out $\lambda_0 = 0$ in Eq. (127). Owing to normalization, $c_0 = \mathrm{tr}\{\rho_0\} = 1$, so

$$\vec{\rho}_t = \vec{\rho}_{\mathrm{ss}} + \sum_{\alpha \neq 0} e^{\lambda_\alpha t} c_\alpha \vec{x}_\alpha. \tag{128}$$

If $\mathrm{Re}(\lambda_\alpha) < 0$ for all $\alpha \neq 0$, the system will always relax to ρ_{ss} as $t \to \infty$ for any initial condition.

The full Liouvillian spectrum can be computed in the case of pure loss models (Torres, 2014; Nakagawa, Kawakami, and Ueda, 2021) and was used by Buča *et al.* (2020) to study the Liouvillian spectrum of the *XXZ* Hamiltonian under pure loss processes. Similar methods were used by Medvedyeva, Essler, and Prosen (2016), Essler and Piroli (2020), and Ziolkowska and Essler (2020) to study models in the presence of bulk noises (Sec. II.J).

The computation of the steady state [Eq. (126)] is equivalent to finding the eigenvector of $\hat{\mathcal{L}}$ with a zero eigenvalue. As this is much simpler for Hermitian problems, Cui, Cirac, and Bañuls (2015) introduced a workaround by instead solving

$$\hat{\mathcal{L}}^\dagger \hat{\mathcal{L}} \vec{\rho}_{\mathrm{ss}} = 0. \tag{129}$$

The eigenvectors of $\hat{\mathcal{L}}^\dagger \hat{\mathcal{L}}$ are different from those of $\hat{\mathcal{L}}$, but the one with $\lambda_\alpha = 0$ is the same since $\hat{\mathcal{L}} \vec{\rho}_{\mathrm{ss}} = 0$ implies that $\hat{\mathcal{L}}^\dagger \hat{\mathcal{L}} \vec{\rho}_{\mathrm{ss}} = 0$. The advantage is that $\hat{\mathcal{L}}^\dagger \hat{\mathcal{L}}$ is also positive semidefinite. This is thus a variational problem, where one searches for the eigenvector of the "effective Hamiltonian" $\hat{\mathcal{L}}^\dagger \hat{\mathcal{L}}$ with the smallest eigenvalue. Unlike in the standard variational principle, here the smallest eigenvalue is explicitly known $\lambda_\alpha = 0$, such that the distance from zero can be used as a measure of convergence.

This method is particularly useful when implemented with a tensor network (Sec. III.E). There are, however, two main disadvantages: First, even if $\hat{\mathcal{L}}$ is local (as in nearest-neighbor interactions), $\hat{\mathcal{L}}^\dagger \hat{\mathcal{L}}$ will in general be nonlocal (Gangat, I, and Kao, 2017). Second, $\hat{\mathcal{L}}^\dagger \hat{\mathcal{L}}$ is often ill conditioned. In fact, if the relaxation gap of $\hat{\mathcal{L}}$ is λ_1, the first excited state of $\hat{\mathcal{L}}^\dagger \hat{\mathcal{L}}$ is $\sim |\lambda_1|^2$, which can be extremely small.

Inverting a matrix is typically a lot simpler than exponentiating it. For this reason, Laplace-transform methods can often provide a convenient advantage. Laplace transforming Eq. (119) leads to $\vec{\rho}(z) = (z - \hat{\mathcal{L}})^{-1} \vec{\rho}(0)$, which has poles at precisely $z_\alpha = \lambda_\alpha$. Steady-state expectation values can be obtained via the final value theorem,

$$\langle A \rangle_{\mathrm{ss}} \equiv \lim_{t \to \infty} \mathrm{tr}\{A \rho(t)\} = \lim_{z \to 0} z\, \mathrm{vec}(\mathbb{1})^\dagger [(A^{\mathrm{T}} \otimes \mathbb{1})(z - \hat{\mathcal{L}})^{-1}] \vec{\rho}(0).$$

In addition, if one can decompose the Liouvillian $\hat{\mathcal{L}} = \hat{\mathcal{L}}_0 + \hat{\mathcal{L}}_1$ into a simple part $\hat{\mathcal{L}}_0$ and a perturbation $\hat{\mathcal{L}}_1$, it is possible to set up a series expansion of the solution as $(z - \hat{\mathcal{L}})^{-1} = \sum_{n=0}^{\infty} [\mathcal{P}_0(z) \hat{\mathcal{L}}_1]^n \mathcal{P}_0(z)$, where $\mathcal{P}_0(z) = (z - \hat{\mathcal{L}}_0)^{-1}$. This is the analog of Eq. (101) in the z domain. When the structure of $\hat{\mathcal{L}}_0$ is simple, it is often possible to transform the solutions back to the time domain. Other perturbative methods are reviewed in Sec. III.D.

The vectorization recipe of Eqs. (117) and (121) chooses a specific basis to represent $\hat{\mathcal{L}}$ and other operators. For instance, in the case of 2×2 matrices this basis is

$$q_1 = \begin{pmatrix} 1 & 0 \\ 0 & 0 \end{pmatrix}, \qquad q_2 = \begin{pmatrix} 0 & 0 \\ 1 & 0 \end{pmatrix},$$
$$q_3 = \begin{pmatrix} 0 & 1 \\ 0 & 0 \end{pmatrix}, \qquad q_4 = \begin{pmatrix} 0 & 0 \\ 0 & 1 \end{pmatrix},$$

which, when vectorized, leads to the four basis vectors $\vec{q}_1 = (1,0,0,0)$, $\vec{q}_2 = (0,1,0,0)$, etc. With the inner product [Eq. (122)], however, one may generalize this for arbitrary bases of operators. For instance, another natural choice involves the Pauli matrices (supplemented by 1), which are orthogonal with respect to Eq. (122) (but not orthonormal). It can also be useful to split populations (diagonals) and coherences (off-diagonals) in some chosen basis, such as in models where their evolutions are decoupled. Given a set of orthogonal matrices $\{q_i\}$, the Liouvillian can always be written as

$$\hat{\mathcal{L}} = \sum_{ij} \mathcal{L}_{ij} \vec{q}_i \vec{q}_j^\dagger, \qquad \mathcal{L}_{ij} = \frac{\mathrm{tr}\{q_i^\dagger \mathcal{L}(q_j)\}}{\mathrm{tr}(q_i^\dagger q_i)\mathrm{tr}(q_j^\dagger q_j)}. \tag{130}$$

For spin chains, a natural choice of basis is the set of tensor products $\sigma^{i_1} \otimes \sigma^{i_2} \otimes \cdots \otimes \sigma^{i_N}$ with $i_n \in \{0, x, y, z\}$. In this case, one also has the freedom of choosing how to order the corresponding vectorized space. In fact, the standard vectorization recipe in Eq. (121) is not good, as it leads to long-range interactions. Alternative orderings were discussed by Casagrande, Poletti, and Landi (2021) and may lead to significant numerical advantages in tensor network simulations (Sec. III.E).

2. Symmetries

Symmetries can significantly reduce the vector space of a computation. For instance, in the unitary (Hamiltonian) dynamics of a spin chain with number conservation, such as the *XXZ* model with L spins [Eq. (12)], one does not need to store 2^L entries, but instead only $\binom{L}{N_u} = L!/[N_u!(L - N_u)!]$, where N_u is the number of spins up. As discussed by Buča and Prosen (2012) for GKSL QMEs, there are two main types of symmetries. A "weak" symmetry is a unitary S obeying

$$S \mathcal{L}(\rho) S^\dagger = \mathcal{L}(S \rho S^\dagger). \tag{131}$$

Conversely, a "strong" symmetry is one in which

$$[S,H]=0, \qquad [S,L_k]=0, \tag{132}$$

where H is the Hamiltonian and L_k are the jump operators. Strong symmetries imply the weak one. As Buča and Prosen (2012) showed, for the strong symmetry there is at least one steady state for each symmetry sector. The evolution of elements within a symmetry sector always remain in that sector, allowing simulations to be performed with a smaller vector space. For instance, if both the Hamiltonian and jump operators preserve the total magnetization (such as an XXZ chain with dephasing), there is a strong symmetry and hence multiple steady states. The dynamics within a subspace with N_u spins up is then represented by a density matrix with $\{(L!)/[N_u!(L-N_u)!]\}^2$ elements, as in the unitary case.

Typically, however, the total magnetization or the total number of particles is not conserved due to the dissipators at the boundaries; cf. Eq. (17a). In this case, only a weak symmetry applies and the steady state is unique. If one is interested solely in $\rho_{\rm ss}$, it may suffice to study much smaller matrices. To see why, consider the XXZ chain under the LME (17a). Instead of using the Pauli basis $|\sigma_1,\ldots,\sigma_L\rangle$, we bundle the states in the form $|\vec{m}_M,M\rangle$, where M is the total magnetization and $\vec{m}_M$ labels all states with magnetization M. We can then decompose

$$\rho=\sum_{M,M'}\sum_{\vec{m}_M,\vec{m}'_{M'}}\rho_{M,M'}^{\vec{m}_M,\vec{m}'_{M'}}|\vec{m}_M,M\rangle\langle\vec{m}'_{M'},M'|. \tag{133}$$

Terms such as $\sigma_i^-\rho\sigma_i^+$ will generate transitions between different M and M'. But they do so by the same amount, i.e., $M\to M-1$ and $M'\to M'-1$. The difference $M-M'$ is hence preserved, which defines the different symmetry sectors. Furthermore, if $\rho_{\rm ss}$ is unique, it must belong to a sector with $M-M'=0$ since these are the only ones with unit trace. Hence, $\rho_{\rm ss}$ lives in a space with dimension $(2L)!/[(L)!(L)!]$. Works relying heavily on symmetries were given by Žnidarič (2013a, 2013b), Guo and Poletti (2017a, 2019), Sá, Ribeiro, and Prosen (2020a), and Lee *et al.* (2022). Some properties of the emerging currents are discussed in Sec. IV. Another example, which can help to build some intuition, is superradiant decay and other Dicke-like collective processes (Gross and Haroche, 1982; Garraway, 2011), where it is much more convenient to use the large-spin representation instead of local Pauli matrices.

B. Noninteracting systems and Lyapunov equation

We consider here a generic fermionic or bosonic system with L sites and annihilation operators a_i. The enormous complexity of boundary-driven systems lies in the exponentially large Hilbert space dimension. In some cases, however, the full dynamics is captured entirely by pairwise correlations such as $\langle a_j^\dagger a_i\rangle$. This will be the case for QMEs such as Eq. (11), where the Hamiltonian is at most quadratic in a_i and $a_i^\dagger$, and the jump operators are at most linear. Systems of this form are said to be *Gaussian*, or *noninteracting*. It is convenient to organize the correlations into an $L\times L$ covariance matrix[14]

$$C_{ij}=\langle a_j^\dagger a_i\rangle-\langle a_j^\dagger\rangle\langle a_i\rangle, \tag{134}$$

where the choice of ordering $a_j^\dagger a_i$, instead of $a_i^\dagger a_j$, is to simplify subsequent calculations. In some cases, a more general definition that includes terms such as $\langle a_i a_j\rangle$ is necessary. This is further discussed later. When the Hamiltonian is quadratic and the jump operators are linear, C will satisfy the Lyapunov equation

$$\frac{dC}{dt}=-(WC+CW^\dagger)+D, \tag{135}$$

where W and D are matrices that depend on the parameters of the QME (see the following example). The solution is

$$C(t)=e^{-Wt}C(0)e^{-W^\dagger t}+\int_0^1 dt'\,e^{-W(t-t')}De^{-W^\dagger(t-t')}. \tag{136}$$

Convergence to a steady state will thus depend on whether the eigenvalues of W have positive real parts. When this is the case, the steady state will satisfy

$$WC+CW^\dagger=D. \tag{137}$$

Routines for solving Eq. (137) can be found in most scientific computing libraries, allowing one to study sizes as large as $L=10\,000$ (Bartels and Stewart, 1972; Golub, Nash, and Van Loan, 1979).

The Lyapunov equation is not restricted to GKSL dynamics, as it also appears in other noninteracting open systems (Purkayastha, 2022). For example, consider a tight-binding Hamiltonian $H_{\rm S}=\sum_{ij}h_{ij}a_i^\dagger a_j$ evolving according to the following GKSL master equation:

$$\frac{d\rho_{\rm S}}{dt}=-\mathrm{i}[H_{\rm S},\rho_{\rm S}]+\sum_{i,j}\gamma_{ji}^-\left[a_i\rho_{\rm S}a_j^\dagger-\frac{1}{2}\{a_j^\dagger a_i,\rho_{\rm S}\}\right]+\gamma_{ij}^+\left[a_i^\dagger\rho_{\rm S}a_j-\frac{1}{2}\{a_ja_i^\dagger,\rho_{\rm S}\}\right] \tag{138}$$

for Hermitian positive semidefinite matrices γ^+ and γ^-, with entries γ_{ij}^+ and γ_{ij}^- (mind the reverse ordering of the indices in γ^-). To derive the Lyapunov equation it suffices to assume that $\langle a_i\rangle=0$ since the form of the final result will not be affected by this term. We thus write $dC_{ij}/dt=\mathrm{tr}\{a_j^\dagger a_i d\rho_{\rm S}/dt\}$ and use Eq. (138), together with the fermionic or bosonic algebras. As a result, we precisely find Eq. (135), with

$$W=\mathrm{i}h+(\gamma^-\pm\gamma^+)/2, \qquad D=\gamma^+, \tag{139}$$

[14]Gaussian states (assuming that $\langle a_i\rangle=0$) have the form $\rho=e^{-\sum_{ij}M_{ij}a_i^\dagger a_j}/Z$, where M is a matrix related to C by $C=(e^M\pm1)^{-1}$ for fermions and bosons, respectively. Moreover, $Z=\det(1\pm e^{-M})^{\pm1}$.

where the upper sign is for fermions and the lower sign is for bosons. In LMEs, $\gamma^{\pm}$ are diagonal (Sec. II.C.4): For fermions, $\gamma^{+}_{ii} = \gamma_i f_i$ and $\gamma^{-}_{ii} = \gamma_i(1-f_i)$, with f_i the Fermi-Dirac distributions. For bosons, one instead has $\gamma^{+}_{ii} = \gamma_i N_i$ and $\gamma^{-}_{ii} = \gamma_i(1+N_i)$, where N_i are now the Bose-Einstein distributions. The Lyapunov matrices therefore become identical for fermions and bosons: $W = \mathrm{i}h + \gamma/2$ and $D_{ii} = \gamma_i n_i$, with n_i either f_i or N_i, and $\gamma = \mathrm{diag}(\gamma_i)$.

Next suppose that one has only nearest-neighbor hopping in H_{S}, such that $h_{ii} = \epsilon$ and $h_{i,i\pm1} = -J$; cf. Eq. (15). Moreover, suppose that the system is coupled to two LME baths in the first and last sites, with equal coupling strengths γ, but different n_1 and n_L. As Karevski and Platini (2009), Žnidarič (2010b), and Asadian *et al.* (2013) showed, the solution of Eq. (135) will be a Toeplitz matrix with diagonals $\langle a_j^{\dagger} a_j\rangle = (n_1+n_L)/2 + (\gamma/2J)x(\delta_{j,L} - \delta_{j,1})$ and a constant first off-diagonal $\langle a_{j+1}^{\dagger} a_j\rangle = \mathrm{i}x$, where $x = \gamma J(n_L - n_1)/(\gamma^2 + 4J^2)$ (with all other entries being zero). The current between sites i and $i+1$ is $I_{\mathrm{N}} = \mathrm{i}J\langle a_{i+1}^{\dagger} a_i - a_i^{\dagger} a_{i+1}\rangle = 2x$. This is the solution discussed in Sec. II.B that provides the prototypical example of ballistic transport, where I_{N} is independent of L and the occupations are uniform along the chain, except in the first and last sites.

The previous example led to a closed set of equations for C_{ij}. This is no longer the case when the Hamiltonian contains pairing or squeezing terms $a_i^{\dagger} a_j^{\dagger}$, or when the dissipators contain terms such as $a_i^{\dagger}\rho_{\mathrm{S}} a_j^{\dagger}$ and $a_i \rho_{\mathrm{S}} a_j$. Examples include the XY spin chain and squeezed baths, respectively. In these cases one may instead use Majorana or quadrature operators $q_i = a_i + a_i^{\dagger}$ and $p_i = \mathrm{i}(a_i^{\dagger} - a_i)$ and define a new $2L \times 2L$ covariance matrix $\Theta_{ij} = (1/2)\langle\{X_i, X_j\}\} - \langle X_i\rangle\langle X_j\rangle$, where $\boldsymbol{X} = (q_1, \ldots, q_L, p_1, \ldots, p_L)$. This will follow a Lyapunov equation of the same form as Eq. (135), but with new matrices W and D of size $2L$ (Barthel and Zhang, 2022).

Next we turn to the somewhat peculiar case of dephasing [Eq. (112)], which is defined by jump operators $L_i = a_i^{\dagger} a_i$. Since they are not linear, the dynamics will not be Gaussian, and one expects the equation for C (or Θ) to no longer be closed (i.e., to depend on higher-order moments). For dephasing, however, it turns out that the equations close. In fact, one may readily verify that $\sum_{\ell} \mathrm{tr}\{a_j^{\dagger} a_i D_{\ell}^{\mathrm{deph}}(\rho_{\mathrm{S}})\} = -C_{ij}(1-\delta_{ij})$, which depends only on C. Dephasing thus causes the off-diagonal elements to decay while keeping the diagonal ones intact. Next suppose that we append to Eq. (138) a set of dephasing baths on all sites $\sum_i \Gamma D[a_i^{\dagger} a_i]$ of strength Γ. The resulting equation for C is then given by (Žnidarič, 2010a, 2011a; Asadian *et al.*, 2013; Malouf *et al.*, 2020)

$$\frac{dC}{dt} = -(WC + CW^{\dagger}) + D - 2\Gamma\Delta(C), \tag{140}$$

where $\Delta(C) = C - \mathrm{diag}(C_{11}, \ldots, C_{LL})$ is the off-diagonal part of C.

Owing to this new element, Eq. (140) is no longer a Lyapunov equation, although it is still a closed set of linear equations for C (and hence still tractable). A proposal to simulate this dynamics in trapped ions was put forth by Bermudez, Bruderer, and Plenio (2013).

The solution for a uniform tight-binding chain can also be obtained analytically when dephasing is present (Žnidarič, 2010a; Asadian *et al.*, 2013). The resulting current is

$$I_{\mathrm{N}} = \frac{2\gamma J}{4J^2 + \gamma^2 + 2\gamma\Gamma(L-1)}(n_L - n_1), \tag{141}$$

which now depends on L. In fact, for any $\Gamma \neq 0$, there is always a sufficiently large size for which $I_{\mathrm{N}} \sim 1/L$. Dephasing therefore renders the transport diffusive for any $\Gamma > 0$. The occupations $\langle a_i^{\dagger} a_i\rangle$ are also modified and vary linearly between n_1 and n_L.

C. Third quantization

This section combines concepts from Secs. III.A and III.B. Equation (118) illustrates how vectorized operators such as $\hat{\mathcal{L}}$ live in a doubled Hilbert space. This is also clear from the Choi-Jamiolkowski isomorphism in Eq. (121). Consider for concreteness a system composed of bosons with operators a_i. Equation (118) then implies that $\mathrm{vec}(a_i\rho) = (\mathbb{1} \otimes a_i)\mathrm{vec}(\rho)$ and $\mathrm{vec}(\rho a_i) = (a_i^{\mathrm{T}} \otimes \mathbb{1})\mathrm{vec}(\rho)$. In the vectorized space, we therefore end up with two species of particles, the "left-multiplying kind" and the "right-multiplying kind." That is, we can define $b_i = \mathbb{1} \otimes a_i$ and $c_i = a_i \otimes \mathbb{1}$, and therefore establish the mappings $(a_i \bullet) \to b_i$ and $(\bullet a_i) \to c_i^{\dagger}$. The problem has thus been recast into a doubled Hilbert space inhabited by two bosonic species. For fermions this recipe also works, but some subtleties arise; see Prosen (2008) for details.

This is the idea behind "third quantization," which was introduced by Prosen (2008) and built upon by Prosen and Seligman (2010), Prosen and Žunkovič (2010), Banchi, Giorda, and Zanardi (2014), Guo and Poletti (2017b, 2018), Prosen (2010), and Yamanaka and Sasamoto (2021). It is equivalent to the superfermion approach taken by Dzhioev and Kosov (2011), although the latter requires only matrices of size $2L$, not $4L$.

The situation simplifies when H_{S} is at most quadratic in the a_i and the jump operators L_k are at most linear (Sec. III.B). In this case, Eq. (120) becomes a quadratic form in the new set of $4L$ operators $\boldsymbol{d} = (b_1, b_1^{\dagger}, c_1, c_1^{\dagger}, , \ldots, b_L, b_L^{\dagger}, c_L, c_L^{\dagger})$:

$$\hat{\mathcal{L}} = \sum_{\mu,\nu=1}^{4L} \Lambda_{\mu\nu} d_{\mu}^{\dagger} d_{\nu}, \tag{142}$$

with a $4L \times 4L$ matrix of coefficients $\Lambda_{\mu\nu}$. For instance, the master equation (138) can be rewritten as $\hat{\mathcal{L}} = -\sum_{ij}(W_{ij} b_i^{\dagger} b_j + W_{ij}^{\dagger} c_i^{\dagger} c_j) + \sum_{ij}(\gamma_{ij}^{-} c_i b_j + \gamma_{ij}^{+} c_j^{\dagger} b_i^{\dagger})$, where W is as defined after Eq. (135).

Third quantization generalizes the Lyapunov equation (135). If one is interested only in the covariance matrix and currents, then Eq. (135) suffices. However, with Eq. (142) one now has access to the full quadratic Liouvillian, and therefore to its entire spectrum. In fact, as Prosen (2008) showed, Eq. (142) can always be put in diagonal form, as

$\hat{\mathcal{L}} = -2\sum_{k=1}^{2L}\lambda_k f'_k f_k$, where f_k and f'_k are normal modes of the Liouvillian that, respectively, annihilate and create a particle in mode k (since $\hat{\mathcal{L}}$ is not Hermitian, $f'_k \neq f_k^\dagger$). In turn, the c-number quantities λ_k are the rapidities in Eq. (125). For tight-binding Hamiltonians or local boundary drives, their computation can simplify considerably and may even allow for solutions in closed form (Yueh, 2005; Kouachi, 2006; Willms, 2008; Da Fonseca and Kowalenko, 2020).

D. Perturbative approaches

It is often impossible to find the steady state analytically [Eq. (116)], but it may be possible to gain important insights using Liouvillian perturbation theory. Consider a Liouvillian of the form $\mathcal{L} = \mathcal{L}_0 + \mu\mathcal{L}_1$, where μ is a small parameter and $\mathcal{L}_0$ and $\mathcal{L}_1$ are in GKSL form. We decompose ρ_S in a power series in μ as $\rho_S = \sum_i \mu^i \rho_i$. The steady-state equation $\mathcal{L}(\rho_S) = 0$ then results in a set of recurrence relations $\mathcal{L}_0(\rho_0) = 0$ and $\mathcal{L}_0(\rho_n) = -\mathcal{L}_1(\rho_{n-1})$ for $n \geq 1$, which can be solved sequentially; see Michel, Gemmer, and Mahler (2004), Lenarčič and Prosen (2015), and Žnidarič (2019). This approach is particularly relevant for boundary-driven problems where the bath couplings are the perturbation.

In some cases the steady state ρ_0 of $\mathcal{L}_0$ may be degenerate, forcing one to resort to degenerate perturbation theory instead. For example, if one chooses $\mathcal{L}_0 = -\mathrm{i}[H_S, \bullet]$, the steady state can be any density matrix diagonal in the eigenbasis of H_S. This degeneracy can be lifted when $\mathcal{L}_0$ also includes local dephasing terms like $D[a_\ell^\dagger a_\ell]$ and $D[\sigma_l^z]$ (Sec. II.J), leading to a unique ρ_0, which is usually the identity matrix (infinite-temperature state). If the Hamiltonian is number conserving (e.g., it conserves the total number of particles or the total magnetization), then ρ_0 would still be degenerate and formed by mixed states proportional to the identity in each number sector.

Perturbation theory for the evaluation of the steady state and the relaxation gap has been used in various works on boundary-driven problems; see Flindt *et al.* (2010), Žnidarič, Žunkovič, and Prosen (2011), Žnidarič (2011b, 2015, 2019), Žnidarič and Horvat (2013), Buča and Prosen (2014), Lenarčič and Prosen (2015), Guo and Poletti (2016), and Žnidarič and Ljubotina (2018). Perturbation theory has also been used for more general problems of open quantum systems; see García-Ripoll *et al.* (2009), Poletti *et al.* (2012, 2013), Cai and Barthel (2013), Sciolla, Poletti, and Kollath (2015), and Medvedyeva, Prosen, and Žnidarič (2016).

E. Tensor network methods

Tensor networks form an extremely effective class of numerical methods for boundary-driven, strongly interacting quantum systems. In the following we review the general ideas and strategies, with a focus on open quantum systems and boundary-driven transport problems. For general reviews see Schollwöck (2005, 2011), Verstraete, Murg, and Cirac (2008), Orús (2014), and Silvi *et al.* (2019), and for reviews addressing open quantum systems see Daley (2014), Bertini *et al.* (2021), and Weimer, Kshetrimayum, and Orús (2021). We also call attention to the work of Brenes *et al.* (2020), who developed tensor network methods for handling dissipative, boundary-driven thermal machines, and we also highlight various publicly available tensor network libraries (Dolfi *et al.*, 2014; Fishman, White, and Stoudenmire; Kao, Hsieh, and Chen, 2015; Al-Assam, Clark, and Jaksch, 2017; Jaschke, Wall, and Carr, 2018; Jaschke, Carr, and de Vega, 2019).

1. Introduction to tensor networks and matrix product states

We consider a state $|\psi\rangle = \sum c_{\sigma_1,\ldots,\sigma_L}|\sigma_1,\ldots,\sigma_L\rangle$ representing a chain with L sites, each with d local levels. One can always write the coefficients $c_{\sigma_1,\ldots,\sigma_L}$ as a product of tensors, each with a number of indices depending on the geometry of the system considered. A particularly effective case is that of 1D systems, in which one can write

$$c_{\sigma_1,\ldots,\sigma_L} = \sum_{a_0,\ldots,a_L} M^{\sigma_1}_{a_0,a_1} M^{\sigma_2}_{a_1,a_2} \cdots M^{\sigma_L}_{a_{L-1},a_L}, \qquad (143)$$

where, for each σ_l, M^{σ_l} is a matrix with auxiliary indices a_{l-1} and a_l. This is referred to as a matrix product state (MPS). MPSs are not the only type of tensor network. But since most boundary-driven systems studied are 1D, where MPSs work particularly well, we henceforth concentrate on this structure. The MPS *Ansatz* is exact if we allow the size of the matrices M^{σ_l} to grow unboundedly. However, this would be of little interest. The advantage instead is that accurate representations can often be obtained even with fixed maximum sizes D_B, called the bond dimension. This is because area laws predict that the entanglement entropy of the ground state of gapped short-range Hamiltonians grows as $L^{D_{\mathrm{dim}}-1}$, where D_{dim} is the dimensionality (Bombelli *et al.*, 1986; Srednicki, 1993; Audenaert *et al.*, 2002; Plenio *et al.*, 2005; Wolf, 2006; Eisert, Cramer, and Plenio, 2010). In 1D critical systems the entropy grows at most logarithmically (Vidal *et al.*, 2003; Latorre, Rico, and Vidal, 2004).

For a fixed D_B, the memory requirements go as $Ld^2{D_B}^2$, i.e., linearly with L, a significant advantage compared to the exponential scaling of the coefficients $c_{\sigma_1,\ldots,\sigma_L}$. Given the MPS *Ansatz* in Eq. (143), tensor network algorithms aim to find the matrices M^{σ_l} that most accurately approximate a particular state for a fixed D_B. From a mathematical point of view, MPSs are thus simply an algorithm to approximate a vector in a high-dimensional space by a product of matrices. It can be implemented beyond the evaluation of ground states to study time evolutions of unitary and dissipative systems and in the computation of steady states. In most of these scenarios, however, there is no guarantee that the *Ansatz* will be accurate. Brandão *et al.* (2015) and Cubitt *et al.* (2015) showed that area laws also exist for rapidly mixing dissipative systems, and Gullans and Huse (2019) showed the existence of NESSs with local equilibrium, which can be effectively represented using tensor networks. In any case, one can systematically study the equilibrium and nonequilibrium properties of a system as a function of the maximum bond dimension D_B and can estimate the accuracy of these results.

2. Tensor networks and boundary-driven systems

Any normalized vector can represent a physical state, but not every matrix, even with unit trace, represents a physical density matrix, since the latter must be positive semidefinite. Various approaches have been suggested to express density matrices as tensor networks in a way that preserves positivity, either using the structure of Eq. (145) (Werner *et al.*, 2016; Minganti *et al.*, 2018; Weimer, Kshetrimayum, and Orús, 2021) or via purification techniques (Nielsen and Chuang, 2000). However, these approaches have not been largely pursued. One possible reason is that QMEs guarantee that any accurate representation of steady states will be physical. In other words, if one approximates the steady state well enough, relevant physical properties can be accurately evaluated, even if the density matrix is not exactly positive semidefinite.

One can thus choose to write the density matrix as a matrix product operator

$$\rho = \sum_{\substack{\sigma_1,\ldots,\sigma_L \\ \sigma'_1,\ldots,\sigma'_L}} \rho^{\sigma'_1,\ldots,\sigma'_L}_{\sigma_1,\ldots,\sigma_L} |\sigma_1,\ldots,\sigma_L\rangle\langle\sigma'_1,\ldots,\sigma'_L| = \sum_{\substack{\sigma_1,\ldots,\sigma_L,\sigma'_1,\ldots,\sigma'_L \\ a_0,\ldots,a_L}} M^{\sigma_1,\sigma'_1}_{a_0,a_1}\cdots M^{\sigma_L,\sigma'_L}_{a_{L-1},a_L} |\sigma_1,\ldots,\sigma_L\rangle\langle\sigma'_1,\ldots,\sigma'_L|, \tag{144}$$

where each M^{σ_l,σ'_l} is a matrix with indices a_{l-1} and a_l of dimension smaller than the bond dimension D_{B}. Taken together with vectorization (Sec. III.A), this *Ansatz* can then be used to directly study the time evolution and the steady state. For a review of methods for time evolving tensor networks, see García-Ripoll (2006), Žnidarič *et al.* (2017), and Paeckel *et al.* (2019). Another approach is to compute the steady state as the ground state of the superoperator $\hat{\mathcal{L}}^\dagger\hat{\mathcal{L}}$, as discussed in Eq. (129) and by Cui, Cirac, and Bañuls (2015). Similarly, one may use ground-state-like search algorithms while looking for the null vector of the non-Hermitian superoperator $\hat{\mathcal{L}}$ (Mascarenhas, Flayac, and Savona, 2015; Bairey *et al.*, 2020). Finally, one may also evolve the density matrix in the Heisenberg picture (Hartmann *et al.*, 2009). Clark *et al.* (2010) showed that, depending on the observables studied, this can lead to significant improvements in efficiency, and even to exact solutions.

An important question is when to stop the simulation. This depends on the quantities of interest, which in our case is usually the current. In the steady state, the current is the same for all bonds of the system, but in the transient this may not be the case. It is thus common to compute the standard deviation of the current over different bonds, and to stop when this falls below a chosen threshold.

3. Approaches to improve the performance

Although tensor networks allow one to study large, strongly interacting boundary-driven systems, the numerical calculations can still be demanding. It is thus worth considering different ways to improve the numerical performance of the algorithm. Tensor networks can be used to describe any type of quantum systems, whether bosonic, fermionic, spins, or mixtures. Bosonic systems can be particularly demanding because the local Hilbert space dimension d may be large. At large temperatures, the relevant terms of M^{σ_l,σ'_l} are usually those for which $\sigma_l \approx \sigma'_l$. Considering only such terms can result in a significant reduction of memory requirements (Guo, Mukherjee, and Poletti, 2015).

Another improvement is to account for symmetries (Sec. III.A.2), more notably the conservation of a quantum number such as total particle number or total magnetization. For instance, in Eq. (143) one can also write $M^{\sigma_l}_{(n_{l-1},a_{l-1}),(n_l,a_l)}$, where a_{l-1} and a_l still represent the auxiliary indices and n_l represents the sum of the physical indices σ_l until site l, i.e., $n_l = \sum_{m=1}^{l}\sigma_m$, which implies that $n_l = \sigma_l + n_{l-1}$. This more detailed data structure allows one to save considerable memory, as one needs to deal with smaller matrices (although many more of them) (McCulloch, 2007; Hubig, McCulloch, and Schollwöck, 2017; Silvi *et al.*, 2019). This can be generalized to open quantum systems, but one needs to account for the quantum numbers in both the bra and the ket of the density matrix. Moreover, while the Hamiltonian does not change the total quantum number, the dissipators generally do. A scheme that automatically adapts to such changes in quantum number was introduced by Guo and Poletti (2019). Taking this into account, however, works best when the fluctuations in the particle number are small, such as when they are far from the infinite-temperature state. In the latter, a simpler non-number-conserving code would typically be more effective. Similar ideas in a system with non-Abelian symmetry were studied by Moca *et al.* (2022).

Parallelization of the time evolution also improves the performance. Schollwöck (2011) discussed how to apply the evolution operator to the MPSs in parallel, alternating between even and odd bonds. This can be done while preserving the canonical structure of the MPSs, allowing one to reduce the local bond dimensions in parallel. An alternative is the algorithm developed by Stoudenmire and White (2013) and recently adapted for time evolution by Secular *et al.* (2020). In this case one divides the sweep over the full system into sweeps over different portions of the system, and distributes these internal sweeps to different computational nodes, letting the nodes communicate once they reach their shared bond.

Recently Rams and Zwolak (2020) and Wójtowicz *et al.* (2020) presented a way to significantly reduce the bond dimension based on the realization that, for fermionic systems, the star configuration (Sec. II.H.2) requires a lower bond dimension than the chain configuration; see also Brenes *et al.* (2020). They also grouped the eigenmodes of the two baths in increasing order of energy, allowing the correlations between baths modes to be concentrated within a narrow energy band close to their Fermi levels. This is particularly effective in the common scenarios in which an energy mode from one bath is scattered to a mode of similar energy in a different bath. Still on the topic of the star-to-chain mapping, Tamascelli *et al.* (2019) and Nüßeler *et al.* (2020) obtained improvements while specifically designing a thermofield transformation approach (Sec. II.H.2) for system-bath couplings with Hermitian bath operators. Tensor network algorithms have also been used to simulate Redfield QMEs [Eqs. (26)

and (27)], reaching system sizes much larger than what can be obtained using exact diagonalization (Xu, Thingna *et al.*, 2019).

F. Analytical solutions for interacting chains

Analytical solutions of interacting boundary-driven models are seldom available due to the enormous mathematical complexities involved. When they are, it usually concerns restricted scenarios or extremes of parameter space. Notwithstanding, these solutions offer invaluable insight, precisely because they are exact. Here we review the most famous example: an XXZ chain (12) under maximally biased local dissipators, which can be solved in terms of MPSs. This was discovered by Prosen (2011a, 2011b) and generalized by Karevski, Popkov, and Schütz (2013). Similar ideas were subsequently used by Popkov, Karevski, and Schütz (2013) and Popkov and Presilla (2016) to show that there are special configurations associated with twisted Lindblad operators of the form $\sigma_x \cos\theta - \mathrm{i}\sigma_y + \sigma_z \sin\theta$, where the NESS is found to be in a product state despite carrying a finite current (which is highly unusual). A matrix product solution, in a similar spirit, was also found by Prosen (2014) and Popkov and Prosen (2015) for the open Fermi-Hubbard chain. Recently these developments were generalized to encompass general XYZ chains and twisted jump operators (Popkov, Prosen, and Zadnik, 2020a, 2020b).

The system is taken to be an XXZ chain [Eq. (12)] with zero magnetic field and LME dissipators acting on the first and last sites, as in Eq. (16). The drives are taken as $f_1 = 1$ and $f_L = 0$, meaning the dissipators try to fully polarize the first and last spins in opposite directions. The master equation (16) is thus described by only the two jump operators $\sqrt{\gamma}\sigma_1^+$ and $\sqrt{\gamma}\sigma_L^-$, where γ is the coupling strength. We mention up front that the solution obtained in this limit is not representative of what is found for other values of f_i. For instance, in this case transport is found to be subdiffusive ($I \sim 1/L^2$) when $\Delta = 1$. Conversely, at high temperatures ($f_1 = 0.5 + \delta$ and $f_L = 0.5 - \delta$) it is superdiffusive (Žnidarič, 2011b); see Sec. IV for more details.

The solution given by Prosen (2011a, 2011b) starts by decomposing the steady state as

$$\rho = \frac{SS^\dagger}{\mathrm{tr}(SS^\dagger)} \tag{145}$$

for some operator S. This is always possible for any ρ since $SS^\dagger$ is always a positive semidefinite operator. However, such a decomposition is often not useful, since, when plugged into the master equation (16), it leads to a nonlinear equation for S. The main innovation of Prosen (2011a, 2011b) was to prove that S in this problem is given by a matrix product *Ansatz*. One can approach the problem as follows. Let $\mathcal{H}_i$ denote the Hilbert space of each spin degree of freedom (so that both ρ and S live in $\mathcal{H}_1 \otimes \cdots \otimes \mathcal{H}_L$). We then introduce an auxiliary space $\mathcal{A}$ and write S as

$$S = \langle\phi|\Omega_1 \otimes \cdots \otimes \Omega_L|\psi\rangle, \tag{146}$$

where $\Omega_i \in \mathcal{H}_i \otimes \mathcal{A}$ are operators that live in the joint Hilbert space of site i and the auxiliary space. Moreover, $|\phi\rangle$ and $|\psi\rangle$ are states that act only on $\mathcal{A}$. As a consequence, the sandwich in Eq. (146) effectively traces out $\mathcal{A}$, leaving S as a state only in $\mathcal{H}_1 \otimes \cdots \otimes \mathcal{H}_L$, as it should.

The goal then is to adjust the parameters in Eq. (146) so that ρ is ultimately a steady-state solution of Eq. (16). This first involves deciding what properties the auxiliary space $\mathcal{A}$ should have. The methods used for doing so are nontrivial, so we state only the result. Since $\Omega_i \in \mathcal{H}_i \otimes \mathcal{A}$, we can parametrize

$$\Omega_i = A_0\sigma_i^0 + A_+\sigma_i^+ + A_-\sigma_i^- + A_z\sigma_i^z, \tag{147}$$

for some operators $A_\alpha \in \mathcal{A}$. This allows us to rewrite Eq. (146) as

$$S = \sum_{\alpha_1,\ldots,\alpha_L \in \{0,+,-,z\}} \langle\phi|A_{\alpha_1},\ldots,A_{\alpha_L}|\psi\rangle \sigma^{\alpha_1} \otimes \cdots \otimes \sigma^{\alpha_L}. \tag{148}$$

Hence, S is written as a linear combination of all possible basis elements $\sigma^{\alpha_1} \otimes \cdots \otimes \sigma^{\alpha_L}$.

Prosen (2011a, 2011b) showed that all coefficients involving σ_i^z can be chosen to vanish. This leaves only three operators to be specified: A_0, A_+, and A_-. Next they showed that $\mathcal{A}$ can be chosen as an infinite-dimensional Hilbert space with basis elements $|r\rangle$, $r = 0, 1, 2, 3, \ldots$ and

$$A_0 = |0\rangle\langle 0| + \sum_{r=1}^{\infty} a_r^0 |r\rangle\langle r|, \tag{149}$$

$$A_+ = (\mathrm{i}\gamma/2)|0\rangle\langle 1| + \sum_{r=1}^{\infty} a_r^+ |r\rangle\langle r+1|, \tag{150}$$

$$A_- = |1\rangle\langle 0| + \sum_{r=1}^{\infty} a_r^- |r+1\rangle\langle r|, \tag{151}$$

where a_r^α are complicated coefficients depending on γ and Δ; see Prosen (2011a) for explicit definitions. For $\Delta \neq 1$, these operators are found to satisfy a q-deformed SU(2) algebra, which reduces to the standard SU(2) algebra for $\Delta = 1$ (Karevski, Popkov, and Schütz, 2013). Finally, it suffices to take both $|\phi\rangle$ and $|\psi\rangle$ to be $|0\rangle$. A systematic calculation of arbitrary correlation functions from this solution was made by Buča and Prosen (2016).

Extracting physical observables from this formal solution is nontrivial for $\Delta \neq 1$. But when $\Delta = 1$, it can be shown that the magnetization current (18) reduces to (Landi and Karevski, 2015)

$$I = \frac{2}{\gamma}\frac{(B^{L-1})_{00}}{(B^L)_{00}},$$
$$B_{k\ell} = 2\left|k - \frac{\mathrm{i}}{2\gamma}\right|^2 \delta_{k\ell} + \ell^2\delta_{k,\ell-1} + \left|\ell - \frac{\mathrm{i}}{\gamma}\right|^2 \delta_{k,\ell+1}, \tag{152}$$

with $k, \ell = 0, 1, 2, \ldots, L$. Equation (152) therefore involves the entries of the powers B^{L-1} and B^L of a $(L+1)$-dimensional matrix, allowing one to compute the current for arbitrarily large sizes. Plots of the behavior of I vs L and γ

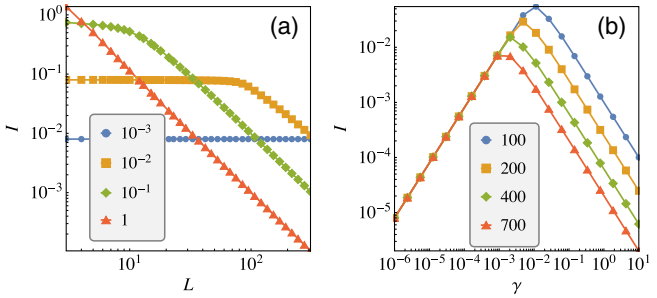

FIG. 9. Steady-state currents in the Heisenberg chain (XXZ with $\Delta = 1$) obtained from the exact solution of Eq. (152). (a) Dependence on the size for different coupling strengths γ. (b) Currents given as a function of γ for different sizes L.

are shown in Fig. 9. As it can be seen, the presence of interactions dramatically alters the current profile, as compared to the ballistic scenario of Sec. III.B. The dependence of I on L is found to depend sensibly on γ. For small γ transport is roughly ballistic, while for large γ it becomes subdiffusive, scaling as $I \propto 1/L^2$. For sufficiently large L, it always eventually becomes subdiffusive for any $\gamma > 0$.

G. Quantum trajectory approach

A method commonly used to describe open quantum systems, including boundary-driven problems (Wichterich *et al.*, 2007), involves *quantum trajectories*, also known as quantum jumps or Monte Carlo wave functions (Dalibard, Castin, and Mølmer, 1992; Dum *et al.*, 1992; Dum, Zoller, and Ritsch, 1992; Carmichael, 1993; Mølmer, Castin, and Dalibard, 1993; Plenio and Knight, 1998; Breuer and Petruccione, 2002; Gardiner and Zoller, 2004; Jacobs and Steck, 2006; Wiseman and Milburn, 2010). The main idea is not to solve the master equation, but rather to stochastically evolve wave functions such that the average of these wave functions reproduces the dynamics of the QME.

A GKSL QME of the form of Eq. (11) can be rewritten as

$$\frac{d\rho_S}{dt} = -i(H_{\text{eff}}\rho_S - \rho_S H_{\text{eff}}^\dagger) + \sum_k L_k \rho_S L_k^\dagger, \tag{153}$$

where H_{eff} is a non-Hermitian Hamiltonian given by

$$H_{\text{eff}} = H_S - \frac{i}{2}\sum_k L_k^\dagger L_k. \tag{154}$$

The last term in Eq. (153) represents discrete jumps, while the first represents a no-jump evolution. As a method for quantum trajectories, one can thus use the following algorithm. Evolve a wave function $|\psi(t)\rangle$ under H_{eff} using a small time δt:

$$|\tilde{\psi}(t+\delta t)\rangle = [\mathbb{1} - iH_{\text{eff}}\delta t]|\psi(t)\rangle. \tag{155}$$

Since H_{eff} is not Hermitian, the norm of the state reduces to $\langle\tilde{\psi}(t+\delta t)|\tilde{\psi}(t+\delta t)\rangle \simeq 1 - \delta p$, where $\delta p = \delta t \sum_k \langle\psi(t)| \times L_k^\dagger L_k|\psi(t)\rangle := \sum_k \delta p_k$. Here δp_k is interpreted as the probability of performing the quantum jump L_k and $1 - \delta p$ is the probability of performing no jump during the time interval δt. Thus, with probability δp_k the state is updated to

$$|\psi(t+\delta t)\rangle \to |\psi_{\text{jump}}^k\rangle = \frac{L_k|\psi(t)\rangle}{\sqrt{\langle\psi(t)|L_k^\dagger L_k|\psi(t)\rangle}}, \tag{156}$$

while with probability $1 - \delta p$ it goes to

$$|\psi(t+\delta t)\rangle \to |\psi_{\text{stay}}\rangle = \frac{|\tilde{\psi}(t+\delta t)\rangle}{\sqrt{\langle\tilde{\psi}(t+\delta t)|\tilde{\psi}(t+\delta t)\rangle}}. \tag{157}$$

One may then verify that the ensemble-averaged evolution $\overline{\rho(t+\delta t)} = (1-\delta p)|\psi_{\text{stay}}\rangle\langle\psi_{\text{stay}}| + \sum_k \delta p_k |\psi_{\text{jump}}^k\rangle\langle\psi_{\text{jump}}^k|$ can be written to order δt^2 as

$$\overline{\rho(t+\delta t)} \simeq \rho(t) - i\delta t[H_{\text{eff}}\rho(t) - \rho(t)H_{\text{eff}}^\dagger] + \delta t\sum_k L_k\rho(t)L_k^\dagger,$$

which is equivalent to Eq. (153).

This implies that the expectation value of any observable O can also be evaluated by averaging over the trajectories $\langle O\rangle = \text{tr}\{\rho(t)O\} = \overline{\langle\psi(t)|O|\psi(t)\rangle}$. Computing a single trajectory this way requires significantly less effort than solving Eq. (153). One has to make sure that this numerical advantage is not scotched by the required sampling (a process that is easily parallelizable, though).

It is natural to try to bring together quantum trajectories with tensor networks (Sec. III.E). This was reviewed by Daley (2014), who also reviewed the quantum trajectory approach in many-body settings. The benefits of such an approach were studied by Bonnes and Lauchli (2014), who analyzed the growth of the bond dimension required for an accurate description of the system. An important element that they identified is the size of the local Hilbert space d, which must be squared for density matrices. This has important consequences on the memory requirements of the algorithms. Quantum trajectories can also be preferred when the relaxation time to the NESS is exponentially long (Benenti, Casati, Prosen, Rossini, and Žnidarič, 2009). Recently Wolff, Sheikhan, and Kollath (2020) considered different ways of computing two-time correlations with quantum trajectories, showing that the preferred approach to this problem also depends on the problem at hand.

IV. PROPERTIES OF BOUNDARY-DRIVEN OPEN SYSTEMS

A. Overview of different types of steady transport regimes

We begin with an introduction to the phenomenology of transport in boundary-driven systems. This is usually characterized by how the current (such as that of energy or matter) I scales with the system size L. For sufficiently large L this usually has the form $I \sim 1/L^\alpha$ [Eq. (2)]. The different transport regimes were discussed in Sec. I and are summarized in Table I. They also manifest as signatures in the expectation values of the quantity considered (such as the spin or energy). For instance, ballistic transport yields roughly constant values through the system that are independent of L. This is illustrated by the blue solid line in

TABLE I. Scaling exponents for different transport regimes when analyzed from the perspective of the current or from the perspective of the spreading of a localized wave packet. The two exponents are connected by $\phi = 1/(\alpha+1)$.

Transport regime	$I \sim 1/L^{\alpha}$	$\sqrt{\langle \Delta x^2 \rangle} \sim t^{\phi}$
Ballistic	$\alpha = 0$	$\phi = 1$
Superdiffusive	$0 < \alpha < 1$	$1/2 < \phi < 1$
Diffusive	$\alpha = 1$	$\phi = 1/2$
Subdiffusive	$\alpha > 1$	$\phi < 1/2$
Localized	$\alpha = \infty$	$\phi = 0$

Fig. 10, which depicts a generic quantity $\langle \mathcal{O}^k \rangle$ as a function of the position k in a chain of length L, when the left (right) bath tries to impose the value 1 (0). Conversely, for diffusive transport one would observe a linear profile (red dashed lines). At the boundaries, however, there is usually a mismatch with respect to the value the baths are trying to impose. Finally, in an insulating regime, since there is no current the profile will be constant over large parts of the chain. But since the quantity must also be adjusted to the one imposed by the baths, this will result in a steplike behavior, as depicted by the green dotted line in Fig. 10.

The classification of transport exponents according to the scaling $I \sim 1/L^{\alpha}$ [Eq. (2)] can alternatively be performed in isolated (unitary) systems by analyzing the spreading of wave packets. An initially localized packet will spread along the system with a standard deviation that scales as

$$\sqrt{\langle \Delta x^2 \rangle} \sim t^{\phi}, \tag{158}$$

with some exponent ϕ. Diffusive transport corresponds to $\phi = 1/2$. Other transport regimes are shown in Table I.

To relate the exponents α and ϕ, we notice from Eq. (158) that the characteristic time it takes for a particle to travel through the chain will be $\tau \sim L^{1/\phi}$. In the NESS, the current should be proportional to the rate of particles flowing through ($I \sim L/\tau \sim L/L^{1/\phi}$). Comparing this to $I \sim 1/L^{\alpha}$ then yields (cf. Table I)

$$\phi = \frac{1}{\alpha+1}. \tag{159}$$

Equation (159), however, crucially relies on the somewhat arbitrary hypothesis of a universal transport exponent. While true in many cases, this has been reported to break down in certain models (Purkayastha, Dhar, and Kulkarni, 2016a; Varma, de Mulatier, and Žnidarič, 2017a).

B. Integrability and transport

One might think that integrable systems are ballistic and nonintegrable systems are diffusive, but reality is much more interesting.[15] For example, integrable systems can present ballistic, diffusive, anomalous, and insulating transport properties (Prosen, 2011b; Žnidarič, 2011b). The mechanisms behind such richness are still a topic of research. Similarly, nonintegrable models can also exhibit ballistic transport. In particular, at $T = 0$ systems with a gapless phase always support ballistic transport, regardless of whether or not they are integrable (Kohn, 1964; Shastry and Sutherland, 1990; Scalapino, White, and Zhang, 1993). See Mastropietro (2013) for a recent study of an XXZ chain equipped with next-nearest-neighbor interactions to break integrability. Away from $T = 0$, transport can be qualitatively different. Ballistic transport has been observed in finite-temperature nonintegrable systems, both classical (Lebowitz and Scaramazza) and quantum (Brenes *et al.*, 2018). In the latter, Brenes *et al.* considered an XXZ chain with a single local impurity in the center, rendering the system nonintegrable. However, since the system is composed of two ballistic halves, ballistic transport was still preserved. A small density of impurities, however, renders the transport diffusive (Žnidarič, 2020). And when the clean system behaves subdiffusively, impurities can also increase transport (Žnidarič, 2022); cf. Sec. IV.E.

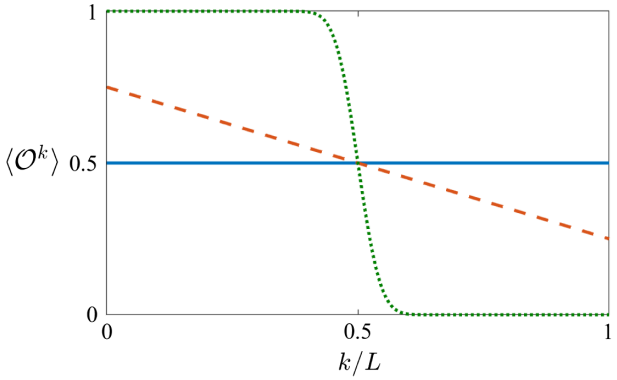

FIG. 10. Qualitative profile of a local quantity $\langle \mathcal{O}^k \rangle$ vs position k for three transport regimes: ballistic (blue solid line), diffusive (red dashed line), and insulating (green dotted line). In all cases the dissipative boundary driving tries to impose the value 1 at the left edge and the value 0 at the right edge, as discussed in Sec. II.D.3.

We now provide an overview of some guiding principles, starting with the concept of Drude weight in linear responses. Considering the conductivity of a system as a function of frequency $\sigma(\omega)$, which can be obtained from Kubo's formula (Green, 1952, 1954; Kubo, 1957), the ac response is obtained when $\omega \to 0$, with ballistic transport signaled by an infinite conductivity. It is thus useful to write the real part of the conductivity $\sigma' = \mathrm{Re}(\sigma)$ as $\sigma'(\omega) = \mathcal{D}_W \delta(\omega) + \sigma_{\mathrm{reg}}(\omega)$, where $\mathcal{D}_W$ is the Drude weight and $\sigma_{\mathrm{reg}}(\omega)$ is the regular portion of the conductivity. A nonzero Drude weight thus implies ballistic transport. The Drude weight of a 1D system in equilibrium with inverse temperature β is given by

$$\mathcal{D}_W = \lim_{t\to\infty} \lim_{L\to\infty} \frac{\beta}{4Lt} \int_{-t}^{t} \langle \mathcal{I}_L(0) \mathcal{I}_L(t') \rangle_{\beta} dt', \tag{160}$$

[15] By integrable, we refer to Bethe-*Ansatz* integrable models that have an infinite number of local conservation laws, as discussed by Bertini *et al.* (2021). For a more exhaustive discussion on integrability in quantum systems, see Caux and Mossel (2011).

where $\langle\cdots\rangle_\beta$ denotes the average over a thermal state at temperature β and $\mathcal{I}_L = \sum_l \mathcal{I}_l$ is the sum of all the local current operators [defined in Eq. (61)].

If the $\mathcal{I}_l$ are conserved at system-internal junctions, transport is guaranteed to be ballistic (Zotos, Naef, and Prelovsek, 1997) because $\langle \mathcal{I}_L(0)\mathcal{I}_L(t')\rangle_\beta$ becomes a constant in t, and hence the Drude weight is finite. For instance, in the XXZ model [Eq. (12)] the energy current operator $\mathcal{I}_E^l$ is given, using Eq. (62), by

$$\mathcal{I}_E^l = \Delta(\mathcal{I}_M^{l-1,l}\sigma_{l+1}^z + \sigma_{l-1}^z\mathcal{I}_M^{l,l+1}) + J\mathcal{I}_M^{l-1,l+1}\sigma_l^z, \tag{161}$$

where $\mathcal{I}_M^{l,l+1} = -2J(\sigma_l^x\sigma_{l+1}^y - \sigma_l^y\sigma_{l+1}^x)$; cf. Eq. (18). It follows that energy transport is ballistic for any parameter value (Zotos, Naef, and Prelovsek, 1997). On the other hand, $[\sum_l \mathcal{I}_M^{l,l+1}, H_{XXZ}] \neq 0$, and hence spin transport is not guaranteed to be ballistic.

A lower bound to the Drude weight is provided by the *Mazur bound* (Mazur, 1969; Suzuki, 1971; Zotos, Naef, and Prelovsek, 1997)

$$\mathcal{D}_W \geq \lim_{L\to\infty} \frac{\beta}{2L} \sum_k \frac{|\langle \mathcal{I}_L Q_k\rangle|^2}{\langle Q_k^\dagger Q_k\rangle}, \tag{162}$$

where Q_k are orthogonal conserved quantities that, if they are (quasi)local, have an overlap with $\mathcal{I}_l$ that is not exponentially small as L increases. If the system has an extensive number of such quantities, then the Drude weight $\mathcal{D}_W$ can be nonzero and transport will be guaranteed to be ballistic. Finding the Q_k may be nontrivial, however. For the XXZ chain they were computed by Prosen (2011b) and Prosen and Ilievski (2013). Using these results, one may show that spin transport in XXZ chains in the zero magnetization sector is ballistic for $|\Delta| < 1$ (Prosen, 2011b), and for any Δ when it is away from the zero magnetization sector (Zotos, Naef, and Prelovsek, 1997). This can also be shown using the Bethe *Ansatz* at $T = 0$ (Shastry and Sutherland, 1990) or with numerical methods (Heidrich-Meisner, Honecker, and Brenig, 2005). In a similar manner one can study the Hubbard model, where the energy current is not conserved but the current operator has a finite overlap with conserved quantities, resulting in a nonzero Mazur bound (Zotos, Naef, and Prelovsek, 1997); see also Karrasch, Kennes, and Heidrich-Meisner (2016), Ilievski and De Nardis (2017), and Karrasch (2017). For charge and spin currents, the current operators have finite overlap with conserved quantities outside of the half-filling sector, and thus transport is ballistic in these regimes (Zotos, Naef, and Prelovsek, 1997; Garst and Rosch, 2001; Ilievski and De Nardis, 2017; Karrasch, 2017).

C. Transport in the XXZ chain

To illustrate the richness of transport behaviors in interacting systems, we review some of the main results for boundary-driven XXZ spin chains [Eq. (12)]; see also Bertini *et al.* (2021) and the following for additional details. We assume the LME boundary driving given by Eq. (17b). The spin current transport diagram as a function of the anisotropy Δ and the bias $\eta_1 = -\eta_L = \eta$ is shown in Fig. 11. For $\Delta < 1$, transport is ballistic for any value of η. For $\Delta = 1$ it is superdiffusive for

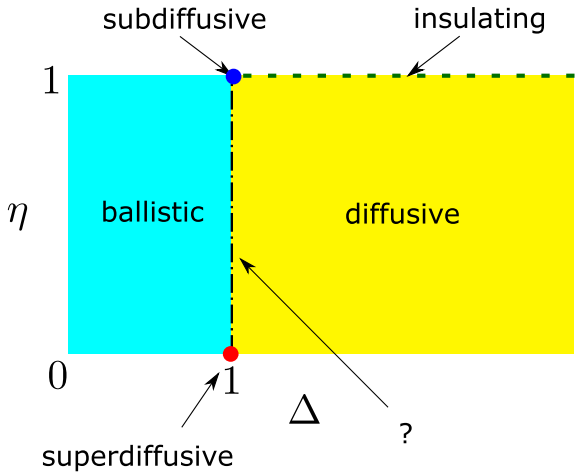

FIG. 11. Phase diagram of magnetization transport regimes in the boundary-driven XXZ chain with driving [Eq. (17b)] for different anisotropies Δ and driving bias η.

$\eta \simeq 0$, with the exponent $\alpha = -1/2$ (Žnidarič, 2011b) but subdiffusive for $\eta = 1$, with exponent $\alpha = -2$ (Prosen, 2011b; Landi and Karevski, 2015); cf. Table I. A superdiffusive regime was also predicted using hydrodynamic theories (De Nardis *et al.*, 2019; Gopalakrishnan and Vasseur, 2019), which were recently verified experimentally in ultracold atoms (Jepsen *et al.*, 2020) and antiferromagnetic materials (Scheie *et al.*, 2021).[16] Superdiffusive transport was also observed for energy transport (Brenes *et al.*, 2020). For $\Delta > 1$ and $\eta < 1$, numerical evidence suggests that spin transport is diffusive (Jesenko and Žnidarič, 2011; Žnidarič, 2011b), but at $\eta = 1$ one finds insulating behavior (Prosen, 2011b). The region $\Delta = 1$ for $0 < \eta < 1$ requires further exploration. Similarly rich behavior can be found in noninteracting systems with long-range tunneling (Purkayastha, Saha, and Agarwalla, 2021).

As mentioned earlier, the energy current through an XXZ chain is ballistic because the corresponding current operator is a conserved quantity. However, for $\eta = 1$ and $\Delta > 1$ the spin current decreases exponentially with L, and the magnetization profile acquires the sigmoid form in Fig. 10. Such insulating spin current behavior may seem at odds with ballistic (without scattering) energy transport. But there is no contradiction because the energy current in this case is exactly 0 due to the symmetries of the system (Schuab, Pereira, and Landi, 2016).

D. Disordered and quasiperiodic systems

Disordered systems have been intensely studied for decades, particularly since the discovery of Anderson localization (Anderson, 1958). For 1D noninteracting systems, any small amount of disorder makes the system an insulator. In interacting systems, Anderson localization, which was studied by Giamarchi and Schulz (1987, 1988), is a line of research that was invigorated after the discovery of many-body

[16]The scenarios reproduced in the experiments are not boundary driven.

localization (Gornyi, Mirlin, and Polyakov, 2005; Basko, Aleiner, and Altshuler, 2006). Comprehensive reviews were given by Nandkishore and Huse (2015), Abanin and Papić (2017), Luitz and Lev (2017), Parameswaran and Vasseur (2018), and Abanin *et al.* (2019). Here we focus on boundary-driven systems of the type of Eq. (17b). The transport properties depend significantly on whether disorder is uncorrelated as in Anderson localization, or correlated as in quasiperiodic potentials, such as in the Aubry-André-Harper (AAH) model (Harper, 1955; Hofstadter, 1976; Aubry and André, 1980). We review them separately in Secs. IV.D.1 and IV.D.2.

1. Uncorrelated disorder

The standard model for the study of transport in disordered systems is an XXZ chain [Eq. (12)] with local potentials h_l. For uncorrelated disorder, h_l is taken from a uniform distribution on $[-h, h]$, where h quantifies the disorder strength. We saw in Fig. 11 that when $h = 0$ and η is small [cf. Eq. (17b)], the system is ballistic for $\Delta < 1$ and diffusive for $\Delta > 1$; for $\Delta = 1$ it is superdiffusive. We also know from the work of Anderson (1958) that, in the absence of interactions, the system becomes an insulator for any value of h. Analytical results for an XX chain with large disorder were given by Monthus (2017).

The high-temperature transport diagram in the XXZ chain is depicted in Fig. 12(a), which was adapted from Žnidarič, Scardicchio, and Varma (2016). These were simulated for small η using tensor networks (Sec. III.E), with L up to 400. For $\Delta > 1$, the transport is subdiffusive for any $h > 0$. Conversely, for $\Delta < 1$ transport is diffusive for $h > h_{c1} = 0$ and subdiffusive for $h > h_{c2}$. For even larger disorder strengths $h > h_{c3}$ [not shown in Fig. 12(a)], the system is localized. The emergence of a subdiffusive region for spin current is aligned with other works (Agarwal *et al.*, 2015, 2017; Bar Lev, Cohen, and Reichman, 2015; Potter, Vasseur, and Parameswaran, 2015; Vosk, Huse, and Altman, 2015; Bera *et al.*, 2017), including experiments (Bordia *et al.*, 2017; Lüschen *et al.*, 2017). However, the origin of the subdiffusive behavior is still under investigation. In particular, Agarwal *et al.* (2015), Potter, Vasseur, and Parameswaran (2015), and Gopalakrishnan *et al.* (2016) pointed to the presence of rare regions with large disorder, known as Griffiths phases (Griffiths, 1969), that can significantly slow down the dynamics. However, subdiffusive transport can also occur in systems with correlated disorder (Sec. IV.D.2), in which the previously mentioned regions do not occur (Weiner, Evers, and Bera, 2019). Numerical simulations initially did not provide any evidence of such regions (Schulz *et al.*, 2020). However, more recent studies involving much larger systems together with local dephasing [cf. Eq. (112)] of random magnitude, and acting on all sites except the boundaries, found clear signatures of the emergence of a Griffiths phase, signaled by power-law tails in the distribution of the resistance (Taylor and Scardicchio, 2021).

We next turn to energy transport. In ordered systems we previously showed that it differs significantly from spin transport since energy is a conserved quantity, while the latter is not. In disordered systems the local energy current is no longer a conserved quantity but, as we later see, transport is strongly affected by the limiting case of disorder going to 0, in which case the current is conserved and transport becomes ballistic. A diagram of the energy transport properties at high temperature and zero magnetization in the disordered XXZ chain [Eq. (12)] is depicted in Fig. 12(b), which was adapted from Mendoza-Arenas *et al.* (2019). The boundary driving is modeled by the two-site reservoirs reviewed in Sec. II.K.2, i.e., baths that act on two sites and that are designed to locally thermalize these sites. In particular, Mendoza-Arenas *et al.* used the target state, acting at the edges, such that $\rho_{T,l} \propto \exp[-\beta_l(H_l - \mu_l M_l)]$, where H_l is the Hamiltonian acting on the two edge sites and M_l is the total magnetization of l and $l+1$. Earlier studies of energy transport in the disordered XXZ model were also given by Varma *et al.* (2017), where two halves of the system were prepared in different states and then allowed to evolve unitarily (cf. Sec. II.H.4); diffusive transport was found for small disorder. In Fig. 12(b) we see that for any value of Δ, as soon as $h > 0$, energy transport goes from ballistic to diffusive, and only at a nonzero critical field can it become subdiffusive. The dashed gray line in Fig. 12(b) shows the boundary between

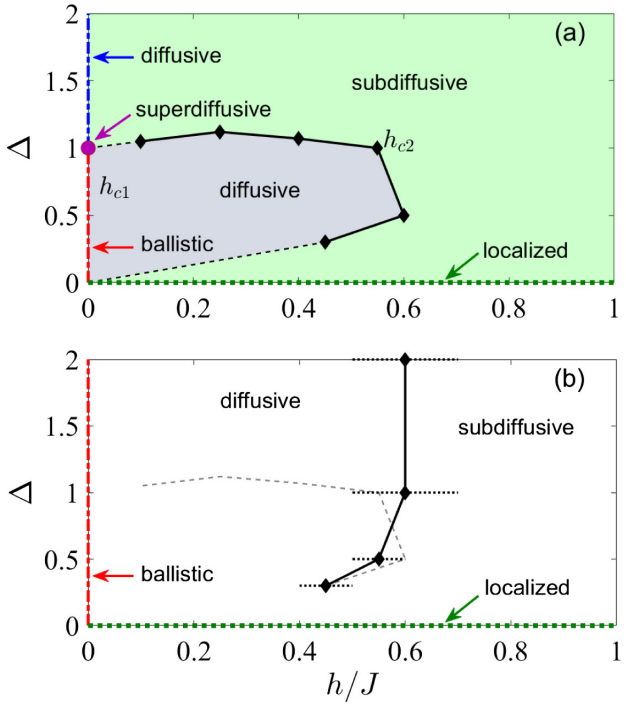

FIG. 12. Maps of (a) spin and (b) energy transport characteristics for the model (12) with local uncorrelated disordered potential h_l. (a) Boundary driving given by Eq. (17a). The transition lines at h_{c1} and h_{c2} represent transitions from ballistic to diffusive and diffusive to subdiffusive, respectively. The transition region, represented by black dots, is evaluated from simulations with L up to 400 spins. Adapted from Žnidarič, Scardicchio, and Varma, 2016. (b) Boundary driving as described in Sec. II.K.2. The black solid line shows the transition line between diffusive and subdiffusive transport, with the dotted lines indicating the confidence level. The gray dashed line represents the transition from diffusive to subdiffusive for the particle transport shown in (a). Adapted from Mendoza-Arenas *et al.*, 2019.

diffusive and subdiffusive transport for spin currents [Fig. 12(a)]. For finite magnetization with $h = 0$, both the particle and the energy current operators are ballistic. In this case, the energy current mimics more closely the particle current (Mendoza-Arenas *et al.*, 2019).

A qualitatively similar description is also found for a non-U(1) symmetric model, such as an XYZ chain with local disorder [Eq. (54)]. Schulz *et al.* (2018) showed that the location of the transition between diffusive and subdiffusive occurs at disorder strengths that depend on the amount of the XY anisotropy $(J_x - J_y)$.

Energy transport was also studied in the localized phase, where it is strongly suppressed. An interesting advantage of the localized phase is that one can exploit the l-bit representation (Huse, Nandkishore, and Oganesyan, 2014; Ros, Müller, and Scardicchio, 2015) based on extensive in number, quasilocal integrals of motion, which can be computed at polynomial cost as a function of the size (Khemani, Pollmann, and Sondhi, 2016; Wahl, Pal, and Simon, 2017; Kulshreshtha *et al.*, 2019). Used by Wu *et al.* (2019), this allowed them to go up to 100 spins. In both the noninteracting and weakly interacting regimes, they found that the temperature T dependence of the heat conductivity σ follows Mott's law (Mott, 1969), $\sigma \propto \exp[(-T_0/T)^{1/(d+1)}]$, where d is the dimensionality of the system and T_0 is an interaction-dependent temperature above which the conductivity becomes more sizable.

We also comment on systems beyond the XXZ chain, but not necessarily studied in the context of boundary-driven open quantum systems. One interesting setup is the Fermi-Hubbard model. It does not fully localize when the disorder does not differentiate between spin-up and spin-down (Prelovšek, Barišič, and Žnidarič, 2016). Instead, the charge degrees of freedom can be localized and nonergodic, while the spin degrees of freedom are delocalized. Full localization can be obtained using spin-dependent tunneling (Środa, Prelovšek, and Mierzejewski, 2019). Iadecola and Žnidarič (2019) considered a spin ladder and showed that the presence of symmetries, independent of the strength of disorder, can be used to construct exponentially large subspaces that can be localized or ballistic. Another interesting setup is a single particle in a lattice with a disordered potential and coupled to a bosonic chain (Prelovšek, Bonča, and Mierzejewski, 2018; Mierzejewski, Prelovšek, and Bonča, 2019; Mierzejewski *et al.*, 2020).[17] The effect of the latter was modeled using Fermi's golden rule and also included a rate equation to describe the injection and removal of particles at the edges. This allowed them to study up to 10^4 sites, and also systems in two dimensions. In one dimension, Mierzejewski, Prelovšek, and Bonča (2019) found that strongly interacting bosons (hard-core bosons) made the transport subdiffusive, while weak interactions resulted in diffusive transport at long times. Conversely, Mierzejewski *et al.* (2020) showed that while transport can be subdiffusive in one dimension, in two dimensions it is always diffusive, even for large disorder.

[17]Note that only Mierzejewski *et al.* (2020) considered a boundary-driven setup.

2. Correlated disorder

As discussed in Sec. IV.D.1, in 1D noninteracting systems any small amount of uncorrelated disorder turns the system into an insulator. In other words, there is no *mobility edge*, i.e., an energy threshold that differentiates localized from delocalized energy states. Mobility edges are possible, however, with correlated disorder, such as quasiperiodic potentials. We consider a noninteracting lattice of free fermions [Eq. (15)], with local potential $h_{\alpha_Q,l} \equiv h_l$ given by (Ganeshan, Pixley, and Das Sarma, 2015)

$$h_{\alpha_Q,l} = \lambda \frac{2\cos(2\pi\beta_Q l + \phi)}{1 - \alpha_Q \cos(2\pi\beta_Q l + \phi)}, \tag{163}$$

where $\beta_Q = (1+\sqrt{5})/2$ is the golden mean (other Diophantine numbers lead to similar results). This is a generalization of the AAH model, which is obtained setting $\alpha_Q = 0$ (Harper, 1955; Hofstadter, 1976; Aubry and André, 1980). In the AAH model there is a critical value of λ below which all eigenstates are delocalized and above which all eigenstates are exponentially localized. This is already a noteworthy difference from uncorrelated noise for which any amount of disorder localizes all eigenstates in one dimension. The transport is found to be ballistic for $\lambda < 1$ and insulating for $\lambda > 1$. At $\lambda = 1$ all eigenstates are critical (Ostlund *et al.*, 1983) and particle transport is subdiffusive, with $I \propto L^{-1.4}$ (Purkayastha, Dhar, and Kulkarni, 2017; Purkayastha *et al.*, 2018).

Here we add a note on the system sizes L considered to compute I. Varma, de Mulatier, and Žnidarič (2017b), Purkayastha *et al.* (2018), and Sutradhar *et al.* (2019) showed that particle transport differs quantitatively whether L is a Fibonacci number or not. For instance, Varma, de Mulatier, and Žnidarič (2017b) showed that in the subdiffusive region ($\lambda = 1$) the current scaled as $I \propto L^{-1.38}$ when L are powers of 2, while $I \propto L^{-1.27}$ when they are Fibonacci numbers. A related study, based on entanglement entropy, was put forth by Roy and Sharma (2019). Another subtlety of the model is that at $\lambda = 1$ one finds different transport coefficients for a boundary-driven system and a unitary Green-Kubo analysis (Purkayastha *et al.*, 2018). In particular, the latter can predict superdiffusion (due to the fast spreading of the tails of a wave packet). This has been shown to be due to the fact that the Green-Kubo formalism takes $L \to \infty$ first, and then $t \to \infty$. Conversely, boundary drives can take only $L \to \infty$ since the infinite time limit is implicit (Purkayastha, 2019). Hence, for systems that are sensitive to boundary conditions (as is the case here), this results in different predictions, depending on the method used. If one is interested in finite systems, then boundary drives are the most accurate approach. Such subtleties are not present for diffusive transport (Žnidarič, 2019).

When $\alpha_Q > 0$ in Eq. (163), the system presents a mobility edge; i.e., below a certain energy all eigenstates are delocalized, and above it they are localized (or vice versa). The presence of a mobility edge shifts the critical value of λ at which transport goes from ballistic to insulating. Furthermore, while the system is still subdiffusive at the critical value the

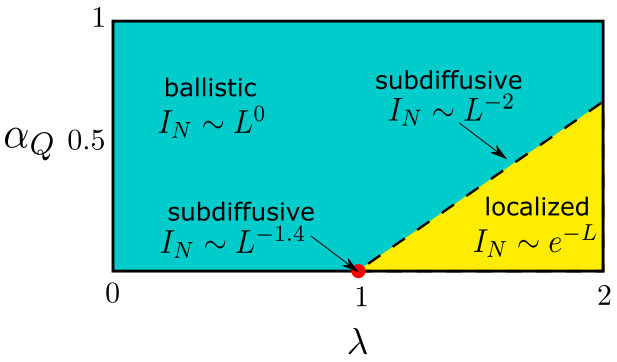

FIG. 13. Phase diagram of the high-temperature particle transport properties of the modified AAH model with potential (163). The ballistic region (top left, turquoise) is separated from the localized region (bottom right, yellow) by a subdiffusive line with $I_N \sim L^{-2}$ and a subdiffusive point at $\alpha_Q = 0$ and $\lambda = 1$ with $I_N \sim L^{-1.4}$. The symbol I_N stands for the NESS particle current and L represents the system size. Adapted from Purkayastha, Dhar, and Kulkarni, 2017.

exponent for $\alpha_Q > 0$ is given by $I_N \propto L^{-2}$, and thus differs from the case $\alpha_Q = 0$. This is illustrated in Fig. 13, based on the work of Purkayastha, Dhar, and Kulkarni (2017), who presented the parameter regions with ballistic and diffusive particle transport, and the critical line with the two scalings for $\alpha_Q = 0$ and $\alpha_Q \neq 0$.

A mobility edge can also be obtained by modifying the AAH model to include beyond-nearest-neighbor tunneling (Das Sarma, He, and Xie, 1988; Boers *et al.*, 2007; Li, Li, and Das Sarma, 2017), which was studied experimentally by Lüschen *et al.* (2018). Power-law hopping can result in algebraically localized modes instead of exponential ones, and this can lead to different forms of zero-temperature particle transport, from ballistic to superdiffusive to insulating, as well as the presence of mobility edges in one dimension (Saha, Maiti, and Purkayastha, 2019). Furthermore, when transport is modeled by Büttiker probes (see Sec. II.J), the current can depend nontrivially on the magnitude of the coupling to the probes (Saha, Venkatesh, and Agarwalla, 2022).

Equilibrium localization properties for an AAH potential ($\alpha_Q = 0$) have also been studied in the presence of interactions, both theoretically (Iyer *et al.*, 2013; Cookmeyer, Motruk, and Moore, 2020) and experimentally (Schreiber *et al.*, 2015; Lüschen *et al.*, 2017), and in higher dimensions (Bordia *et al.*, 2017). Interactions with $\alpha_Q \neq 0$ were studied by Li *et al.* (2015), Modak and Mukerjee (2015), and Modak, Ghosh, and Mukerjee (2018). Additionally, the possible existence of a nonergodic phase violating the eigenstate thermalization hypothesis while having volume law entanglement entropy was studied by Srednicki (1994).

Focusing on $\alpha_Q = 0$, Žnidarič and Ljubotina (2018) showed that for the region of $\lambda \lesssim 1.5$ any small Δ makes the particle and magnetization transport diffusive. However, this requires much larger system sizes, even up to sizes of $L = 1000$ sites (Žnidarič, 2021). Since for $\Delta = 0$ the system is insulating when $\lambda > 1$, the diffusion constant diverges as $\Delta \to 0$ when $\lambda < 1$ and tends to zero otherwise. These results indicate that, even for strongly localized integrable systems, small integrability-breaking perturbations can result in diffusive dynamics. Žnidarič and Ljubotina (2018) showed that altering the potential at chosen sites can significantly affect the transport, thus opening another door to engineer transport properties in quantum systems.

Another particularly interesting quasiperiodic potential is the *Fibonacci chain* defined by the local potential (Kohmoto, Kadanoff, and Tang, 1983; Ostlund *et al.*, 1983; Kalugin, Kitaev, and Levitov, 1986; Kohmoto, Sutherland, and Tang, 1987; Sutherland and Kohmoto, 1987; Hiramoto and Abe, 1988; Hiramoto and Kohmoto, 1992)

$$h_l = \frac{h}{2}[2V(lg) - 1], \tag{164}$$

where h is the magnitude, $g = (1+\sqrt{5})/2$, and $V(x) = \lfloor x+g \rfloor - \lfloor x \rfloor$, with $\lfloor x \rfloor$ denoting the integer part of x. Unlike the AAH model, the noninteracting ($\Delta = 0$) Fibonacci model is critical for any value of h, showing eigensystem fractality, and anomalous transport (Kohmoto, Kadanoff, and Tang, 1983; Ostlund *et al.*, 1983; Kalugin, Kitaev, and Levitov, 1986; Kohmoto, Sutherland, and Tang, 1987; Hiramoto and Abe, 1988; Hiramoto and Kohmoto, 1992; Macé, Jagannathan, and Piéchon, 2016). In fact, the particle transport varies continuously from ballistic to insulating as h increases. This is illustrated in Fig. 14, which shows simulations computed using the Lyapunov equation [Sec. III.B].

Concerning interacting Fibonacci chains, in the low-temperature regime bosonization techniques showed that repulsive interactions can lead to a metal-insulator transition and a power-law dependence of the conductivity with L (Vidal, Mouhanna, and Giamarchi, 1999, 2001). The high-temperature case was studied by Macé, Laflorencie, and Alet (2019) and Varma and Žnidarič (2019), who showed that for large enough h and Δ the system becomes subdiffusive and can show many-body localization. However, we point out that, independent of the magnitude of h, for small Δ the current is diffusive. Further studies are required for larger values of Δ, especially close to $\Delta = 1$. Although they did not employ a boundary-driven setup, Chiaracane *et al.* (2021) found signatures of superdiffusive behavior for $h < \Delta$, and subdiffusive to insulating behavior for $h > \Delta$. Similar results were also found by Chiaracane *et al.* (2022) for the energy current.

In the AAH model [Eq. (163) with $\alpha_Q = 0$], the eigenstates for $\lambda = 1$ are neither localized nor delocalized. Instead, they are critical and display fractal properties. Conversely, in the Fibonacci model [Eq. (164)] they are critical for any value of h. The fractal nature of the steady-state magnetization profile was shown by Varma, de Mulatier, and Žnidarič (2017b). To characterize said fractal structure, they had go to almost 40 000 sites, which was made possible by recasting the problem as a Lyapunov equation (Sec. III.B). To conclude, we mention that contrasting the AAH potential (163) with a uniform distribution may not provide a fair comparison between uncorrelated and correlated disorder, since the potential magnitudes are significantly different. A noteworthy workaround was pursued by Setiawan, Deng, and Pixley (2017),

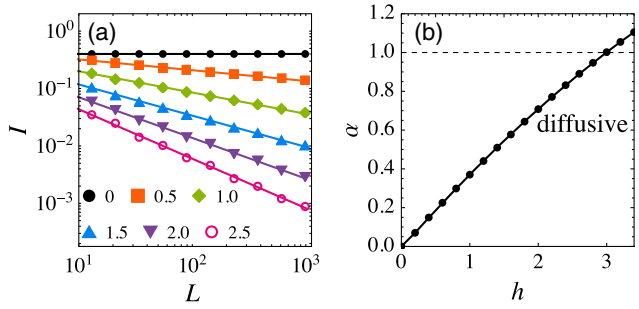

FIG. 14. (a) Magnetization current as a function of L for the noninteracting Fibonacci model (164), for different values of h ranging from $h = 0$ (top) to $h = 2.5$ (bottom) in steps of 0.5. For sufficiently large L, all curves behave like $I \sim 1/L^{\alpha}$ [Eq. (2)], with an exponent α that depends on h. (b) α vs h, extracted from the simulations in (a). Adapted from Lacerda, Goold, and Landi, 2021.

who used the AAH potential (163) but with randomly chosen local phases ϕ on each site. With this they showed that for small λ and high temperatures, the correlated disordered model led to a higher current when compared to the uncorrelated one. Conversely, for large λ the situation was inverted (although for both setups the currents decayed exponentially with L since both are insulators).

E. Dephasing and transport

In this section we discuss how transport is affected by the presence of dephasing baths (Sec. II.J) acting locally on all sites of a chain. In short, dephasing is expected to always render the transport diffusive for a sufficiently large chain size L. This is based on evidence from various models: first in noninteracting chains with homogeneous (Žnidarič, 2010a, 2011a; Asadian *et al.*, 2013; Bermudez, Bruderer, and Plenio, 2013; Malouf *et al.*, 2020), disordered (Žnidarič and Horvat, 2013; Taylor and Scardicchio, 2021), and quasiperiodic (Dwiputra and Zen, 2021; Lacerda, Goold, and Landi, 2021) potentials, and second in interacting systems both homogeneous (Mendoza-Arenas, Grujic *et al.*, 2013) and disordered (Žnidarič *et al.*, 2017).

To illustrate the idea, consider the nearest-neighbor homogeneous tight-binding chain studied in Sec. III.B. The current in this case is given by Eq. (141), which scales as

$$I = \frac{a}{b + \Gamma L}, \tag{165}$$

where a and b are constants. In the absence of dephasing ($\Gamma \equiv 0$), the transport is ballistic. But for any nonzero Γ there will always be a sufficiently large L for which the current starts to behave diffusively, as $I \sim 1/L$.

For other models involving interactions, disorder, etc., the functional form of the current $I(\Gamma, L)$ will no longer be given by Eq. (165). Notwithstanding, one can still predict that if Γ is much larger than any other scale in the problem, any Hamiltonian contribution should be washed away, so the current is expected to behave similarly to Eq. (165):

$$I(\Gamma, L) = \frac{c_{\mathrm{deph}}}{\Gamma L} \qquad (\Gamma \text{ large}), \tag{166}$$

where c_{deph} is a constant. The interesting case, therefore, is when Γ is moderate, as this should lead to an intricate competition between the Hamiltonian, which is responsible for the system's natural transport $I \sim 1/L^{\alpha}$, and the dephasing, which tends to make the transport diffusive ($I \sim 1/L$). In fact, in this case there should be a characteristic length scale L_{Γ} at which the system transitions from one regime to the other (Žnidarič *et al.*, 2017). That is,

$$I(\Gamma, L) = \begin{cases} c_0/L^{\alpha}, & L \ll L_{\Gamma}, \\ c_{\Gamma}/L, & L \gg L_{\Gamma}, \end{cases} \tag{167}$$

where c_0 and c_{Γ} are constants, with the former independent of Γ. The length scale L_{Γ}, where the transition occurs, can be estimated if one assumes the single-transport exponent hypothesis [Eqs. (158) and (159)], from which the typical length scale for the spreading of wave packets is found to behave as $\sqrt{\langle \Delta x^2 \rangle} \sim \tau^{1/(\alpha+1)}$. Since dephasing introduces a characteristic timescale $\tau \sim 1/\Gamma$, L_{Γ} should scale as

$$L_{\Gamma} \sim \Gamma^{-1/(\alpha+1)}. \tag{168}$$

Since $\alpha > 0$, L_{Γ} is always decreasing in Γ. Hence, for large Γ the diffusive behavior should become visible for small chain sizes, while for low Γ large L's might be necessary.

Finally, the functional dependence of c_{Γ} in Eq. (167) can also be estimated by requiring continuity when $L = L_{\Gamma}$. That is, $c_0/L_{\Gamma}^{\alpha} = c_{\Gamma}/L$, which yields

$$c_{\Gamma} = c_0 \Gamma^{(\alpha-1)/(\alpha+1)}. \tag{169}$$

One can use this to predict the following: Suppose that L is sufficiently large such that $L \gg L_{\Gamma}$ for a wide range of Γ's. Both Eqs. (166) and (167) will predict diffusive transport, but with a nontrivial dependence on Γ:

$$I(\Gamma, L)L = \begin{cases} c_0 \Gamma^{(\alpha-1)/(\alpha+1)}, & \Gamma \text{ small}, \\ c_{\mathrm{deph}}/\Gamma, & \Gamma \text{ large}, \end{cases} \tag{170}$$

where "small" and "large" are defined with respect to the energy scales of the system Hamiltonian. Particularly noteworthy, even though the transport is diffusive due to dephasing, is that the exponent α of the dephasing-free system still plays a clear role.

The presence of noise is often expected to reduce the current and thus is deleterious for transport. For instance, in the ballistic example of Eq. (165), the current with dephasing is always smaller than that without it ($\Gamma = 0$). There are situations, however, where noise can actually be beneficial. The term *dephasing-assisted transport* (or noise-assisted transport) is used to describe those situations in which an additional noise source increases the current.

This effect was first investigated by Olaya-Castro *et al.* (2008) and Plenio and Huelga (2008) and in a series of follow-up papers (Caruso *et al.*, 2009; Rebentrost *et al.*, 2009; Chin, Datta *et al.*, 2010; Chin, Huelga, and Plenio, 2012; del Rey

et al., 2013; Manzano, 2013; Contreras-Pulido *et al.*, 2014). Interest was on light harvesting in biological molecules, modeled by spin 1/2 (or tight-binding) networks. The noise was introduced by means of a dephasing dissipator (Sec. II.J) acting on all sites of the lattice. Experimental simulations were carried out in optical setups (Viciani *et al.*, 2015; Biggerstaff *et al.*, 2016) and trapped ions (Cormick and Schmiegelow, 2016; Maier *et al.*, 2019). Related studies were also carried out using Büttiker probes (Sec. II.J) by Kilgour and Segal (2015, 2016).

Dephasing-assisted transport always occurs in systems exhibiting *subdiffusive* transport (Žnidarič *et al.*, 2017) (with insulators being a limiting case). This can be seen in Eq. (170): Subdiffusivity implies that $\alpha > 1$, and hence $(\alpha-1)/(\alpha+1) > 0$. For small Γ the function $I \sim \Gamma^{(\alpha-1)/(\alpha+1)}$ will thus be monotonically increasing in Γ, which is exactly the dephasing-assisted transport. This was explored by Žnidarič and Horvat (2013) and Lacerda, Goold, and Landi (2021), who studied the XX model in the presence of disorder and Fibonacci potentials, respectively. Mobility edges were studied by Dwiputra and Zen (2021), and Chiaracane *et al.* (2022) addressed applications to thermal machines. In the context of many-body systems, this was studied by Mendoza-Arenas, Al-Assam *et al.* (2013) and Mendoza-Arenas, Grujic *et al.* (2013), who considered interacting fermionic chains with LME dissipators (17b) at the boundaries, and dephasing dissipators at all sites. The system was simulated using tensor network methods (Sec. III.E) up to 120 sites. Finally, Mendoza-Arenas *et al.* (2014) considered a system made by multiple lattices and found an even larger transport enhancement by a type of noise that induces incoherent coupling to neighboring lattices.

F. Negative differential conductance

In linear response, the greater the bias at the boundaries of a driven system, the larger the response. For example, the larger the temperature difference, the larger the heat current, as indicated by Fourier's law [Eq. (1)]. The early works of Esaki (1958), Esaki and Stiles (1966), and Esaki and Tsu (1970) showed that it is possible to have negative differential conductance (NDC) or resistance, which means that an increase of the bias would result in a decrease of the response. NDC is a key ingredient in the realization of transistors, including thermal ones (Li, Wang, and Casati, 2006).

Esaki and Tsu (1970) showed that superlattices, and the consequent presence of a structured density of states, can result in a resonant response that naturally leads to NDC. Many other mechanisms resulting in resonant behavior do as well, such as Coulomb blockade (Heij *et al.*, 1999), spin-charge separation (Cavaliere *et al.*, 2004), ferromagnetic interactions (Rolf-Pissarczyk *et al.*, 2017), conformational changes (Mujica *et al.*, 2003), and electron interactions with vibrational modes (Gaudioso, Lauhon, and Ho, 2000; Galperin, Ratner, and Nitzan, 2005) in molecules.

NDC has been observed in semiconductor quantum dots (Weis *et al.*, 1993), carbon nanotubes (Zhou *et al.*, 2000; Pop *et al.*, 2005), and small molecular systems (Chen *et al.*, 1999; Halbritter *et al.*, 2008). This was reviewed, with an emphasis on molecular electronics, by Zimbovskaya and Pederson (2011) and Xu and Dubi (2015), and in more general reviews on nanoelectronics (Kastner, 1992; Anantram and Léonard, 2006). We thus focus on reviewing negative differential conductance in boundary-driven, strongly interacting spin systems, which were not discussed in the previous reviews.

Owing to interactions, spin chains are an ideal setup for the emergence of NDC. Recently it was shown that this can also appear in classical Heisenberg chain models with varying magnetic field (Bagchi, 2015). Benenti, Casati, Prosen, and Rossini (2009) and Benenti, Casati, Prosen, Rossini, and Žnidarič (2009) showed that strongly interacting XXZ chains [Eq. (12)] can present strong NDC under LME boundary driving. In the notation of Eq. (17a), strong bias ($f_1 = 1 - f_L = 0$) forces the edge spins to be either up or down. If $\Delta > 1$, the bulk Hamiltonian, together with the large bias, will favor the presence of two large ferromagnetic domains at the edges. Because of their insulating nature this lowers the current, and for large enough interactions and biases the system can turn into an insulator. The stability of such an insulating phase is due to the properties of the Hamiltonian, and for large enough interactions the steady state is given by two large domains that can be destabilized only by magnons: excitations at the boundary between the domains. However, for large enough Δ, such excitations are gapped and thus exponentially localized. As a consequence they cannot propagate and reach the baths, thereby prohibiting the decay of the system to a different state. A different explanation of the phenomenon was given by Mendoza-Arenas, Al-Assam *et al.* (2013), who stressed that for $\Delta \gg 1$ the baths preferentially couple to high energy states with low conductivity. Specifically, one configuration becomes particularly important, which is the one with two half-chain-long ferromagnetic domains, as this is a dark state of the baths alone, for which the domain boundary is farthest from the baths. All other states are exponentially suppressed.

One can also examine the robustness of NDC. First, it is robust against various types of integrability-breaking terms; thus, it is not related to the integrable nature of the XXZ chain. For instance, Benenti, Casati, Prosen, and Rossini (2009) also added an integrability-breaking staggered magnetic field and still observed it. Mendoza-Arenas, Grujic *et al.* (2013) and Droenner and Carmele (2017) instead considered a dissipative perturbation as an additional dephasing in the local σ^z basis [Eq. (113)]. Since the mechanism for such strong rectification is related to the properties of the bulk Hamiltonian, dephasing is found to significantly reduce, or even remove, NDC. This is another manifestation of dephasing-assisted transport (Sec. IV.E). Another way to remove NDR is to increase the range of the spin-spin interactions or add strong disorder, as studied by Droenner and Carmele (2017). Long-range interactions oppose the formation of two large and opposite domains at the edges, thus resulting in a more gradual spin magnetization profile. Particularly chosen local potentials can also significantly reduce the NDC for one bias and reinforce it for the opposite one, thus resulting in strong spin current rectification (Lenarčič and Prosen, 2015; Lee *et al.*, 2020) (Sec. IV.G).

G. Rectification

Rectification is an effect that has widespread applications in electronics. It describes, in the widest sense, an asymmetric response of a two-terminal system to reflection. The *electric diode* makes the flow of electric current in one direction significantly different from the other if the driving bias is inverted. While electric diodes are widespread, the implementation of a *heat diode* appears to be much more challenging. A key requirement is the presence of reflection symmetry breaking in the system. Given our focus on quantum boundary-driven systems, we discuss rectification of different quantities, such as spin, particle, and heat currents. We also mention key developments in classical rectification, which form the basis for the developments in quantum systems; for comprehensive reviews, see Li *et al.* (2012) and Benenti *et al.* (2016). There has also been significant interest in the experimental realization of thermal rectifiers in various setups, such as oxides (Starr, 1936; Brattain, 1951), nanotubes (Chang *et al.*, 2006), nanoribbons (Hu, Ruan, and Chen, 2009), quantum dots (Scheibner *et al.*, 2008), and systems with superconducting components (Fornieri, Martínez-Pérez, and Giazotto, 2015; Martínez-Pérez, Fornieri, and Giazotto, 2015; Bours *et al.*, 2019; Iorio *et al.*, 2021). A review of the experimental efforts was given by Roberts and Walker (2011).

The rectification performance is measured by the rectification coefficient $\mathcal{R}$ defined as $\mathcal{R} = -I_f/I_b$, where I_f and I_b are the current with the bias in the forward and backward (swapped) directions. The minus sign is used because the current, after inverting the bias driving the current, is in the opposite direction. An alternative figure of merit is $\mathcal{C} = |(I_f + I_b)/(I_f - I_b)|$, which is sometimes also denoted as the rectification coefficient, but which we refer to as *contrast*. A system that does not rectify has $\mathcal{R} = 1$ and $\mathcal{C} \to 0$, while a perfect rectifier (where the system is an insulator in one direction) has $\mathcal{R} \to 0, \infty$ and $\mathcal{C} \to 1$. Since $\mathcal{C}$ is confined between 0 and 1, it helps to observe sharp transitions between nonrectifying and strongly rectifying behavior (Balachandran *et al.*, 2018).

To better understand the requirements for rectification, we consider the heat current through a system coupled to two baths (L and R) at temperatures T_L and T_R. We can thus write $I_f = I(\bar{T}, \Delta T)$ and $I_b = I(\bar{T}, -\Delta T)$, where $\bar{T} = (T_L + T_R)/2$ and $\Delta T = T_L - T_R$. Each current can be written as a series expansion in powers of ΔT:

$$I(\bar{T}, \Delta T) = \sum_{n>0} \alpha_n I_n(\bar{T}) \Delta T^n. \tag{171}$$

It is thus clear that in order to have rectification $I(\bar{T}, \Delta T)$ should be nonlinear in ΔT, and the expansion in Eq. (171) should include even powers of n. For a study of the role of quadratic and quartic conductivities as a function of temperature, see Yang *et al.* (2018).

For rectification to occur, it is necessary to break reflection symmetry. This can be done by considering (i) a non–reflection-symmetric system (Wang *et al.*, 2019; Chioquetta *et al.*, 2021), (ii) equivalent baths with asymmetric couplings (Purkayastha, Dhar, and Kulkarni, 2016a), or (iii) different baths [such as baths with different magnetic fields (Arrachea, Lozano, and Aligia, 2009) or different statistics (Wu and Segal, 2009b; Wu, Yu, and Segal, 2009)]. These conditions, however, are necessary but not sufficient.

Interactions tend to play a key role in rectification. For instance, considering the Landauer formula (84), for noninteracting transport one finds that when the transmission function is reflection symmetric, there will be no rectification: Reversing the bias amounts to exchanging $f_L(\omega) \leftrightarrow f_R(\omega)$ and the current simply reverses sign. This therefore excludes rectification effects for a broad class of models. In contrast, Meir and Wingreen (1992) provided a formally exact current formula for transport through an interacting region, which was also recently done in boundary-driven LMEs (Jin, Filippone, and Giamarchi, 2020). This formula is not antisymmetric under reservoir exchanges, and hence rectification is in principle possible. In the remainder of this section we review general ways of obtaining nonlinear responses and thus rectification. Section IV.G.1 discusses the role of nonlinearities and interactions within the system, while Sec. IV.G.2 considers asymmetric baths.

1. Nonlinearities and interactions within the system

Terraneo, Peyrard, and Casati (2002) and Li, Wang, and Casati (2004) greatly advanced our understanding of heat rectification in classical systems. They showed that to obtain a nonlinear response one can build rectifiers from a concatenation of chains of nonlinear oscillators. In this case, rectification occurs because each portion of the chain has a distinct, temperature-dependent power spectrum. It results that for a certain pair of temperatures T_L and T_R there is a large overlap between the spectra of the different portions of the chain (resulting in large currents), but if the temperatures are swapped this overlap is significantly suppressed (resulting in small currents).

Nonlinear responses have been used to rectify the propagation of waves (Lepri and Casati, 2011; Mascarenhas *et al.*, 2016), and they have also been employed in quantum many-body systems. A prototypical example was presented by Werlang *et al.* (2014), who considered two spins coupled via a $\sigma_1^z \sigma_2^z$ coupling. Each spin feels a different local magnetic field and is coupled to a different heat bath. The interplay between the structure of the system Hamiltonian and the coupling of the system to the baths can result in perfect rectification (zero current in one direction). This approach was later pursued for more than two spins by Pereira (2019).

Considering extended boundary-driven systems, one of the first works to give strong rectification was by Balachandran *et al.* (2018), who considered an XXZ chain [Eq. (12)] segmented in two halves,[18] one with anisotropy $\Delta = 0$ and the other with $\Delta \neq 0$. They considered spin transport with LME dissipators acting on the first and last sites, as in Eq. (17a). One bath had $f = 0.5$ (infinite temperature) and the other had $f = 0$. It was shown that for an anisotropy

[18]With a Jordan-Wigner transformation [Eq. (14)], the XXZ chain can be seen as a fermionic lattice where the anisotropy plays the role of the interactions.

$\Delta > 1 + \sqrt{2}$ the system had large rectification ($\mathcal{R} \approx 10^4$) even for small chains. And in the thermodynamic limit, the system became a perfect heat diode. This occurs because, in reverse bias, the baths drive the system toward a state with a large excitation gap, which thus is stable toward spin excitations arising from the Hamiltonian. In the forward bias the state is not gapped, so excitations can propagate.

An analysis of the stability of this rectifier, as well as further properties, was provided by Balachandran *et al.* (2018) and Lee *et al.* (2020, 2022). For instance, if Δ is nonzero on both sides of the chain, then the value of Δ at which the energy gap occurs in reverse bias increases with the system size (Lee, Balachandran, and Poletti, 2021). As a result, there is no perfect insulator in the thermodynamic limit, although the system can still become a strong rectifier. This setup can also be used to rectify heat, as done by Balachandran, Clark *et al.* (2019), with possibly large values of heat current rectification ($\mathcal{R} \approx 400$). Adding a ring structure in the middle of the chain can increase rectification, which occurs together with the formation of entanglement between the spins in the ring (Poulsen *et al.*, 2022).

An XXZ spin chain that also shows large-spin rectification is one with homogeneous anisotropy but local magnetic fields pointing in different directions in each half of the chain (Lenarčič and Prosen, 2015; Lee *et al.*, 2020). Gradual changes of the local magnetic field also result in rectification (Zhang *et al.*, 2009; Landi *et al.*, 2014; Pereira, 2017a). In particular, Landi *et al.* (2014) showed that when $\Delta \equiv 0$ the rectification is identically zero, underlining once again the importance of interactions. Moreover, Pereira (2017a) showed that in spin chains described by LMEs rectification can also reach an extreme situation where even the direction of the current does not change sign, as the baths are inverted; i.e., the energy current flows in the same direction even after inverting the baths. Even though this seems thermodynamically inconsistent at first sight, it can actually be explained by the existence of a work term in LMEs (De Chiara *et al.*, 2018; Pereira, 2018); cf. Eq. (73).

The role of interactions in rectification is also prominent in bosonic chains (Purkayastha, Dhar, and Kulkarni, 2016a) and quantum dots (Stopa, 2002; Michaelis, Emary, and Beenakker, 2006; Scheibner *et al.*, 2008; Xue-Ou, Bing, and Xiao-Lin, 2008; Pöltl, Emary, and Brandes, 2009; Kuo and Chang, 2010; Svensson *et al.*, 2013; Sierra and Sánchez, 2014; Marcos-Vicioso *et al.*, 2018; Tang, Zhang, and Wang, 2018; Zimbovskaya, 2020). Schaller, Giusteri, and Celardo (2016) relied on collective effects such as *configurational blockades* to significantly enhance the rectification. Alternatively, rectification can also be enhanced using long-range interactions (Pereira and Ávila, 2013; Chen, Pereira, and Casati, 2015).

2. Nonlinearities in the baths and role of quantum statistics

Important insights into the origin of nonlinear terms in Eq. (171) were developed by Segal (2008), Wu and Segal (2009b), and Wu, Yu, and Segal (2009). They considered systems coupled to two reservoirs and found two sufficient conditions for the emergence of thermal rectification: baths with different energy-dependent densities of states and different statistical properties of system and baths, plus asymmetric system-bath couplings. They studied the Hamiltonian $H_S = \sum_n E_n |n\rangle\langle n|$, weakly coupled to the baths via $H_I = \sum_\nu S \lambda_\nu B_\nu$, with B_ν an operator acting on bath ν, λ_ν a coupling constant, and $S = \sum_{nm} S_{n,m} |n\rangle\langle m|$, an operator acting only in the system. They considered Markovian baths and weak coupling, such that the evolution can be described using a Pauli master equation for the populations p_n of the system energy levels [see Eq. (36)]:

$$\dot{p}_n = \sum_{\nu,m} |S_{n,m}|^2 p_m(t) k^\nu_{m\to n}(T_\nu) - p_n(t) \sum_{\nu,m} |S_{n,m}|^2 k^\nu_{n\to m}(T_\nu),$$

with transition rates

$$k^\nu_{m\to n}(T_\nu) = \lambda_\nu^2 \int_{-\infty}^{\infty} d\tau e^{\mathrm{i}(E_m - E_n)\tau} \langle B_\nu(\tau) B_\nu(0)\rangle_{T_\nu}, \tag{172}$$

where $\langle B_\nu(\tau) B_\nu(0)\rangle_{T_\nu}$ are bath correlation functions [Eq. (23)]. Segal (2008), Wu and Segal (2009b), and Wu, Yu, and Segal (2009) then observed that if the system is a harmonic oscillator with $H_S = \omega a^\dagger a$ and $S \propto a + a^\dagger$, then

$$I_{\mathrm{HO}}(T_L, T_R) = -\frac{\omega[n_B(\omega, T_L) - n_B(\omega, T_R)]}{n_B(-\omega, T_L)/k^L(T_L) + n_B(-\omega, T_R)/k^R(T_R)},$$

where $k^\nu(T_\nu) = k^\nu(T_\nu)_{n\to n-1}$ is independent of n and $n_B(\omega, T_\nu) = (e^{\omega/T_\nu} - 1)^{-1}$. Conversely, if one has a two-level system $H_S = (\omega/2)\sigma^z$, with $S = \sigma^x$, then

$$I_S(T_L, T_R) = -\frac{\omega[n_S(\omega, T_L) - n_S(\omega, T_R)]}{n_S(-\omega, T_L)/k^L(T_L) + n_S(-\omega, T_R)/k^R(T_R)},$$

with $n_S(\omega, T_\nu) = (e^{\omega/T_\nu} + 1)^{-1}$. In both cases the numerator is antisymmetric with respect to a swap $T_L \leftrightarrow T_R$, but the denominator may not be. It is thus sufficient to study the denominator to find criteria for the occurrence of rectification.

The decay rate $k^\nu(T)$ can be written as (Wu, Yu, and Segal, 2009)

$$k^\nu(T) = 2\pi\lambda_\nu^2 \frac{\int d\epsilon e^{-\epsilon/T} \rho_{\mathrm{d},\nu}(\epsilon) g_\nu(\epsilon, \omega)}{\int d\epsilon e^{-\beta\epsilon} \rho_{\mathrm{d},\nu}(\epsilon)}, \tag{173}$$

where $\rho_{\mathrm{d},\nu}(\epsilon)$ is the density of states (see Sec. II.K.1) of bath ν, while $\lambda_\nu^2 g_\nu(\epsilon, \omega)$ characterizes the system-bath coupling; cf. Eq. (87). Assuming that $\lambda_L = \lambda_R$ and $g_L = g_R$, it follows that if

$$\frac{\int d\epsilon e^{-\epsilon/T} \rho_{\mathrm{d},L}(\epsilon) g_L(\epsilon, \omega)}{\int d\epsilon e^{-\beta\epsilon} \rho_{\mathrm{d},L}(\epsilon)} \neq \frac{\int d\epsilon e^{-\epsilon/T} \rho_{\mathrm{d},R}(\epsilon) g_R(\epsilon, \omega)}{\int d\epsilon e^{-\beta\epsilon} \rho_{\mathrm{d},R}(\epsilon)}, \tag{174}$$

then rectification is possible. For example, as long as $g_\nu(\epsilon, \omega)$ depends on ϵ, it is sufficient that $\rho_{\mathrm{d},L}(\epsilon) \neq \rho_{\mathrm{d},R}(\epsilon)$, and at least one of them depends on ϵ as well. Thus, if both baths are harmonic with a constant density of states, there is no rectification.

An example of this behavior, in the context of quantum spin chains, was given by Arrachea, Lozano, and Aligia (2009). They considered an XX chain coupled on one edge to a

semi-infinite XY chain and on the other to a semi-infinite XX chain, which assumed the role of the reservoirs. Each bath was subject to different magnetic field biases, resulting in rectification. Kalantar, Agarwalla, and Segal (2021) showed that while it is not possible to obtain rectification in a completely harmonic system plus bath setup, it is possible to obtain rectification when different portions of each edge of the chain are coupled to baths at different temperatures. Similarly, Pereira (2017b) showed that classical harmonic chains subject to temperature-dependent potentials could also lead to rectification.

Another sufficient condition for the emergence of rectification, first discussed by Wu and Segal (2009b) and Wu, Yu, and Segal (2009), is when the system and baths are composed of particles with different statistics. An intuitive way to think about it is that if the bath is harmonic and the system is a spin, the latter can be thought of as a strongly anharmonic system (as exemplified by a Holstein-Primakoff transform), and thus there is an effective nonlinearity in the overall system plus bath setup. Another way to look at this is to note that different quantum statistics make it impossible to describe transport with linear scattering theory; see Benenti *et al.* (2017). A difference in statistics is in fact the mechanism that allows the linear models described by Yan, Wu, and Li (2009), Balachandran, Benenti *et al.* (2019), and Silva *et al.* (2020) to show rectification.

The fact that rectification is possible does not imply that it will be strong. Balachandran, Benenti *et al.* (2019) considered a bosonic chain with a quasiperiodic potential [introduced by Ganeshan, Pixley, and Das Sarma (2015)] and two identical spins baths at different temperatures. This setup allows rectification because of the different statistics in the system and in the baths, and because the quasiperiodic potential breaks reflection symmetry. The quasiperiodic potential also induces mobility edges [cf. Eq. (163)], which significantly enhances the rectification. In fact, Ganeshan, Pixley, and Das Sarma showed that this could be used to tune the magnitude of the rectification over 3 orders of magnitude. This is because localized modes can be moved into different positions by tuning the potential parameters, and in the scenarios in which one localized mode is at one of the edges of the system but no other localized mode is present at the other edge, strong rectification emerges.

H. Beyond 1D systems

Thus far we have discussed transport in boundary-driven systems that are mainly 1D. Extending beyond 1D geometries opens various possibilities. First, systems that are integrable in one dimension may not be integrable in two dimensions: e.g., the 1D XXZ chain is integrable, but an XXZ ladder, or the 2D XXZ model, is not. Second, there is more flexibility on what parameters to tune, and one can also introduce qualitatively different new terms, such as gauge fields, in the Hamiltonian. Here we focus on ladders dissipatively driven far from equilibrium. Results obtained via the Kubo formula for closed quantum systems were reviewed by Bertini *et al.* (2021).

Spin ladders are setups that show neither that integrability is strictly associated with ballistic transport nor that nonintegrability corresponds to diffusive transport. The following refers to results for local dissipators of the form of Eq. (17b). Žnidarič (2013b) considered an integrable spin ladder and showed that while for finite magnetization the transport is ballistic, in the zero magnetization sector transport it can be anomalous. For nonintegrable ladders Žnidarič found numerical evidence of diffusive transport. However, Žnidarič (2013a) showed that a nonintegrable spin ladder with XX coupling for bonds in the legs and XXZ coupling within the rungs (i.e., $\Delta \neq 0$) has invariant subspaces that permit ballistic spin transport within them. The existence of such subspaces, with different transport properties, has been investigated as a tool to control the transport properties of the system (Manzano and Hurtado, 2014, 2018; Manzano, Chuang, and Cao, 2016; Thingna, Manzano, and Cao, 2016, 2020). In the Fermi-Hubbard model analyzed by Prosen and Žnidarič (2012) for small driving η_i [see Eq. (17b) after conversion from fermions to spins], they showed the emergence of diffusive transport except for the noninteracting limit, where it was ballistic, and for infinite interaction strengths, where it was anomalous. Moreover, for extreme boundary drivings $\eta_i = \pm 1$, the system became an insulator.

The addition of an extra dimension also allows one to explore the effect of different Hamiltonian terms and the resulting phases of matter. For instance, one can consider the following noninteracting bosonic ladder with gauge fields in each leg:

$$H_{\mathrm{VM}} = -\left(J^{\parallel}\sum_{l,p} e^{i(-1)^{p+1}\phi/2} {a^{\dagger}}_{l,p} a_{l+1,p} + J^{\perp}\sum_{l} {a^{\dagger}}_{l,1} a_{l,2} + \mathrm{H.c.}\right) + V\sum_{l,p} {a^{\dagger}}_{l,p} a_{l,p}. \tag{175}$$

In Eq. (175) ϕ is the gauge field phase, $a_{l,p}$ ($ {a^{\dagger}}_{l,p}$) is the bosonic annihilation (creation) operator at the lth rung and pth leg of the ladder, and $J^{\parallel}$ and $J^{\perp}$ are the tunneling amplitudes along the legs and rungs, respectively. Such a system presents a phase transition between a Meissner phase, in which the ground state has a current circulating on the edges but not within the rungs (known as chiral current), and a vortex phase for which the current in the ground state presents a different number of vortices (Kardar, 1986; Granato, 1990). This system has been studied both theoretically (including interactions) and experimentally, with different techniques and experimental setups (Kardar, 1986; Granato, 1990; Denniston and Tang, 1995; van Oudenaarden and Mooij, 1996; Nishiyama, 2000; Donohue and Giamarchi, 2001; Orignac and Giamarchi, 2001; Atala *et al.*, 2014). However, only recently have the effects of the phase transition on the boundary-driven transport properties been explored (Guo and Poletti, 2016, 2017a; Rivas and Martin-Delgado, 2017; Xing *et al.*, 2020).

Given the noninteracting nature of the problem, transport is always ballistic, regardless of the strength of the gauge field ϕ. However, tuning ϕ can significantly alter the current across the ladder and within the system. For instance, Guo and Poletti (2016) considered LME baths of the type of Eq. (17b) (adapted for bosons) and showed that chiral currents can emerge, but only if the baths are coupled to certain sites. They also showed that it is possible to tune the system into a perfect

insulator. The nonequilibrium properties of this system depend significantly on whether or not the two bands of the spectrum have an energy gap between them (see the further discussion in Sec. IV.I on phase transitions). As the gap opens between the bands, such as by varying ϕ or $J^{\perp}$, the current is significantly reduced. Rivas and Martin-Delgado (2017) considered a similar setup under the effect of GME thermal baths [as in Eq. (32)] and showed the robustness of the chiral, heat, and particle currents versus the presence of disorder. Xing *et al.* (2020) used nonequilibrium Green's functions, which unlike GMEs and LMEs is exact, to study chiral, heat, and particle currents for a broad range of system parameters. They showed how, at low temperatures, these three currents are significantly different depending on whether the underlying ground state is in the Meissner or vortex phase, and on the presence or absence of a gap between the two bands of the energy spectrum of the system. For instance, if one of the temperatures is large enough to allow transport via the upper band, then even a small amount of particle current in this band would result in a significant change to the heat current, especially if the gap between the bands is large. If one compares the current pattern in the ground state to the one in a low-temperature NESS, it can be found that the pattern is more robust to the coupling with the baths for parameters such that the ground state is in the Meissner phase, while it is less robust for an underlying vortex phase. The boundary-driven bosonic system with a gauge field has also been studied for interacting particles, in particular, the hard-core bosons discussed by Guo and Poletti (2017a), who found that the effect of the gauge field on the current becomes less prominent as the filling increases.

As in ladders, in ring configurations the magnetic field can significantly affect the transport properties. To be more specific, we focus on rings with two external baths coupled to different sites. A ring can behave as an Aharonov-Bohm interferometer (Aharonov and Bohm, 1959) that is sensitive to an external magnetic field, as long as the ring is smaller than the phase-coherence length. Ring setups have been studied intensively, particularly when they contain quantum dots; see Yacoby *et al.* (1995), Schuster *et al.* (1997), Holleitner *et al.* (2001), and Sigrist *et al.* (2004) and Akera (1993), Yeyati and Büttiker (1995), Bruder, Fazio, and Schoeller (1996), and Hackenbroich and Weidenmüller (1996) for pioneering experimental and theoretical works, respectively. Various phenomena have been observed, including resonant tunneling (Shahbazyan and Raikh, 1994; Mourokh, Horing, and Smirnov, 2002) and cotunneling (Akera, 1993; Loss and Sukhorukov, 2000), Fano physics (Kubala and König, 2002; Silva, Oreg, and Gefen, 2002; Kobayashi *et al.*, 2003; Ueda *et al.*, 2003), Kondo correlations (Gerland *et al.*, 2000; Hofstetter, König, and Schoeller, 2001; Boese, Hofstetter, and Schoeller, 2002; Kim and Hershfield, 2002), the influence of Coulomb interaction on transport, quantum coherence, and current statistics (Bruder, Fazio, and Schoeller, 1996; Hackenbroich and Weidenmüller, 1996; König and Gefen, 2001, 2002; Weidenmüller, 2003; Urban, König, and Fazio, 2008; Urban and König, 2009; Hiltscher, Governale, and König, 2010), and entanglement (Loss and Sukhorukov, 2000). We have provided here some of the key references, but we acknowledge that a fair discussion of transport in rings and quantum-dot setups would require its own review. One interesting aspect of rings is that currents can follow different paths, depending on the parameters. For instance, while overall the current enters the system at one point and leaves in another, within the ring it could follow an overall clockwise or counterclockwise path, or even move on both sides of the ring in the same direction (Xu, Choo *et al.*, 2019), while spin and energy currents can follow different patterns.

Last, we also point out that molecules are a prominent example of beyond 1D systems, in which it is important to study transport properties. Given the vastness of the research done on molecular transport, we direct the interested reader to Nitzan and Ratner (2003), Tao (2009), Dubi and Di Ventra (2011), Zimbovskaya and Pederson (2011), and Segal and Agarwalla (2016).

I. Phase transitions

Phase transitions represent abrupt transitions that take place when one changes an external parameter such as the temperature. In classical phase transitions, such as the melting of ice, the driver of the transition is thermal fluctuations, while quantum phase transitions (QPTs) (Sachdev, 2011), such as the superfluid-to-Mott-insulator transition (Fisher *et al.*, 1989; Jaksch *et al.*, 1998; Greiner *et al.*, 2002), are driven by quantum fluctuations.[19] Conversely, *dissipative phase transitions* are driven by a competition between nonequilibrium fluctuations produced by the coupling to the environment and internal system parameters.

As an example of a dissipative phase transition, consider the electron shuttle, which [in analogy with a ball pendulum between two capacitor plates (Kim *et al.*, 2015)] can be realized by a single electron transistor mounted on a harmonic oscillator system (Gorelik *et al.*, 1998). The single electron transistor can be modeled by a LME such as of the Redfield type as in Eq. (28) to describe electronic tunneling to the leads and the oscillator by a local Fokker-Planck equation (equivalent to an oscillator-local master equation of the Redfield type in the classical limit) (Novotný, Donarini, and Jauho, 2003; Strasberg, Wächtler, and Schaller, 2021). The tunneling depends nonlinearly on the oscillator position, and the phase transition manifests as a sharp onset of autonomous self-oscillations. This transition has been studied in various works, highlighting the FCS of electron transfers (Flindt, Novotný, and Jauho, 2004) (Sec. II.I) or its thermodynamic properties (Wächtler *et al.*, 2019) (Sec. II.D). Further experimental (Park *et al.*, 2000; Scheible and Blick, 2004; Moskalenko *et al.*, 2009; König and Weig, 2012) and theoretical (Joachim, Gimzewski, and Aviram, 2000; Shekhter *et al.*, 2003; Galperin, Ratner, and Nitzan, 2007; Galperin *et al.*, 2008)

[19]This includes not only the more common ground-state transitions, but also excited-state phase transitions (Cejnar *et al.*, 2021), in which the level density changes abruptly, and topological phase transitions (Hasan and Kane, 2010), where some eigenstates undergo topological changes.

studies demonstrate the use of LMEs to explain dissipative nonequilibrium phenomena.

There are many natural questions that one can then ask regarding phase transitions and boundary-driven systems, such as (i) How does a phase transition affect the transport properties of a system? (ii) Can transport be used as an indicator of the occurrence of a phase transition? (iii) Are the character and position of the critical point and the nature of the phases altered or induced by the presence of the reservoirs?

In Markovian systems described by the GKSL master equation (11), the Liouvillian $\mathcal{L}$, not the Hamiltonian, becomes the central object of interest (Morrison and Parkins, 2008; Kessler *et al.*, 2012; Minganti *et al.*, 2018). Thus, while a QPT can be associated with the ground state of the Hamiltonian, a dissipative transition is associated with the NESS, which is simply the right eigenstate of $\mathcal{L}$ with a vanishing eigenvalue; cf. Eq. (124). Similarly, the Hamiltonian energy gap that closes at the critical point for QPTs is replaced by the gap with the next eigenvalue of $\mathcal{L}$ (Minganti *et al.*, 2018). In some systems, dissipation affects only a transition that already occurs in the isolated system, e.g., by shifting the critical point (Morrison and Parkins, 2008; Dalidovich and Kennett, 2009; Bhaseen *et al.*, 2012). In other models, it may induce entirely new behavior.

In previous sections we saw that in systems driven by LMEs transport properties can be significantly altered at the transition point. For instance, in the XXZ chain, transport changes from ballistic to diffusive to insulating as Δ crosses the critical value $\Delta_c = 1$ (Fig. 11). At $\Delta_c = 1$, transport can be superdiffusive for small boundary driving, and subdiffusive for large boundary driving. As mentioned in Sec. IV.D, it is also possible to have phase transitions without interaction. For instance, in the AAH model, which uses the potential of Eq. (163), the system is insulating in one phase and ballistic in the other and shows anomalous tranport at the transition (Fig. 13). Another well-studied example (see also Sec. IV.H) is a ladder in the presence of a magnetic field; cf. Eq. (175). The QPT takes the ground state from a Meissner phase, characterized by currents only at the edges, to a vortex phase, in which the ground state has vortices of currents. The transport properties of this setup were discussed in Sec. IV.H. Here we add that there is also a significant change in the relaxation timescale toward the steady state (Guo and Poletti, 2017b). More precisely, the rapidity of the slowest decaying state scales as L^{-3}, except at the phase transition where it scales as L^{-5}. As shown by Prosen (2008) and Žnidarič (2015), this is due to the change in the momentum k dependence of the energy dispersion relation from $\omega(k) \propto k^2$ to k^4. The model in Eq. (175) also shows an excited-state QPT in which a gap opens in the density of states.

Continuing the review of noninteracting systems, Prosen and Pižorn (2008) considered the XY model [Eq. (54) with $J_z = 0$]. In particular, they parametrized the Hamiltonian with $J_x = J(1+\delta)/2$, $J_y = J(1-\delta)/2$, $h_i = h$, and a coupling to baths described by a LME of the type of Eq. (9). They found the existence of a critical magnetic field magnitude $h_c/J = 1 - \delta^2$: Below this critical value, the single-particle correlations present long-range order and the operator space entanglement entropy (OSEE), which is a measure of the complexity of the operator (Prosen and Pižorn, 2007; Prosen and Žnidarič, 2009), grows linearly with L. Above the critical value the correlations decay and the OSEE saturates to a constant value. This transition is related not to a phase transition in the ground state of the system but to dynamical properties of the system (Pižorn and Prosen, 2009). The out-of-equilibrium transition can also be observed when using the Redfield-II master equation (27), as shown by Prosen and Žunkovič (2010).

In bosonic systems one can also consider the effects of Bose-Einstein condensation. Vorberg *et al.* (2013) showed that the presence of multiple macroscopically occupied states can significantly enhance transport in noninteracting bosonic chains.

As mentioned, the fact that a phase transition affects transport also implies that with GMEs one can use the current to identify signatures of phase transitions that occurred in the isolated systems discussed by Vogl, Schaller, and Brandes (2011) and Schaller, Vogl, and Brandes (2014). An example is the critical nature of the eigenstates of the AAH or Fibonacci model (Sec. IV.D). In such scenarios, Varma, de Mulatier, and Žnidarič (2017b) found that the magnetization profile shows a fractal behavior.

Phase transitions can turn systems into a strong rectifier (see Sec. IV.G for a more in-depth discussion), and this phenomenology can in itself be a probe of the phase transition; see Balachandran *et al.* (2018) and Sec. IV.G. In a completely different setup, Schaller, Giusteri, and Celardo (2016) considered a system coupled differently to each of the two baths and observed that when the system undergoes a phase transition the rectification becomes significantly stronger. It is a challenging task to develop accurate models to describe the out-of-equilibrium dynamics close to criticality. Recent advances in this direction were obtained by Wächtler and Schaller (2020), who used polaron transforms and reaction coordinates (Secs. II.H.1 and II.H.3) to obtain thermodynamically consistent equations.

V. SUMMARY AND OUTLOOK

In this review we have examined theoretical aspects of boundary-driven systems, focusing on models to describe them (Sec. II), techniques to analyze them (Sec. III), and the emerging phenomenology (Sec. IV). The models studied in Sec. II have revealed that the local and global master equations are complementary tools capable of addressing different parameter regimes of open nonequilibrium systems. Transport theory shows, in particular, that for a proper thermodynamic interpretation the computed currents must properly reflect the corresponding energy balances between the system and the reservoirs. We have also exposed methods to explore the strong-coupling regime. However, apart from exact solutions, these methods are capable of exploring only small regions of the parameter space. This means that none of these methods should be used naively beyond their range of validity. In particular, GKSL approaches can be deceptive in the sense that a formally correct solution can be far from being physically correct.

Many important questions remain largely unexplored. For example, within the exposed theoretical framework it would

be interesting to consider varying degrees of locality by treating only certain internal junctions of a multipartite system perturbatively. This would yield dissipators acting nontrivially only on a few sites of a larger system, and it would be interesting to learn how the spectral changes of random Liouvillians (Timm, 2009; Can, 2019; Lange and Timm, 2021), as a function of locality (Denisov *et al.*, 2019; Wang, Piazza, and Luitz, 2020), are linked to physical phenomena. Furthermore, while symmetries in the full counting statistics such as the fluctuation theorem (Crooks, 1999) are naturally reflected in GMEs (Esposito, Harbola, and Mukamel, 2009; Campisi, Hänggi, and Talkner, 2011), they are less well explored in LMEs. For example, the standard thermodynamic uncertainty relation for Pauli-type rate equations (Barato and Seifert, 2015; Gingrich *et al.*, 2016) need not be respected by LMEs or Redfield equations (Liu and Segal, 2021). The fluctuation theorem alone would enforce weaker uncertainty relations (Hasegawa and Van Vu, 2019; Timpanaro *et al.*, 2019). To explore the long-time limit of strongly interacting systems, or simply large systems with small energy gaps, would also require us to advance the corresponding theoretical description. Here both GMEs and LMEs have issues since approximations like the secular one may fail. With such issues resolved, it would be interesting to consider the dynamics and transport characteristics of larger and strongly interacting systems (Navez and Schützhold, 2010; Queisser *et al.*, 2014). Systems for which a rich dynamics can be expected are Fermi-Hubbard models (Wu and Eckardt, 2019; Kleinherbers *et al.*, 2020; Kolovsky, 2020; Wu and Eckardt, 2020) or higher-dimensional spin systems [such as higher-dimensional lattices or irregular spin networks (Farhi *et al.*, 2001) with quantum information applications]. One could then go beyond mere heat transport applications, and also revisit the development of correlations inside the system from the perspective of information processing. Still, with their contractive properties GKSL master equations can treat only a fraction of all possible dynamics. Self-oscillatory systems (Gorelik *et al.*, 1998; Novotný, Donarini, and Jauho, 2003) require a nonlinear ingredient, and it is questionable whether this can be achieved with GKSL approaches.

These arguments encourage the search for alternative approaches for treating open systems. The few exactly solvable models can assist as benchmarks in this endeavor. Small steps include discarding or avoiding certain approximations, such as the secular one (Hartmann and Strunz, 2020; McCauley *et al.*, 2020). More ambitiously, one may also consider methods to find approximations to the full Kraus map dynamics, aiming at a picture consistent with thermodynamic laws.

As for the methods discussed in Sec. III, we want to add a few comments. Boundary-driven problems are usually difficult to solve owing to the large Hilbert space dimension, together with the need to work with density matrices instead of pure states. In this aspect, the use of tensor network methods is currently revolutionizing the field, with new approaches being invented all the time; see Sec. III.E. Tools such as entanglement entropy have greatly assisted in the development of tensor networks for closed systems but are not readily extensible to open dynamics. This is one of the challenges that must be overcome. The other challenge is to gain a better understanding of the typical tensor structures of boundary-driven systems. Most open system models use MPSs. But other structures such as tree tensor networks and neural-network states could offer advantages in certain cases.

Once again analytical solutions offer valuable insight. The results discussed in Sec. III.F highlight the underlying tensor structure of the NESS but hold only for special setups. In parallel to the development of novel tensor network algorithms, the discovery of new models amenable to analytical treatment is therefore highly desirable.

Another related challenge is in the description of boundary-driven systems with different geometries. This does not necessarily indicate higher dimensionality; it could instead suggest more complex bond structures, such as the network illustrated in Fig. 2. These systems appear frequently in biological processes, molecular transport, nuclear magnetic resonance, optomechanics, and quantum-dot devices. Most solution methods can handle this kind of geometry, but few are actually optimized for it. Bridging this gap is another important open challenge in the field.

In Sec. IV we have reviewed the different transport properties and phenomena that can emerge in boundary-driven quantum systems. We have described systems with distinct transport properties (i.e., insulating, subdiffusive, diffusive, superdiffusive, and ballistic) and have showed phase diagrams for prototypical models in clean conditions with disorder and with a quasiperiodic potential (Figs. 11–13). Many of these diagrams, however, are still incomplete. For instance, in Fig. 11 the transport properties in the vertical line for anisotropy $\Delta = 1$ are still unknown. The models presented are also often studied only close to infinite temperature, as only in this regime can one investigate large enough systems to be able to extract the transport exponent. This is made worse by the small values that the currents tend to reach. The same type of problem occurs when studying negative differential conductance (Sec. IV.F) or rectification (Sec. IV.G), which occurs primarily when the bath imposes large biases and not small ones near the infinite-temperature state.

For interacting systems, most studies have relied on tensor network methods to describe the steady states (Sec. III.E). However, for large system sizes the bond dimensions needed to describe the steady state accurately can be too large to make computations practical. This is particularly relevant in systems beyond the nearest-neighbor 1D chains. In Sec. IV.H we have showed that geometries such as ladders, or 2D systems, can have significantly different properties than their 1D counterpart. For instance, an XXZ chain could be integrable and ballistic, while an XXZ ladder with the same magnitude of anisotropy would be nonintegrable and diffusive (Žnidarič, 2013b). Because of the presence of ulterior symmetries in the ladders, it is even possible that the same system is ballistic in some symmetry sectors but diffusive in others (Žnidarič, 2013a).

Going beyond 1D nearest-neighbor chains also allows one to introduce other terms in the Hamiltonian, such as gauge fields on plaquettes, which can induce quantum phase transitions in the ground state or abrupt changes in the density

of states (excited-state QPTs), significantly affecting transport across the system. In ladders such QPTs can already occur in noninteracting systems (Kardar, 1986; Granato, 1990), and hence can be studied up to large system sizes. However, interactions can affect their transport properties, and this is still a vastly unexplored area.

Phase transitions can significantly affect the transport properties of the system, as reviewed in Sec. IV.I. We stress here that this can be seen from two parallel and equally interesting points of view. From one side, one can vary a parameter to induce a phase transition as a way to control transport properties in a device. Conversely, since a phase transition can drastically change the transport properties, one can design detectors that function by measuring currents in systems that can go through a phase transition if some external parameters are varied. Additionally, the impact of topological and excited-state phase transition on transport properties requires more research (Benito *et al.*, 2016).

Another topic currently under intense study concerns the complexity of boundary-driven steady states. This has been analyzed through the OSEE (Sec. IV.I), the levels statistics of the steady state (Prosen and Žnidarič, 2013), or the effective Hamiltonian (Sá, Ribeiro, and Prosen, 2020b). The OSEE in 1D steady states may follow an area or a volume law. The level spacing of the steady state or the effective Hamiltonian can follow a Poisson distribution for integrable or localized systems, or a Wigner-Dyson distribution for nonintegrable ones. This mirrors the behavior of unitary chaotic systems, in which the change from Poisson to Wigner-Dyson statistics of the energy level spacing is associated with a passage from regular to chaotic dynamics (Casati, Valz-Gris, and Guarnieri, 1980; Bohigas, Giannoni, and Schmit, 1984; D'Alessio *et al.*, 2016). For the overall open system setup, one needs to take into account that rapidities, unlike eigenvalues of a Hamiltonian, can be complex numbers, and one thus needs to consider the distance in a 2D space (Sá, Ribeiro, and Prosen, 2020a; Li, Prosen, and Chan, 2021). Recently it was shown that Liovillians of GKSL form with randomly chosen jump operators (Can, 2019; Can *et al.*, 2019) tend, in the thermodynamic limit, to a universal lemon shaped spectrum of rapidities in the complex plane (Timm, 2009; Denisov *et al.*, 2019; Wang, Piazza, and Luitz, 2020). Further analyses on random Liouvillians were undertaken by Can *et al.* (2019), Sá, Ribeiro, and Prosen (2020b), Sá *et al.* (2020), and Lange and Timm (2021). Depending on the symmetries in the system, other universality classes in the level-spacing distribution of the rapidities have been uncovered (Hamazaki *et al.*, 2020), and it has been shown in an increasing number of works that the level-spacing statistics of nonintegrable open systems tend to be one of these classes (Akemann *et al.*, 2019; Hamazaki *et al.*, 2020; Sá, Ribeiro, and Prosen, 2020a; Li, Prosen, and Chan, 2021; Rubio-García, Molina, and Dukelsky, 2022). There have also been recent developments in understanding the relation between the scaling of the rapidities with system size and the scaling of the current (Mori and Shirai, 2020). The relaxation gap, in particular, does not necessarily scale in the same way as the current (Žnidarič, 2015).

A more recent field of research that was not covered in this review is that of periodically driven systems. Prosen and Ilievski (2011) found that the driving could result in the emergence of long-range spin-spin correlations. Purkayastha and Dubi (2017) realized that the instantaneous current can be orders of magnitude larger than the average current, making it experimentally measurable. Periodic drivings bring an entirely new dimension to the study of transport because they can be used to model engines, refrigerators, and heat pumps; cf. Thouless (1983), Switkes *et al.* (1999), Xiao, Chang, and Niu (2010), Kosloff (2013), Pekola *et al.* (2013), Kaestner and Kashcheyevs (2015), Van den Broeck and Esposito (2015), Goold *et al.* (2016), Millen and Xuereb (2016), Vinjanampathy and Anders (2016), Benenti *et al.* (2017), and Lacerda *et al.* (2022). The modeling of open quantum systems subject to time-dependent driving must be considered carefully, however. For periodic driving and weak coupling, one may rely on Floquet master equations (Grifoni and Hänggi, 1998; Breuer and Petruccione, 2002). In the strong-coupling regime, one may instead employ methods simulating both the system and the bath (Secs. II.H.2 and II.H.4), which are extendable to driven systems.

Finally, in this review we have not covered experimental papers in detail, although we have cited a number of experimental results in various sections. An important direction for future research is the proposal of novel experiments in new setups, such as ultracold atoms (Damanet *et al.*, 2019) and trapped ions (Bermudez, Bruderer, and Plenio, 2013), both of which allow a high degree of control (Bloch, Dalibard, and Zwerger, 2008; Blatt and Roos, 2012) and can lead to applications in atomtronics (Seaman *et al.*, 2007; Amico *et al.*, 2017, 2021). We have highlighted experiments that use ultracold atoms to create two reservoirs, connected by a tunable channel through which both particles and energy can flow (Brantut *et al.*, 2012, 2013; Stadler *et al.*, 2012; Husmann *et al.*, 2015, 2018; Krinner *et al.*, 2015, 2016; Lebrat *et al.*, 2018). Experiments would be the first step toward the design and production of new materials and devices, such as tunable spin and heat current rectifiers, transistors, and sensors.

ACKNOWLEDGMENTS

We thank the referees involved in the peer-review process for the detailed and constructive reports, which helped us to significantly improve the quality of this review. We also thank B. K. Agarwalla, V. Balachandran, G. Benenti, B. Buča, A. Eckardt, J. P. Garrahan, J. Goold, C. Guo, Z. L. Lim, J. J. Mendoza-Arenas, E. Pereira, T. Prosen, A. Purkayastha, L. Sá, A. Scardicchio, D. Segal, P. Stegmann, S. R. Taylor, J. Thingna, X. Xu, and M. Žnidarič for feedback on early draft of this review. We thank, in particular, J. J. Mendoza-Arenas and M. Žnidarič for sharing their data for Fig. 12. D. P. acknowledges support from the Ministry of Education of Singapore AcRF MOE Tier-II (Projects No. MOE2018-T2-2-142 and No. MOE-T2EP50120-0019). G. S. acknowledges support from the Helmholtz high-potential program and previous support from the DFG (Project No. 278162697-CRC 1242). G. T. L. and D. P. acknowledge the financial support and hospitality of the International Centre

for Theoretical Physics (ICTP) in Trieste, Italy, where this project began.

APPENDIX: EXACT SOLUTION VIA LAPLACE TRANSFORMS

Here we provide details for the exact time-dependent solution discussed in Sec. II.G. The star representation has the advantage that, by computing the Laplace transform $C_{k\alpha}(z) = \int_0^\infty \boldsymbol{c}_{k\alpha}(t) e^{-zt} dt$, we can eliminate the reservoir modes

$$C_{kL}(z) = \frac{c_{kL}}{z + \mathrm{i}\epsilon_{kL}} - \mathrm{i}\frac{t_{kL} D_1(z)}{z + \mathrm{i}\epsilon_{kL}},$$
$$C_{kR}(z) = \frac{c_{kR}}{z + \mathrm{i}\epsilon_{kR}} - \mathrm{i}\frac{t_{kR} D_N(z)}{z + \mathrm{i}\epsilon_{kR}}, \tag{A1}$$

leaving only the following Laplace-transformed equations for the system operators to solve:

$$\begin{aligned} z D_a(z) - d_a &= -\mathrm{i}\sum_j h_{aj} D_j(z):\ 2 \le a \le N-1, \\ z D_1(z) - d_1 &= -\mathrm{i}\sum_j h_{1j} D_j(z) - \mathrm{i}\sum_k \frac{t_{kL} c_{kL}}{z + \mathrm{i}\epsilon_{kL}} \\ &\quad - \sum_k \frac{|t_{kL}|^2}{z + \mathrm{i}\epsilon_{kL}} D_1(z), \\ z D_N(z) - d_N &= -\mathrm{i}\sum_j h_{Nj} D_j(z) - \mathrm{i}\sum_k \frac{t_{kR} c_{kR}}{z + \mathrm{i}\epsilon_{kR}} \\ &\quad - \sum_k \frac{|t_{kR}|^2}{z + \mathrm{i}\epsilon_{kR}} D_N(z). \end{aligned} \tag{A2}$$

Thereby one can express the Laplace-transformed system operators $D_j(z)$ in terms of the initial system (d_j) and reservoir ($c_{k\alpha}$) operators, and by performing inverse Laplace transforms one can in principle compute all observables exactly.

To be more specific, we now consider the case $N = 2$. We can recast the equations for the system annihilation operators as

$$G^{-1}(z) \begin{pmatrix} D_1(z) \\ D_2(z) \end{pmatrix} = \begin{pmatrix} d_1 \\ d_2 \end{pmatrix} - \mathrm{i}\sum_k \begin{pmatrix} [t_{kL}/(z+\mathrm{i}\epsilon_{kL})] c_{kL} \\ [t_{kR}/(z+\mathrm{i}\epsilon_{kR})] c_{kR} \end{pmatrix},$$
$$G^{-1}(z) = \left[z \cdot \mathbb{1} + \mathrm{i} \begin{pmatrix} h_{11} & h_{12} \\ h_{21} & h_{22} \end{pmatrix} + \sum_k \begin{pmatrix} |t_{kL}|^2/(z+\mathrm{i}\epsilon_{kL}) & 0 \\ 0 & |t_{kR}|^2/(z+\mathrm{i}\epsilon_{kR}) \end{pmatrix} \right], \tag{A3}$$

where $G_{ij}(z)$ is the Green's function. By inversion, we can write this in the form

$$D_i(z) = G_{i1}(z) d_1 + G_{i2}(z) d_2 - \mathrm{i}\sum_k \frac{t_{kL} G_{i1}(z)}{z + \mathrm{i}\epsilon_{kL}} c_{kL} - \mathrm{i}\sum_k \frac{t_{kR} G_{i2}(z)}{z + \mathrm{i}\epsilon_{kR}} c_{kR}. \tag{A4}$$

Employing the initial product assumption

$$\rho_0 = \rho_S^0 \otimes \frac{e^{-\beta_L (H_B^{(L)} - \mu_L N_B^{(L)})}}{Z_B^{(L)}} \otimes \frac{e^{-\beta_R (H_B^{(R)} - \mu_R N_B^{(R)})}}{Z_B^{(R)}}, \tag{A5}$$

one then finds via the inverse Laplace transform (Bromwich integral) that the system observables can be expressed in terms of the initial expectation values as

$$\begin{aligned} \langle d_i^\dagger d_j \rangle_t &= g_{i1}^*(t) g_{j1}(t) \langle d_1^\dagger d_1 \rangle_0 + g_{i2}^*(t) g_{j2}(t) \langle d_2^\dagger d_2 \rangle_0 \\ &\quad + g_{i1}^*(t) g_{j2}(t) \langle d_1^\dagger d_2 \rangle_0 + g_{i2}^*(t) g_{j1}(t) \langle d_2^\dagger d_1 \rangle_0 \\ &\quad + \sum_k |t_{kL}|^2 g_{i1kL}^*(t) g_{j1kL}(t) f_L(\epsilon_{kL}) \\ &\quad + \sum_k |t_{kR}|^2 g_{i2kR}^*(t) g_{j2kR}(t) f_R(\epsilon_{kR}), \end{aligned} \tag{A6}$$

where the initial reservoir properties are encoded in the Fermi functions $f_\alpha(\epsilon_{k\alpha})$ and $g_{ij}(t)$ and $g_{ijk\alpha}(t)$ are the inverse Laplace transforms of $G_{ij}(z)$ and $-\mathrm{i}G_{ij}(z)/(z + \mathrm{i}\epsilon_{k\alpha})$, respectively.

As a first observation, although for finite L_α the evolution is quasiperiodic, a stationary long-term limit may arise from the exact dynamics. When we make the reservoirs larger ($L_\alpha \to \infty$), their single-particle spectra from Eq. (75) continuously cover the interval $[\epsilon - 2\tau, \epsilon + 2\tau]$ and we can use the spectral coupling density of Eq. (77). To invert the Laplace transform, we can then analytically calculate expressions like

$$\sum_k \frac{|t_{k\alpha}|^2}{z + \mathrm{i}\epsilon_{k\alpha}} = \frac{1}{2\pi} \int \frac{\Gamma_\alpha(\omega)}{z + \mathrm{i}\omega} d\omega = \frac{\tau_\alpha^2}{2\tau^2} \left(\sqrt{1 + \frac{4\tau^2}{(z + \mathrm{i}\epsilon)^2}} - 1 \right) (z + \mathrm{i}\epsilon), \tag{A7}$$

which has a branch cut discontinuity along the imaginary axis in the interval $\mathrm{i}[-\epsilon - 2\tau, -\epsilon + 2\tau]$ that has to be considered when inverting the Laplace transform.

REFERENCES

Abanin, D. A., E. Altman, I. Bloch, and M. Serbyn, 2019, Rev. Mod. Phys. **91**, 021001.

Abanin, D. A., and Z. Papić, 2017, Ann. Phys. (Berlin) **529**, 1700169.

Aeberhard, U., 2011, J. Comput. Electron. **10**, 394.

Agarwal, K., E. Altman, E. Demler, D. Gopalakrishnan, Sarang Huse, and M. Knap, 2017, Ann. Phys. (Berlin) **529**, 1600326.

Agarwal, K., S. Gopalakrishnan, M. Knap, M. Müller, and E. Demler, 2015, Phys. Rev. Lett. **114**, 160401.

Aharonov, Y., and D. Bohm, 1959, Phys. Rev. **115**, 485.

Ajisaka, S., and F. Barra, 2013, Phys. Rev. B **87**, 195114.

Ajisaka, S., F. Barra, C. Mejía-Monasterio, and T. Prosen, 2012, Phys. Rev. B **86**, 125111.

Akemann, G., M. Kieburg, A. Mielke, and T. Prosen, 2019, Phys. Rev. Lett. **123**, 254101.

Akera, H., 1993, Phys. Rev. B **47**, 6835.

Al-Assam, S., S. R. Clark, and D. Jaksch, 2017, J. Stat. Mech. 093102.

Albert, V. V., and L. Jiang, 2014, Phys. Rev. A **89**, 022118.
Aleiner, I., P. Brouwer, and L. Glazman, 2002, Phys. Rep. **358**, 309.
Alicki, R., 1979, J. Phys. A **12**, L103.
Amato, G., H.-P. Breuer, S. Wimberger, A. Rodríguez, and A. Buchleitner, 2020, Phys. Rev. A **102**, 022207.
Amico, L., G. Birkl, M. Boshier, and L.-C. Kwek, 2017, New J. Phys. **19**, 020201.
Amico, L., *et al.*, 2021, AVS Quantum Sci. **3**, 039201.
Anantram, M. P., and F. Léonard, 2006, Rep. Prog. Phys. **69**, 507.
Anderson, P. W., 1958, Phys. Rev. **109**, 1492.
Anto-Sztrikacs, N., and D. Segal, 2021, New J. Phys. **23**, 063036.
Aoki, K., and D. Kusnezov, 2001, Phys. Rev. Lett. **86**, 4029.
Araki, H., and E. J. Woods, 1963, J. Math. Phys. (N.Y.) **4**, 637.
Arrachea, L., G. S. Lozano, and A. A. Aligia, 2009, Phys. Rev. B **80**, 014425.
Asadian, A., D. Manzano, M. Tiersch, and H. J. Briegel, 2013, Phys. Rev. E **87**, 012109.
Atala, M., M. Aidelsburger, M. Lohse, J. T. Barreiro, B. Paredes, and I. Bloch, 2014, Nat. Phys. **10**, 588.
Aubry, S., and G. André, 1980, Ann. Isr. Phys. Soc. **3**, 133.
Audenaert, K., J. Eisert, M. B. Plenio, and R. F. Werner, 2002, Phys. Rev. A **66**, 042327.
Aurell, E., 2018, Phys. Rev. E **97**, 042112.
Baer, R., and R. Kosloff, 1997, J. Chem. Phys. **106**, 8862.
Bagchi, D., 2015, J. Stat. Mech. P02015.
Bairey, E., C. Guo, D. Poletti, N. H. Lindner, and I. Arad, 2020, New J. Phys. **22**, 032001.
Balachandran, V., G. Benenti, E. Pereira, G. Casati, and D. Poletti, 2018, Phys. Rev. Lett. **120**, 200603.
Balachandran, V., G. Benenti, E. Pereira, G. Casati, and D. Poletti, 2019, Phys. Rev. E **99**, 032136.
Balachandran, V., S. R. Clark, J. Goold, and D. Poletti, 2019, Phys. Rev. Lett. **123**, 020603.
Banchi, L., P. Giorda, and P. Zanardi, 2014, Phys. Rev. E **89**, 022102.
Barato, A. C., and U. Seifert, 2015, Phys. Rev. Lett. **114**, 158101.
Bargmann, V., 1961, Commun. Pure Appl. Math. **14**, 187.
Bar Lev, Y., G. Cohen, and D. R. Reichman, 2015, Phys. Rev. Lett. **114**, 100601.
Barra, F., 2015, Sci. Rep. **5**, 14873.
Bartels, R. H., and G. W. Stewart, 1972, Commun. ACM **15**, 820.
Barthel, T., and Y. Zhang, 2022, arXiv:2112.08344.
Basko, D. M., L. Aleiner, and B. L. Altshuler, 2006, Ann. Phys. (N.Y.) **321**, 1126.
Baumgartner, B., and H. Narnhofer, 2008, J. Phys. A **41**, 395303.
Benenti, G., G. Casati, C. Mejía-Monasterio, and M. Peyrard, 2016, in *Thermal Transport in Low Dimensions: From Statistical Physics to Nanoscale Heat Transfer*, edited by S. Lepri (Springer International Publishing, Cham, Switzerland), Chap. 10, pp. 365–407.
Benenti, G., G. Casati, T. Prosen, and D. Rossini, 2009, Europhys. Lett. **85**, 37001.
Benenti, G., G. Casati, T. Prosen, D. Rossini, and M. Žnidarič, 2009, Phys. Rev. B **80**, 035110.
Benenti, G., G. Casati, K. Saito, and R. S. Whitney, 2017, Phys. Rep. **694**, 1.
Benito, M., M. Niklas, and S. Kohler, 2016, Phys. Rev. B **94**, 195433.
Benito, M., M. Niklas, G. Platero, and S. Kohler, 2016, Phys. Rev. B **93**, 115432.
Bera, S., G. De Tomasi, F. Weiner, and F. Evers, 2017, Phys. Rev. Lett. **118**, 196801.
Bermudez, A., M. Bruderer, and M. B. Plenio, 2013, Phys. Rev. Lett. **111**, 040601.
Bertini, B., F. Heidrich-Meisner, C. Karrasch, T. Prosen, R. Steinigeweg, and M. Žnidarič, 2021, Rev. Mod. Phys. **93**, 025003.
Bhandari, B., R. Fazio, F. Taddei, and L. Arrachea, 2021, Phys. Rev. B **104**, 035425.
Bhaseen, M. J., J. Mayoh, B. D. Simons, and J. Keeling, 2012, Phys. Rev. A **85**, 013817.
Biella, A., M. Collura, D. Rossini, A. De Luca, and L. Mazza, 2019, Nat. Commun. **10**, 4820.
Biella, A., A. De Luca, J. Viti, D. Rossini, L. Mazza, and R. Fazio, 2016, Phys. Rev. B **93**, 205121.
Biggerstaff, D. N., R. Heilmann, A. A. Zecevik, M. Gräfe, M. A. Broome, A. Fedrizzi, S. Nolte, A. Szameit, A. G. White, and I. Kassal, 2016, Nat. Commun. **7**, 11282.
Blasone, M., P. Jizba, and G. Vitiello, 2011, *Quantum Field Theory and Its Macroscopic Manifestations: Boson Condensation, Ordered Patterns and Topological Defects* (World Scientific, Singapore).
Blatt, R., and C. F. Roos, 2012, Nat. Phys. **8**, 277.
Bloch, I., J. Dalibard, and W. Zwerger, 2008, Rev. Mod. Phys. **80**, 885.
Boers, D. J., B. Goedeke, D. Hinrichs, and M. Holthaus, 2007, Phys. Rev. A **75**, 063404.
Boese, D., W. Hofstetter, and H. Schoeller, 2002, Phys. Rev. B **66**, 125315.
Bohigas, O., M. J. Giannoni, and C. Schmit, 1984, Phys. Rev. Lett. **52**, 1.
Bolsterli, M., M. Rich, and W. M. Visscher, 1970, Phys. Rev. A **1**, 1086.
Bombelli, L., R. K. Koul, J. Lee, and R. D. Sorkin, 1986, Phys. Rev. D **34**, 373.
Bonnes, L., and A. Lauchli, 2014, arXiv:1411.4831.
Bordia, P., H. Lüschen, S. Scherg, S. Gopalakrishnan, M. Knap, U. Schneider, and I. Bloch, 2017, Phys. Rev. X **7**, 041047.
Bours, L., B. Sothmann, M. Carrega, E. Strambini, A. Braggio, E. M. Hankiewicz, L. W. Molenkamp, and F. Giazotto, 2019, Phys. Rev. Appl. **11**, 044073.
Braggio, A., C. Flindt, and T. Novotný, 2009, J. Stat. Mech. P01048.
Brandão, F. G. S. L., T. S. Cubitt, A. Lucia, S. Michalakis, and D. Perez-Garcia, 2015, J. Math. Phys. (N.Y.) **56**, 102202.
Brandes, T., 2005, Phys. Rep. **408**, 315.
Brandes, T., 2008, Ann. Phys. (Berlin) **17**, 477.
Brandes, T., 2010, Phys. Rev. Lett. **105**, 060602.
Brantut, J.-P., C. Grenier, J. Meineke, D. Stadler, S. Krinner, C. Kollath, T. Esslinger, and A. Georges, 2013, Science **342**, 713.
Brantut, J.-P., J. Meineke, D. Stadler, S. Krinner, and T. Esslinger, 2012, Science **337**, 1069.
Brattain, W. H., 1951, Rev. Mod. Phys. **23**, 203.
Brenes, M., E. Mascarenhas, M. Rigol, and J. Goold, 2018, Phys. Rev. B **98**, 235128.
Brenes, M., J. J. Mendoza-Arenas, A. Purkayastha, M. T. Mitchison, S. R. Clark, and J. Goold, 2020, Phys. Rev. X **10**, 031040.
Breuer, H.-P., 2012, J. Phys. B **45**, 154001.
Breuer, H.-P., E.-M. Laine, J. Piilo, and B. Vacchini, 2016, Rev. Mod. Phys. **88**, 021002.
Breuer, H.-P., and F. Petruccione, 2002, *The Theory of Open Quantum Systems* (Oxford University Press, New York).
Bruder, C., R. Fazio, and H. Schoeller, 1996, Phys. Rev. Lett. **76**, 114.
Bruderer, M., L. D. Contreras-Pulido, M. Thaller, L. Sironi, D. Obreschkow, and M. B. Plenio, 2014, New J. Phys. **16**, 033030.
Buča, B., C. Booker, and D. Jaksch, 2022, SciPost Phys. **12**, 97.

Buča, B., C. Booker, M. Medenjak, and D. Jaksch, 2020, New J. Phys. **22**, 123040.
Buča, B., and T. Prosen, 2012, New J. Phys. **14**, 073007.
Buča, B., and T. Prosen, 2014, Phys. Rev. Lett. **112**, 067201.
Buča, B., and T. Prosen, 2016, J. Stat. Mech. 023102.
Buča, B., J. Tindall, and D. Jaksch, 2019, Nat. Commun. **10**, 1730.
Bulla, R., T. A. Costi, and T. Pruschke, 2008, Rev. Mod. Phys. **80**, 395.
Bulla, R., H.-J. Lee, N.-H. Tong, and M. Vojta, 2005, Phys. Rev. B **71**, 045122.
Büttiker, M., 1986, Phys. Rev. Lett. **57**, 1761.
Cabot, A., F. Galve, and R. Zambrini, 2017, New J. Phys. **19**, 113007.
Caffarel, M., and W. Krauth, 1994, Phys. Rev. Lett. **72**, 1545.
Cai, Z., and T. Barthel, 2013, Phys. Rev. Lett. **111**, 150403.
Campisi, M., P. Hänggi, and P. Talkner, 2011, Rev. Mod. Phys. **83**, 771.
Can, T., 2019, J. Phys. A **52**, 485302.
Can, T., V. Oganesyan, D. Orgad, and S. Gopalakrishnan, 2019, Phys. Rev. Lett. **123**, 234103.
Carmichael, H. J., 1993, *An Open Systems Approach to Quantum Optics* (Springer, Berlin).
Caroli, C., R. Combescot, P. Nozieres, and D. Saint-James, 1971, J. Phys. C **4**, 916.
Carollo, F., J. P. Garrahan, and I. Lesanovsky, 2018, Phys. Rev. B **98**, 094301.
Carollo, F., J. P. Garrahan, I. Lesanovsky, and C. Pérez-Espigares, 2017, Phys. Rev. E **96**, 052118.
Caruso, F., A. W. Chin, A. Datta, S. F. Huelga, and M. B. Plenio, 2009, J. Chem. Phys. **131**, 105106.
Casagrande, H. P., D. Poletti, and G. T. Landi, 2021, Comput. Phys. Commun. **267**, 108060.
Casati, G., J. Ford, F. Vivaldi, and W. M. Visscher, 1984, Phys. Rev. Lett. **52**, 1861.
Casati, G., F. Valz-Gris, and I. Guarnieri, 1980, Lett. Nuovo Cimento Soc. Ital. Fis. **28**, 279.
Cattaneo, M., G. De Chiara, S. Maniscalco, R. Zambrini, and G. L. Giorgi, 2021, Phys. Rev. Lett. **126**, 130403.
Caux, J.-S., and J. Mossel, 2011, J. Stat. Mech. P02023.
Cavaliere, F., A. Braggio, J. T. Stockburger, M. Sassetti, and B. Kramer, 2004, Phys. Rev. Lett. **93**, 036803.
Cejnar, P., P. Stránský, M. Macek, and M. Kloc, 2021, J. Phys. A **54**, 133001.
Chang, C. W., D. Okawa, A. Majumdar, and A. Zettl, 2006, Science **314**, 1121.
Chen, J., M. A. Reed, A. M. Rawlett, and J. M. Tour, 1999, Science **286**, 1550.
Chen, Shunda, Emmanuel Pereira, and Giulio Casati, 2015, Europhys. Lett. **111**, 30004.
Chen, T., V. Balachandran, C. Guo, and D. Poletti, 2020, Phys. Rev. E **102**, 012155.
Chiaracane, C., F. Pietracaprina, A. Purkayastha, and J. Goold, 2021, Phys. Rev. B **103**, 184205.
Chiaracane, C., A. Purkayastha, M. T. Mitchison, and J. Goold, 2022, Phys. Rev. B **105**, 134203.
Chin, A. W., A. Datta, F. Caruso, S. F. Huelga, and M. B. Plenio, 2010, New J. Phys. **12**, 065002.
Chin, A. W., S. F. Huelga, and M. B. Plenio, 2012, Phil. Trans. R. Soc. A **370**, 3638.
Chin, A. W., A. Rivas, S. F. Huelga, and M. B. Plenio, 2010, J. Math. Phys. (N.Y.) **51**, 092109.
Chioquetta, A., E. Pereira, G. T. Landi, and R. C. Drumond, 2021, Phys. Rev. E **103**, 032108.
Choi, M.-D., 1975, Linear Algebra Appl. **10**, 285.
Clark, S. R., J. Prior, M. J. Hartmann, D. Jaksch, and P. M. B., 2010, New J. Phys. **12**, 025005.
Coffey, W. T., Y. P. Kalmykov, and J. T. Waldron, 2004, *The Langevin Equation: With Applications to Stochastic Problems in Physics, Chemistry and Electrical Engineering*, 2nd ed. (World Scientific, Singapore).
Cohen-Tannoudji, C., and J. Dalibar, 1986, Europhys. Lett. **1**, 441.
Contreras-Pulido, L. D., M. Bruderer, S. F. Huelga, and M. B. Plenio, 2014, New J. Phys. **16**, 113061.
Cookmeyer, T., J. Motruk, and J. E. Moore, 2020, Phys. Rev. B **101**, 174203.
Cormick, C., and C. T. Schmiegelow, 2016, Phys. Rev. A **94**, 053406.
Correa, L. A., B. Xu, and B. M. G. Adesso, 2019, J. Chem. Phys. **151**, 094107.
Crooks, G. E., 1999, Phys. Rev. E **60**, 2721.
Cubitt, T. S., A. Lucia, S. Michalakis, and D. Perez-Garcia, 2015, Commun. Math. Phys. **337**, 1275.
Cuetara, G. B., M. Esposito, and G. Schaller, 2016, Entropy **18**, 447.
Cui, J., J. I. Cirac, and M. C. Bañuls, 2015, Phys. Rev. Lett. **114**, 220601.
D'Abbruzzo, A., and D. Rossini, 2021, Phys. Rev. A **103**, 052209.
Da Fonseca, C., and V. Kowalenko, 2020, Acta Math. Acad. Sci. Hung. **160**, 376.
D'Alessio, L., Y. Kafri, A. Polkovnikov, and M. Rigol, 2016, Adv. Phys. **65**, 239.
Daley, A. J., 2014, Adv. Phys. **63**, 77.
Dalibard, J., Y. Castin, and K. Mølmer, 1992, Phys. Rev. Lett. **68**, 580.
Dalidovich, D., and M. P. Kennett, 2009, Phys. Rev. A **79**, 053611.
Damanet, F., E. Mascarenhas, D. Pekker, and A. J. Daley, 2019, New J. Phys. **21**, 115001.
Das Sarma, S., S. He, and X. C. Xie, 1988, Phys. Rev. Lett. **61**, 2144.
De Chiara, G., G. Landi, A. Hewgill, B. Reid, A. Ferraro, A. J. Roncaglia, and M. Antezza, 2018, New J. Phys. **20**, 113024.
del Rey, M., A. W. Chin, S. F. Huelga, and M. B. Plenio, 2013, J. Phys. Chem. Lett. **4**, 903.
De Nardis, J., M. Medenjak, C. Karrasch, and E. Ilievski, 2019, Phys. Rev. Lett. **123**, 186601.
Denisov, S., T. Laptyeva, W. Tarnowski, D. Chruściński, and K. Życzkowski, 2019, Phys. Rev. Lett. **123**, 140403.
Denniston, C., and C. Tang, 1995, Phys. Rev. Lett. **75**, 3930.
de Vega, I., and D. Alonso, 2017, Rev. Mod. Phys. **89**, 015001.
de Vega, I., and M.-C. Bañuls, 2015, Phys. Rev. A **92**, 052116.
de Vega, I., U. Schollwöck, and F. A. Wolf, 2015, Phys. Rev. B **92**, 155126.
Dhar, A., 2008, Adv. Phys. **57**, 457.
Dhar, A., K. Saito, and P. Hänggi, 2012, Phys. Rev. E **85**, 011126.
Dolfi, M., B. Bauer, S. Keller, A. Kosenkov, T. Ewart, A. Kantian, T. Giamarchi, and M. Troyer, 2014, Comput. Phys. Commun. **185**, 3430.
Donohue, P., and T. Giamarchi, 2001, Phys. Rev. B **63**, 180508.
Dorda, A., M. Nuss, W. von der Linden, and E. Arrigoni, 2014, Phys. Rev. B **89**, 165105.
Droenner, L., and A. Carmele, 2017, Phys. Rev. B **96**, 184421.
Dubi, Y., and M. Di Ventra, 2011, Rev. Mod. Phys. **83**, 131.
Dum, R., A. S. Parkins, P. Zoller, and C. W. Gardiner, 1992, Phys. Rev. A **46**, 4382.
Dum, R., P. Zoller, and H. Ritsch, 1992, Phys. Rev. A **45**, 4879.
Dümcke, R., and H. Spohn, 1979, Z. Phys. B **34**, 419.
Dwiputra, D., and F. P. Zen, 2021, Phys. Rev. A **104**, 022205.
Dzhioev, A. A., and D. S. Kosov, 2011, J. Chem. Phys. **134**, 1.

Economou, E. N., 2006, *Green's Functions in Quantum Physics* (Springer, Berlin).
Ehrlich, T., and G. Schaller, 2021, Phys. Rev. B **104**, 045424.
Eisert, J., M. Cramer, and M. B. Plenio, 2010, Rev. Mod. Phys. **82**, 277.
Englert, B.-G., and G. Morigi, 2002, in *Coherent Evolution in Noisy Environments*, Lecture Notes in Physics Vol. 611, edited by A. Buchleitner and K. Hornberger (Springer, Berlin), p. 611.
Esaki, L., 1958, Phys. Rev. **109**, 603.
Esaki, L., and P. J. Stiles, 1966, Phys. Rev. Lett. **16**, 1108.
Esaki, L., and R. Tsu, 1970, IBM J. Res. Dev. **14**, 61.
Esposito, M., U. Harbola, and S. Mukamel, 2007, Phys. Rev. B **75**, 155316.
Esposito, M., U. Harbola, and S. Mukamel, 2009, Rev. Mod. Phys. **81**, 1665.
Esposito, M., K. Lindenberg, and C. V. den Broeck, 2010, New J. Phys. **12**, 013013.
Esposito, M., and S. Mukamel, 2006, Phys. Rev. E **73**, 046129.
Essler, F. H. L., and L. Piroli, 2020, Phys. Rev. E **102**, 062210.
Evans, D. E., 1977, Commun. Math. Phys. **54**, 293.
Evans, D. E., and H. Hanche-Olsen, 1979, J. Funct. Anal. **32**, 207.
Farhi, E., J. Goldstone, S. Gutmann, J. Lapan, A. Lundgren, and D. Preda, 2001, Science **292**, 472.
Farina, D., G. De Filippis, V. Cataudella, M. Polini, and V. Giovannetti, 2020, Phys. Rev. A **102**, 052208.
Farina, D., and V. Giovannetti, 2019, Phys. Rev. A **100**, 012107.
Finazzi, S., A. Le Boité, F. Storme, A. Baksic, and C. Ciuti, 2015, Phys. Rev. Lett. **115**, 080604.
Fisher, M. P. A., P. B. Weichman, G. Grinstein, and D. S. Fisher, 1989, Phys. Rev. B **40**, 546.
Fishman, M., S. R. White, and E. M. Stoudenmire, 2020, arXiv: 2007.14822.
Fleming, C. H., and N. I. Cummings, 2011, Phys. Rev. E **83**, 031117.
Flindt, C., A. Braggio, and T. Novotný, 2007, AIP Conf. Proc. **922**, 531.
Flindt, C., C. Fricke, F. Hohls, T. Novotný, K. Netocny, T. Brandes, and R. J. Haug, 2009, Proc. Natl. Acad. Sci. U.S.A. **106**, 10116.
Flindt, C., T. Novotný, A. Braggio, and A.-P. Jauho, 2010, Phys. Rev. B **82**, 155407.
Flindt, C., T. Novotný, A. Braggio, M. Sassetti, and A.-P. Jauho, 2008, Phys. Rev. Lett. **100**, 150601.
Flindt, C., T. Novotný, and A.-P. Jauho, 2004, Phys. Rev. B **70**, 205334.
Fornieri, A., M. J. Martínez-Pérez, and F. Giazotto, 2015, AIP Adv. **5**, 053301.
Fourier, J., 1822, *Théorie Analytique de la Chaleur* (Firmin Didot, Paris).
Friedman, H. M., B. K. Agarwalla, and D. Segal, 2018, New J. Phys. **20**, 083026.
Friedman, H. M., and D. Segal, 2019, Phys. Rev. E **100**, 062112.
Frigerio, A., 1978, Commun. Math. Phys. **63**, 269.
Fujisawa, T., T. Hayashi, R. Tomita, and Y. Hirayama, 2006, Science **312**, 1634.
Galperin, M., M. A. Ratner, and A. Nitzan, 2005, Nano Lett. **5**, 125.
Galperin, M., M. A. Ratner, and A. Nitzan, 2007, J. Phys. Condens. Matter **19**, 103201.
Galperin, M., M. A. Ratner, A. Nitzan, and A. Troisi, 2008, Science **319**, 1056.
Ganeshan, S., J. H. Pixley, and S. Das Sarma, 2015, Phys. Rev. Lett. **114**, 146601.
Gangat, A. A., T. I, and Y.-J. Kao, 2017, Phys. Rev. Lett. **119**, 010501.
García-Ripoll, J. J., 2006, New J. Phys. **8**, 305.
García-Ripoll, J. J., S. Dürr, N. Syassen, D. M. Bauer, M. Lettner, G. Rempe, and J. I. Cirac, 2009, New J. Phys. **11**, 013053.
Gardiner, C., and P. Zoller, 2004, *Quantum Noise*, 3rd ed. (Springer, New York).
Garrahan, J. P., and I. Lesanovsky, 2010, Phys. Rev. Lett. **104**, 160601.
Garraway, B. M., 1997a, Phys. Rev. A **55**, 4636.
Garraway, B. M., 1997b, Phys. Rev. A **55**, 2290.
Garraway, B. M., 2011, Phil. Trans. R. Soc. A **369**, 1137.
Garst, M., and A. Rosch, 2001, Europhys. Lett. **55**, 66.
Gaspard, P., and M. Nagaoka, 1999, J. Chem. Phys. **111**, 5668.
Gaudioso, J., L. J. Lauhon, and W. Ho, 2000, Phys. Rev. Lett. **85**, 1918.
Gautschi, W., 2005, J. Comput. Appl. Math. **178**, 215.
Gelbwaser-Klimovsky, D., and A. Aspuru-Guzik, 2015, J. Phys. Chem. Lett. **6**, 3477.
Gerland, U., J. von Delft, T. A. Costi, and Y. Oreg, 2000, Phys. Rev. Lett. **84**, 3710.
Giamarchi, T., and H. J. Schulz, 1987, Europhys. Lett. **3**, 1287.
Giamarchi, T., and H. J. Schulz, 1988, Phys. Rev. B **37**, 325.
Gingrich, T. R., J. M. Horowitz, N. Perunov, and J. L. England, 2016, Phys. Rev. Lett. **116**, 120601.
Golub, G. H., S. Nash, and C. F. Van Loan, 1979, IEEE Trans. Autom. Control **24**, 909.
González, J. O., L. A. Correa, G. Nocerino, J. P. Palao, D. Alonso, and G. Adesso, 2017, Open Syst. Inf. Dyn. **24**, 1740010.
Goold, J., M. Huber, A. Riera, L. del Rio, and P. Skrzypczyk, 2016, J. Phys. A **49**, 143001.
Gopalakrishnan, S., K. Agarwal, E. A. Demler, D. A. Huse, and M. Knap, 2016, Phys. Rev. B **93**, 134206.
Gopalakrishnan, S., and R. Vasseur, 2019, Phys. Rev. Lett. **122**, 127202.
Gorelik, L. Y., A. Isacsson, M. V. Voinova, B. Kasemo, R. I. Shekhter, and M. Jonson, 1998, Phys. Rev. Lett. **80**, 4526.
Gorini, V., A. Kossakowski, and E. C. G. Sudarshan, 1976, J. Math. Phys. (N.Y.) **17**, 821.
Gornyi, I. V., A. D. Mirlin, and D. G. Polyakov, 2005, Phys. Rev. Lett. **95**, 206603.
Granato, E., 1990, Phys. Rev. B **42**, 4797.
Green, M. S., 1952, J. Chem. Phys. **20**, 1281.
Green, M. S., 1954, J. Chem. Phys. **22**, 398.
Greiner, M., O. Mandel, T. Esslinger, T. Hänsch, and I. Bloch, 2002, Nature (London) **415**, 39.
Griffiths, R. B., 1969, Phys. Rev. Lett. **23**, 17.
Grifoni, M., and P. Hänggi, 1998, Phys. Rep. **304**, 229.
Gross, M., and S. Haroche, 1982, Phys. Rep. **93**, 301.
Guimarães, P. H., M. J. de Oliveira, and G. T. Landi, 2016, Phys. Rev. E **94**, 032139.
Gullans, M. J., and D. A. Huse, 2019, Phys. Rev. X **9**, 021007.
Guo, C., I. de Vega, U. Schollwöck, and D. Poletti, 2018, Phys. Rev. A **97**, 053610.
Guo, C., M. Mukherjee, and D. Poletti, 2015, Phys. Rev. A **92**, 023637.
Guo, C., and D. Poletti, 2016, Phys. Rev. A **94**, 033610.
Guo, C., and D. Poletti, 2017a, Phys. Rev. B **96**, 165409.
Guo, C., and D. Poletti, 2017b, Phys. Rev. A **95**, 052107.
Guo, C., and D. Poletti, 2018, Phys. Rev. A **98**, 052126.
Guo, C., and D. Poletti, 2019, Phys. Rev. B **100**, 134304.
Gustavsson, S., R. Leturcq, B. Simovič, R. Schleser, T. Ihn, P. Studerus, K. Ensslin, D. C. Driscoll, and A. C. Gossard, 2006, Phys. Rev. Lett. **96**, 076605.
Hackenbroich, G., and H. A. Weidenmüller, 1996, Phys. Rev. Lett. **76**, 110.

Halbritter, A., P. Makk, S. Csonka, and G. Mihály, 2008, Phys. Rev. B **77**, 075402.
Hamazaki, R., K. Kawabata, N. Kura, and M. Ueda, 2020, Phys. Rev. Res. **2**, 023286.
Harper, P. G., 1955, Proc. Phys. Soc. London Sect. A **68**, 874.
Hartmann, M. J., and G. Carleo, 2019, Phys. Rev. Lett. **122**, 250502.
Hartmann, M. J., J. Prior, S. R. Clark, and M. B. Plenio, 2009, Phys. Rev. Lett. **102**, 057202.
Hartmann, R., and W. T. Strunz, 2020, Phys. Rev. A **101**, 012103.
Hasan, M. Z., and C. L. Kane, 2010, Rev. Mod. Phys. **82**, 3045.
Hasegawa, Y., and T. Van Vu, 2019, Phys. Rev. Lett. **123**, 110602.
Haug, H., and A.-P. Jauho, 2008, *Quantum Kinetics in Transport and Optics of Semiconductors* (Springer-Verlag, Berlin).
Heidrich-Meisner, F., A. Honecker, and W. Brenig, 2005, Phys. Rev. B **71**, 184415.
Heij, C. P., D. C. Dixon, P. Hadley, and J. E. Mooij, 1999, Appl. Phys. Lett. **74**, 1042.
Hiltscher, B., M. Governale, and J. König, 2010, Phys. Rev. B **82**, 165452.
Hiramoto, H., and S. Abe, 1988, J. Phys. Soc. Jpn. **57**, 230.
Hiramoto, H., and M. Kohmoto, 1992, Int. J. Mod. Phys. B **06**, 281.
Hofer, P. P., M. Perarnau-Llobet, L. David, M. Miranda, G. Haack, R. Silva, J. B. Brask, and N. Brunner, 2017, New J. Phys. **19**, 123037.
Hofstadter, D. R., 1976, Phys. Rev. B **14**, 2239.
Hofstetter, W., J. König, and H. Schoeller, 2001, Phys. Rev. Lett. **87**, 156803.
Holleitner, A. W., C. R. Decker, H. Qin, K. Eberl, and R. H. Blick, 2001, Phys. Rev. Lett. **87**, 256802.
Hu, J., X. Ruan, and Y. P. Chen, 2009, Nano Lett. **9**, 2730.
Hubig, C., I. P. McCulloch, and U. Schollwöck, 2017, Phys. Rev. B **95**, 035129.
Huh, J., S. Mostame, T. Fujita, M.-H. Yung, and A. Aspuru-Guzik, 2014, New J. Phys. **16**, 123008.
Huse, D. A., R. Nandkishore, and V. Oganesyan, 2014, Phys. Rev. B **90**, 174202.
Husmann, D., M. Lebrat, S. Häusler, J.-P. Brantut, L. Corman, and T. Esslinger, 2018, Proc. Natl. Acad. Sci. U.S.A. **115**, 8563.
Husmann, D., S. Uchino, S. Krinner, M. Lebrat, T. Giamarchi, T. Esslinger, and J.-P. Brantut, 2015, Science **350**, 1498.
Hussein, R., and S. Kohler, 2014, Phys. Rev. B **89**, 205424.
Hützen, R., S. Weiss, M. Thorwart, and R. Egger, 2012, Phys. Rev. B **85**, 121408.
Iadecola, T., and M. Žnidarič, 2019, Phys. Rev. Lett. **123**, 036403.
Iles-Smith, J., A. G. Dijkstra, N. Lambert, and A. Nazir, 2016, J. Chem. Phys. **144**, 044110.
Iles-Smith, J., N. Lambert, and A. Nazir, 2014, Phys. Rev. A **90**, 032114.
Ilievski, E., and J. De Nardis, 2017, Phys. Rev. B **96**, 081118.
Imamoğlu, A., 1994, Phys. Rev. A **50**, 3650.
Iorio, A., E. Strambini, G. Haack, M. Campisi, and F. Giazotto, 2021, Phys. Rev. Appl. **15**, 054050.
Iyer, S., V. Oganesyan, G. Refael, and D. A. Huse, 2013, Phys. Rev. B **87**, 134202.
Jacobs, K., and D. A. Steck, 2006, Contemp. Phys. **47**, 279–303.
Jaksch, D., C. Bruder, J. I. Cirac, C. W. Gardiner, and P. Zoller, 1998, Phys. Rev. Lett. **81**, 3108.
Jamiolkowski, A., 1972, Rep. Math. Phys. **3**, 275.
Jang, S., J. Cao, and R. J. Silbey, 2002, J. Chem. Phys. **116**, 2705.
Jaschke, D., L. D. Carr, and I. de Vega, 2019, Quantum Sci. Technol. **4**, 034002.
Jaschke, D., M. L. Wall, and L. D. Carr, 2018, Comput. Phys. Commun. **225**, 59.
Jepsen, P. N., J. Amato-Grill, I. Dimitrova, W. W. Ho, E. Demler, and W. Ketterle, 2020, Nature (London) **588**, 403.
Jesenko, S., and M. Žnidarič, 2011, Phys. Rev. B **84**, 174438.
Jin, J., A. Biella, O. Viyuela, L. Mazza, J. Keeling, R. Fazio, and D. Rossini, 2016, Phys. Rev. X **6**, 031011.
Jin, J., M. W.-Y. Tu, W.-M. Zhang, and Y. Yan, 2010, New J. Phys. **12**, 083013.
Jin, T., M. Filippone, and T. Giamarchi, 2020, Phys. Rev. B **102**, 205131.
Joachim, C., J. Gimzewski, and A. Aviram, 2000, Nature (London) **408**, 541.
Jordan, P., and E. Wigner, 1928, Z. Phys. **47**, 631.
Jussiau, E., M. Hasegawa, and R. S. Whitney, 2019, Phys. Rev. B **100**, 115411.
Kaestner, B., and V. Kashcheyevs, 2015, Rep. Prog. Phys. **78**, 103901.
Kalantar, N., B. K. Agarwalla, and D. Segal, 2021, Phys. Rev. E **103**, 052130.
Kalugin, P. A., A. Y. Kitaev, and L. Levitov, 1986, Sov. Phys. JETP **64**, 410, http://www.jetp.ras.ru/cgi-bin/e/index/e/64/2/p410?a=list.
Kamiya, N., 2015, Prog. Theor. Exp. Phys. 043A02.
Kao, Y.-J., Y.-D. Hsieh, and P. Chen, 2015, J. Phys. Conf. Ser. **640**, 012040.
Kardar, M., 1986, Phys. Rev. B **33**, 3125.
Karevski, D., and T. Platini, 2009, Phys. Rev. Lett. **102**, 207207.
Karevski, D., V. Popkov, and G. M. Schütz, 2013, Phys. Rev. Lett. **110**, 047201.
Karrasch, C., 2017, New J. Phys. **19**, 033027.
Karrasch, C., J. H. Bardarson, and J. E. Moore, 2012, Phys. Rev. Lett. **108**, 227206.
Karrasch, C., R. Ilan, and J. E. Moore, 2013, Phys. Rev. B **88**, 195129.
Karrasch, C., D. M. Kennes, and F. Heidrich-Meisner, 2016, Phys. Rev. Lett. **117**, 116401.
Karrlein, R., and H. Grabert, 1997, Phys. Rev. E **55**, 153.
Kast, D., and J. Ankerhold, 2013, Phys. Rev. B **87**, 134301.
Kastner, M. A., 1992, Rev. Mod. Phys. **64**, 849.
Katz, G., and R. Kosloff, 2016, Entropy **18**, 186.
Kessler, E. M., G. Giedke, A. Imamoğlu, S. F. Yelin, M. D. Lukin, and J. I. Cirac, 2012, Phys. Rev. A **86**, 012116.
Khemani, V., F. Pollmann, and S. L. Sondhi, 2016, Phys. Rev. Lett. **116**, 247204.
Kilgour, M., B. K. Agarwalla, and D. Segal, 2019, J. Chem. Phys. **150**, 084111.
Kilgour, M., and D. Segal, 2015, J. Chem. Phys. **143**, 024111.
Kilgour, M., and D. Segal, 2016, J. Chem. Phys. **144**, 124107.
Kim, C., M. Prada, H. Qin, H.-S. Kim, and R. H. Blick, 2015, Appl. Phys. Lett. **106**, 061909.
Kim, T.-S., and S. Hershfield, 2002, Phys. Rev. Lett. **88**, 136601.
Kimura, G., S. Ajisaka, and K. Watanabe, 2017, Open Syst. Inf. Dyn. **24**, 1740009.
Kiršanskas, G., M. Franckié, and A. Wacker, 2018, Phys. Rev. B **97**, 035432.
Kleinekathöfer, U., 2004, J. Chem. Phys. **121**, 2505.
Kleinherbers, E., N. Szpak, J. König, and R. Schützhold, 2020, Phys. Rev. B **101**, 125131.
Klich, I., 2003, in *Quantum Noise in Mesoscopic Physics*, NATO Science Series II Vol. 97, edited by Y. V. Nazarov (Springer, Dordrecht), p. 397.
Kobayashi, K., H. Aikawa, S. Katsumoto, and Y. Iye, 2003, Phys. Rev. B **68**, 235304.
Kohler, S., J. Lehmann, and P. Hänggi, 2005, Phys. Rep. **406**, 379.

Kohmoto, M., L. P. Kadanoff, and C. Tang, 1983, Phys. Rev. Lett. **50**, 1870.
Kohmoto, M., B. Sutherland, and C. Tang, 1987, Phys. Rev. B **35**, 1020.
Kohn, W., 1964, Phys. Rev. **133**, A171.
Kolovsky, A. R., 2020, Phys. Rev. B **102**, 174310.
König, D. R., and E. M. Weig, 2012, Appl. Phys. Lett. **101**, 213111.
König, J., and Y. Gefen, 2001, Phys. Rev. Lett. **86**, 3855.
König, J., and Y. Gefen, 2002, Phys. Rev. B **65**, 045316.
Kosloff, R., 2013, Entropy **15**, 2100.
Kouachi, S., 2006, Electron. J. Linear Algebra **15**, 115.
Kraus, K., 1971, Ann. Phys. (N.Y.) **64**, 311.
Krause, T., T. Brandes, M. Esposito, and G. Schaller, 2015, J. Chem. Phys. **142**, 134106.
Krinner, S., M. Lebrat, D. Husmann, C. Grenier, J.-P. Brantut, and T. Esslinger, 2016, Proc. Natl. Acad. Sci. U.S.A. **113**, 8144.
Krinner, S., D. Stadler, D. Husmann, J.-P. Brantut, and T. Esslinger, 2015, Nature (London) **517**, 64.
Kubala, B., and J. König, 2002, Phys. Rev. B **65**, 245301.
Kubo, R., 1957, J. Phys. Soc. Jpn. **12**, 570.
Kulshreshtha, A. K., A. Pal, T. B. Wahl, and S. H. Simon, 2019, Phys. Rev. B **99**, 104201.
Kuo, D. M.-T., and Y.-c. Chang, 2010, Phys. Rev. B **81**, 205321.
Kurzmann, A., P. Stegmann, J. Kerski, R. Schott, A. Ludwig, A. D. Wieck, J. König, A. Lorke, and M. Geller, 2019, Phys. Rev. Lett. **122**, 247403.
Lacerda, A. M., J. Goold, and G. T. Landi, 2021, Phys. Rev. B **104**, 174203.
Lacerda, A. M., A. Purkayastha, M. Kewming, G. T. Landi, and J. Goold, 2022, arXiv:2206.01090.
Laird, B. B., 1991, J. Chem. Phys. **94**, 4391.
Landauer, R., 1957, IBM J. Res. Dev. **1**, 223.
Landi, G. T., and D. Karevski, 2015, Phys. Rev. B **91**, 174422.
Landi, G. T., E. Novais, M. J. de Oliveira, and D. Karevski, 2014, Phys. Rev. E **90**, 042142.
Landi, G. T., and M. Paternostro, 2021, Rev. Mod. Phys. **93**, 035008.
Lang, I. G., and Y. A. Firsov, 1963, Sov. Phys. JETP **16**, 1301, http://www.jetp.ras.ru/cgi-bin/e/index/e/16/5/p1301?a=list.
Lange, S., and C. Timm, 2021, Chaos **31**, 023101.
Latorre, J. I., E. Rico, and G. Vidal, 2004, Quantum Inf. Comput. **4**, 48.
Lebowitz, J. L., and J. A. Scaramazza, 2018, arXiv:1801.07153.
Lebrat, M., P. Grišins, D. Husmann, S. Häusler, L. Corman, T. Giamarchi, J.-P. Brantut, and T. Esslinger, 2018, Phys. Rev. X **8**, 011053.
Lee, K., V. Balachandran, C. Guo, and D. Poletti, 2020, Entropy **22**, 1311.
Lee, K. H., V. Balachandran, C. Guo, and D. Poletti, 2022, Phys. Rev. E **105**, 024120.
Lee, K. H., V. Balachandran, and D. Poletti, 2021, Phys. Rev. E **103**, 052143.
Leggett, A. J., S. Chakravarty, A. T. Dorsey, M. P. A. Fisher, A. Garg, and W. Zwerger, 1987, Rev. Mod. Phys. **59**, 1.
Lenarčič, Z., and T. Prosen, 2015, Phys. Rev. E **91**, 030103.
Lepri, S., and G. Casati, 2011, Phys. Rev. Lett. **106**, 164101.
Levitov, L. S., H. Lee, and G. B. Lesovik, 1996, J. Math. Phys. (N.Y.) **37**, 4845.
Levitov, L. S., and G. B. Lesovik, 1993, JETP Lett. **58**, 230, http://jetpletters.ru/ps/1186/article_17907.shtml.
Levy, A., and R. Kosloff, 2014, Europhys. Lett. **107**, 20004.
Li, B., L. Wang, and G. Casati, 2004, Phys. Rev. Lett. **93**, 184301.
Li, B., L. Wang, and G. Casati, 2006, Appl. Phys. Lett. **88**, 143501.
Li, J., T. c. v. Prosen, and A. Chan, 2021, Phys. Rev. Lett. **127**, 170602.
Li, N., J. Ren, L. Wang, G. Zhang, P. Hänggi, and B. Li, 2012, Rev. Mod. Phys. **84**, 1045.
Li, X., S. Ganeshan, J. H. Pixley, and S. Das Sarma, 2015, Phys. Rev. Lett. **115**, 186601.
Li, X., X. Li, and S. Das Sarma, 2017, Phys. Rev. B **96**, 085119.
Lidar, D. A., Z. Bihary, and K. B. Whaley, 2001, Chem. Phys. **268**, 35.
Lieb, E. H., T. Schultz, and D. Mattis, 1961, Ann. Phys. (N.Y.) **16**, 407.
Lindblad, G., 1976, Commun. Math. Phys. **48**, 119.
Linden, N., S. Popescu, and P. Skrzypczyk, 2010, Phys. Rev. Lett. **105**, 130401.
Liu, J., and D. Segal, 2021, Phys. Rev. E **103**, 032138.
Ljubotina, M., M. Znidaric, and T. Prosen, 2017, Nat. Commun. **8**, 16117.
Longhi, S., 2007, Eur. Phys. J. B **57**, 45.
Loss, D., and E. V. Sukhorukov, 2000, Phys. Rev. Lett. **84**, 1035.
Lu, Y., X. Cao, P. Hansmann, and M. W. Haverkort, 2019, Phys. Rev. B **100**, 115134.
Luitz, D. J., and Y. B. Lev, 2017, Ann. Phys. (Berlin) **529**, 1600350.
Luo, D., Z. Chen, J. Carrasquilla, and B. K. Clark, 2020, arXiv:2009.05580.
Lüschen, H. P., P. Bordia, S. Scherg, F. Alet, E. Altman, U. Schneider, and I. Bloch, 2017, Phys. Rev. Lett. **119**, 260401.
Lüschen, H. P., S. Scherg, T. Kohlert, M. Schreiber, P. Bordia, X. Li, S. Das Sarma, and I. Bloch, 2018, Phys. Rev. Lett. **120**, 160404.
Macé, N., A. Jagannathan, and F. Piéchon, 2016, Phys. Rev. B **93**, 205153.
Macé, N., N. Laflorencie, and F. Alet, 2019, SciPost Phys. **6**, 50.
Maier, C., T. Brydges, P. Jurcevic, N. Trautmann, C. Hempel, B. P. Lanyon, P. Hauke, R. Blatt, and C. F. Roos, 2019, Phys. Rev. Lett. **122**, 050501.
Mäkelä, H., and M. Möttönen, 2013, Phys. Rev. A **88**, 052111.
Malouf, W. T. B., J. Goold, G. Adesso, and G. Landi, 2020, J. Phys. A **53**, 305302.
Mandel, L., and E. Wolf, 1995, *Optical Coherence and Quantum Optics* (Cambridge University Press, Cambridge, England).
Maniscalco, S., 2007, Phys. Rev. A **75**, 062103.
Manzano, D., 2013, PLoS One **8**, e57041.
Manzano, D., C. Chuang, and J. Cao, 2016, New J. Phys. **18**, 043044.
Manzano, D., and P. I. Hurtado, 2014, Phys. Rev. B **90**, 125138.
Manzano, D., and P. I. Hurtado, 2018, Adv. Phys. **67**, 1.
Marcos-Vicioso, A., C. López-Jurado, M. Ruiz-Garcia, and R. Sánchez, 2018, Phys. Rev. B **98**, 035414.
Martensen, N., and G. Schaller, 2019, Eur. Phys. J. B **92**, 30.
Martin, P. C., and J. Schwinger, 1959, Phys. Rev. **115**, 1342.
Martinazzo, R., B. Vacchini, K. H. Hughes, and I. Burghardt, 2011, J. Chem. Phys. **134**, 011101.
Martínez-Pérez, M. J., A. Fornieri, and F. Giazotto, 2015, Nat. Nanotechnol. **10**, 303.
Mascarenhas, E., F. Damanet, S. Flannigan, L. Tagliacozzo, A. J. Daley, J. Goold, and I. de Vega, 2019, Phys. Rev. B **99**, 245134.
Mascarenhas, E., H. Flayac, and V. Savona, 2015, Phys. Rev. A **92**, 022116.
Mascarenhas, E., G. Giudice, and V. Savona, 2017, Quantum **1**, 40.
Mascarenhas, E., M. F. Santos, A. Auffèves, and D. Gerace, 2016, Phys. Rev. A **93**, 043821.
Mascherpa, F., A. Smirne, A. D. Somoza, P. Fernández-Acebal, S. Donadi, D. Tamascelli, S. F. Huelga, and M. B. Plenio, 2020, Phys. Rev. A **101**, 052108.
Mastropietro, V., 2013, Phys. Rev. E **87**, 042121.
Mazur, P., 1969, Physica (Amsterdam) **43**, 533.
McCauley, G., B. Cruikshank, D. I. Bondar, and K. Jacobs, 2020, npj Quantum Inf. **6**, 74.

McCulloch, I. P., 2007, J. Stat. Mech. P10014.
McCutcheon, D. P. S., N. S. Dattani, E. M. Gauger, B. W. Lovett, and A. Nazir, 2011, Phys. Rev. B **84**, 081305.
Medvedyeva, M. V., F. H. L. Essler, and T. Prosen, 2016, Phys. Rev. Lett. **117**, 137202.
Medvedyeva, M. V., T. Prosen, and M. Žnidarič, 2016, Phys. Rev. B **93**, 094205.
Meir, Y., and N. S. Wingreen, 1992, Phys. Rev. Lett. **68**, 2512.
Meir, Y., N. S. Wingreen, and P. A. Lee, 1993, Phys. Rev. Lett. **70**, 2601.
Mendoza-Arenas, J. J., S. Al-Assam, S. R. Clark, and D. Jaksch, 2013, J. Stat. Mech. P07007.
Mendoza-Arenas, J. J., S. R. Clark, and D. Jaksch, 2015, Phys. Rev. E **91**, 042129.
Mendoza-Arenas, J. J., T. Grujic, D. Jaksch, and S. R. Clark, 2013, Phys. Rev. B **87**, 235130.
Mendoza-Arenas, J. J., M. T. Mitchison, S. R. Clark, J. Prior, D. Jaksch, and M. B. Plenio, 2014, New J. Phys. **16**, 053016.
Mendoza-Arenas, J. J., M. Žnidarič, V. K. Varma, J. Goold, S. R. Clark, and A. Scardicchio, 2019, Phys. Rev. B **99**, 094435.
Michaelis, B., C. Emary, and C. W. J. Beenakker, 2006, Europhys. Lett. **73**, 677.
Michel, M., J. Gemmer, and G. Mahler, 2004, Eur. Phys. J. B **42**, 555.
Mierzejewski, M., P. Prelovšek, and J. Bonča, 2019, Phys. Rev. Lett. **122**, 206601.
Mierzejewski, M., and M. Środa, J. Herbrych, and P. Prelovšek, 2020, Phys. Rev. B **102**, 161111.
Millen, J., and A. Xuereb, 2016, New J. Phys. **18**, 011002.
Minganti, F., A. Biella, N. Bartolo, and C. Ciuti, 2018, Phys. Rev. A **98**, 042118.
Mitchison, M. T., and M. B. Plenio, 2018, New J. Phys. **20**, 033005.
Moca, C. P., M. A. Werner, O. Legeza, T. Prosen, M. Kormos, and G. Zaránd, 2022, Phys. Rev. B **105**, 195144.
Modak, R., S. Ghosh, and S. Mukerjee, 2018, Phys. Rev. B **97**, 104204.
Modak, R., and S. Mukerjee, 2015, Phys. Rev. Lett. **115**, 230401.
Mølmer, K., Y. Castin, and J. Dalibard, 1993, J. Opt. Soc. Am. B **10**, 524.
Monthus, C., 2017, J. Stat. Mech. 043303.
Mori, T., and S. Miyashita, 2008, J. Phys. Soc. Jpn. **77**, 124005.
Mori, T., and T. Shirai, 2020, Phys. Rev. Lett. **125**, 230604.
Morrison, S., and A. S. Parkins, 2008, Phys. Rev. Lett. **100**, 040403.
Moskalenko, A. V., S. N. Gordeev, O. F. Koentjoro, P. R. Raithby, R. W. French, F. Marken, and S. E. Savel'ev, 2009, Phys. Rev. B **79**, 241403.
Mott, N. F., 1969, Philos. Mag. **19**, 835.
Mourokh, L. G., N. J. M. Horing, and A. Y. Smirnov, 2002, Phys. Rev. B **66**, 085332.
Mu, A., B. K. Agarwalla, G. Schaller, and D. Segal, 2017, New J. Phys. **19**, 123034.
Mühlbacher, L., and E. Rabani, 2008, Phys. Rev. Lett. **100**, 176403.
Mujica, V., A. Nitzan, S. Datta, M. A. Ratner, and C. P. Kubiak, 2003, J. Phys. Chem. B **107**, 91.
Nagy, A., and V. Savona, 2018, Phys. Rev. A **97**, 052129.
Nagy, A., and V. Savona, 2019, Phys. Rev. Lett. **122**, 250501.
Nakagawa, M., N. Kawakami, and M. Ueda, 2021, Phys. Rev. Lett. **126**, 110404.
Nakajima, S., 1958, Prog. Theor. Phys. **20**, 948.
Nandkishore, R., and D. Huse, 2015, Annu. Rev. Condens. Matter Phys. **6**, 15.
Navez, P., and R. Schützhold, 2010, Phys. Rev. A **82**, 063603.
Nazarov, Y. V., and Y. M. Blanter, 2009, *Quantum Transport: Introduction to Nanoscience* (Cambridge University Press, Cambridge, England).
Nazir, A., and G. Schaller, 2019, in *Thermodynamics in the Quantum Regime: Recent Progress and Outlook*, Fundamental Theories of Physics Vol. 195, edited by F. Binder, L. A. Correa, C. Gogolin, J. Anders, and G. Adesso (Springer, Cham, Switzerland), p. 551.
Newns, D. M., 1969, Phys. Rev. **178**, 1123.
Nielsen, M. A., and I. L. Chuang, 2000, *Quantum Computation and Quantum Information* (Cambridge University Press, Cambridge, England).
Nigro, D., 2019, J. Stat. Mech. 043202.
Nikolić, B. K., K. K. Saha, T. Markussen, and K. S. Thygesen, 2012, J. Comput. Electron. **11**, 78.
Nishiyama, Y., 2000, Eur. Phys. J. B **17**, 295.
Nitzan, A., and M. A. Ratner, 2003, Science **300**, 1384.
Nordsieck, A., W. E. Lamb, and G. E. Uhlenbeck, 1940, Physica (Amsterdam) **7**, 344.
Novotný, T., A. Donarini, and A.-P. Jauho, 2003, Phys. Rev. Lett. **90**, 256801.
Nüßeler, A., I. Dhand, S. F. Huelga, and M. B. Plenio, 2020, Phys. Rev. B **101**, 155134.
Olaya-Castro, A., C. F. Lee, F. F. Olsen, and N. F. Johnson, 2008, Phys. Rev. B **78**, 085115.
Orignac, E., and T. Giamarchi, 2001, Phys. Rev. B **64**, 144515.
Orús, R., 2014, Ann. Phys. (N.Y.) **349**, 117.
Ostlund, S., R. Pandit, D. Rand, H. J. Schellnhuber, and E. D. Siggia, 1983, Phys. Rev. Lett. **50**, 1873.
Paeckel, S., T. Köhler, A. Swoboda, S. R. Manmana, U. Schollwöck, and C. Hubig, 2019, Ann. Phys. (N.Y.) **411**, 167998.
Palmer, P. F., 1977, J. Math. Phys. (N.Y.) **18**, 527.
Palmero, M., X. Xu, C. Guo, and D. Poletti, 2019, Phys. Rev. E **100**, 022111.
Parameswaran, S. A., and R. Vasseur, 2018, Rep. Prog. Phys. **81**, 082501.
Park, H., J. Park, A. K. L. Lim, E. H. Anderson, A. P. Alivisatos, and P. L. McEuen, 2000, Nature (London) **407**, 57.
Pekola, J. P., O.-P. Saira, V. F. Maisi, A. Kemppinen, M. Möttönen, Y. A. Pashkin, and D. V. Averin, 2013, Rev. Mod. Phys. **85**, 1421.
Perarnau-Llobet, M., H. Wilming, A. Riera, R. Gallego, and J. Eisert, 2018, Phys. Rev. Lett. **120**, 120602.
Pereira, E., 2017a, Phys. Rev. E **95**, 030104.
Pereira, E., 2017b, Phys. Rev. E **96**, 012114.
Pereira, E., 2018, Phys. Rev. E **97**, 022115.
Pereira, E., 2019, Phys. Rev. E **99**, 032116.
Pereira, E., and R. R. Ávila, 2013, Phys. Rev. E **88**, 032139.
Pižorn, I., and T. Prosen, 2009, Phys. Rev. B **79**, 184416.
Pleasance, G., B. M. Garraway, and F. Petruccione, 2020, Phys. Rev. Res. **2**, 043058.
Plenio, M. B., J. Eisert, J. Dreißig, and M. Cramer, 2005, Phys. Rev. Lett. **94**, 060503.
Plenio, M. B., and S. F. Huelga, 2008, New J. Phys. **10**, 113019.
Plenio, M. B., and P. L. Knight, 1998, Rev. Mod. Phys. **70**, 101.
Poletti, D., P. Barmettler, A. Georges, and C. Kollath, 2013, Phys. Rev. Lett. **111**, 195301.
Poletti, D., J.-S. Bernier, A. Georges, and C. Kollath, 2012, Phys. Rev. Lett. **109**, 045302.
Polkovnikov, A., 2011, Ann. Phys. (N.Y.) **326**, 486.
Pöltl, C., C. Emary, and T. Brandes, 2009, Phys. Rev. B **80**, 115313.
Ponomarev, A. V., S. Denisov, and P. Hänggi, 2011, Phys. Rev. Lett. **106**, 010405.
Pop, E., D. Mann, J. Cao, Q. Wang, K. Goodson, and H. Dai, 2005, Phys. Rev. Lett. **95**, 155505.

Popkov, V., D. Karevski, and G. M. Schütz, 2013, Phys. Rev. E **88**, 062118.
Popkov, V., and C. Presilla, 2016, Phys. Rev. A **93**, 022111.
Popkov, V., and T. Prosen, 2015, Phys. Rev. Lett. **114**, 127201.
Popkov, V., T. Prosen, and L. Zadnik, 2020a, Phys. Rev. Lett. **124**, 160403.
Popkov, V., T. Prosen, and L. Zadnik, 2020b, Phys. Rev. E **101**, 042122.
Potter, A. C., R. Vasseur, and S. A. Parameswaran, 2015, Phys. Rev. X **5**, 031033.
Potts, P. P., A. A. S. Kalaee, and A. Wacker, 2021, New J. Phys. **23**, 123013.
Poulsen, K., A. C. Santos, L. B. Kristensen, and N. T. Zinner, 2022, Phys. Rev. A **105**, 052605.
Prelovšek, P., O. S. Barišič, and M. Žnidarič, 2016, Phys. Rev. B **94**, 241104.
Prelovšek, P., J. Bonča, and M. Mierzejewski, 2018, Phys. Rev. B **98**, 125119.
Prior, J., A. W. Chin, S. F. Huelga, and M. B. Plenio, 2010, Phys. Rev. Lett. **105**, 050404.
Prociuk, A., H. Phillips, and B. D. Dunietz, 2010, J. Phys. Conf. Ser. **220**, 012008.
Prosen, T., 2008, New J. Phys. **10**, 043026.
Prosen, T., 2010, J. Stat. Mech. P07020.
Prosen, T., 2011a, Phys. Rev. Lett. **107**, 137201.
Prosen, T., 2011b, Phys. Rev. Lett. **106**, 217206.
Prosen, T., 2014, Phys. Rev. Lett. **112**, 030603.
Prosen, T., and E. Ilievski, 2011, Phys. Rev. Lett. **107**, 060403.
Prosen, T., and E. Ilievski, 2013, Phys. Rev. Lett. **111**, 057203.
Prosen, T., and I. Pižorn, 2007, Phys. Rev. A **76**, 032316.
Prosen, T., and I. Pižorn, 2008, Phys. Rev. Lett. **101**, 105701.
Prosen, T., and T. H. Seligman, 2010, J. Phys. A **43**, 392004.
Prosen, T., and M. Žnidarič, 2009, J. Stat. Mech. P02035.
Prosen, T., and M. Žnidarič, 2012, Phys. Rev. B **86**, 125118.
Prosen, T., and M. Žnidarič, 2013, Phys. Rev. Lett. **111**, 124101.
Prosen, T., and B. Žunkovič, 2010, New J. Phys. **12**, 025016.
Ptaszyński, K., and M. Esposito, 2019, Phys. Rev. Lett. **122**, 150603.
Purkayastha, A., 2019, J. Stat. Mech. 043101.
Purkayastha, A., 2022, arXiv:2201.00677.
Purkayastha, A., A. Dhar, and M. Kulkarni, 2016a, Phys. Rev. A **94**, 052134.
Purkayastha, A., A. Dhar, and M. Kulkarni, 2016b, Phys. Rev. A **93**, 062114.
Purkayastha, A., A. Dhar, and M. Kulkarni, 2017, Phys. Rev. B **96**, 180204.
Purkayastha, A., and Y. Dubi, 2017, Phys. Rev. B **96**, 085425.
Purkayastha, A., G. Guarnieri, S. Campbell, J. Prior, and J. Goold, 2021, Phys. Rev. B **104**, 045417.
Purkayastha, A., M. Saha, and B. K. Agarwalla, 2021, Phys. Rev. Lett. **127**, 240601.
Purkayastha, A., S. Sanyal, A. Dhar, and M. Kulkarni, 2018, Phys. Rev. B **97**, 174206.
Queisser, F., K. V. Krutitsky, P. Navez, and R. Schützhold, 2014, Phys. Rev. A **89**, 033616.
Rams, M. M., and M. Zwolak, 2020, Phys. Rev. Lett. **124**, 137701.
Rau, J., 1963, Phys. Rev. **129**, 1880.
Rebentrost, P., M. Mohseni, I. Kassal, S. Lloyd, and A. Aspuru-Guzik, 2009, New J. Phys. **11**, 033003.
Redfield, A. G., 1965, *Advances in Magnetic and Optical Resonance*, Vol. 1 (Academic Press, New York).
Restrepo, S., S. Böhling, J. Cerrillo, and G. Schaller, 2019, Phys. Rev. B **100**, 035109.
Ribeiro, P., and V. R. Vieira, 2015, Phys. Rev. B **92**, 100302(R).
Rieder, Z., J. L. Lebowitz, and E. Lieb, 1967, J. Math. Phys. (N.Y.) **8**, 1073.
Riera-Campeny, A., A. Sanpera, and P. Strasberg, 2022, Phys. Rev. E **105**, 054119.
Rivas, Á., and S. F. Huelga, 2012, *Open Quantum Systems: An Introduction* (Springer, Heidelberg).
Rivas, Á., S. F. Huelga, and M. B. Plenio, 2014, Rep. Prog. Phys. **77**, 094001.
Rivas, Á., and M. A. Martin-Delgado, 2017, Sci. Rep. **7**, 6350.
Rivas, Á., A. D. K. Plato, S. F. Huelga, and M. B. Plenio, 2010, New J. Phys. **12**, 113032.
Roberts, N. A., and D. G. Walker, 2011, Int. J. Therm. Sci. **50**, 648.
Rolf-Pissarczyk, S., S. Yan, L. Malavolti, J. A. J. Burgess, G. McMurtrie, and S. Loth, 2017, Phys. Rev. Lett. **119**, 217201.
Ros, V., M. Müller, and A. Scardicchio, 2015, Nucl. Phys. **B891**, 420.
Roy, N., and A. Sharma, 2019, Phys. Rev. B **100**, 195143.
Rubio-García, Á., R. A. Molina, and J. Dukelsky, 2022, SciPost Phys. Core **5**, 26.
Ryndyk, D., 2016, *Theory of Quantum Transport at Nanoscale*, Springer Series in Solid-State Sciences Vol. 184 (Springer International Publishing, Cham, Switzerland).
Sá, L., P. Ribeiro, T. Can, and T. Prosen, 2020, Phys. Rev. B **102**, 134310.
Sá, L., P. Ribeiro, and T. Prosen, 2020a, Phys. Rev. X **10**, 021019.
Sá, L., P. Ribeiro, and T. Prosen, 2020b, J. Phys. A **53**, 305303.
Sachdev, S., 2011, *Quantum Phase Transitions* (Cambridge University Press, Cambridge, England).
Saha, M., S. K. Maiti, and A. Purkayastha, 2019, Phys. Rev. B **100**, 174201.
Saha, M., B. P. Venkatesh, and B. K. Agarwalla, 2022, arXiv:2202.14033.
Saito, K., and Y. Utsumi, 2008, Phys. Rev. B **78**, 115429.
Scalapino, D. J., S. R. White, and S. Zhang, 1993, Phys. Rev. B **47**, 7995.
Scali, S., J. Anders, and L. A. Correa, 2021, Quantum **5**, 451.
Scarani, V., M. Ziman, P. Štelmachovič, N. Gisin, V. Bužek, and V. Bužek, 2002, Phys. Rev. Lett. **88**, 097905.
Schaller, G., 2014, *Open Quantum Systems Far from Equilibrium*, Lecture Notes in Physics Vol. 881, (Springer, Cham, Switzerland).
Schaller, G., J. Cerrillo, G. Engelhardt, and P. Strasberg, 2018, Phys. Rev. B **97**, 195104.
Schaller, G., G. G. Giusteri, and G. L. Celardo, 2016, Phys. Rev. E **94**, 032135.
Schaller, G., G. Kießlich, and T. Brandes, 2010, Phys. Rev. B **81**, 205305.
Schaller, G., T. Krause, T. Brandes, and M. Esposito, 2013, New J. Phys. **15**, 033032.
Schaller, G., C. Nietner, and T. Brandes, 2014, New J. Phys. **16**, 125011.
Schaller, G., F. Queisser, N. Szpak, J. König, and R. Schützhold, 2022, Phys. Rev. B **105**, 115139.
Schaller, G., M. Vogl, and T. Brandes, 2014, J. Phys. Condens. Matter **26**, 265001.
Schaller, G., P. Zedler, and T. Brandes, 2009, Phys. Rev. A **79**, 032110.
Scheible, D. V., and R. H. Blick, 2004, Appl. Phys. Lett. **84**, 4632.
Scheibner, R., M. Konig, D. Reuter, A. Weick, C. Gould, H. Buhmann, and L. Molenkamp, 2008, New J. Phys. **10**, 083016.
Scheie, A., N. E. Sherman, M. Dupont, S. E. Nagler, M. B. Stone, G. E. Granroth, J. E. Moore, and D. A. Tennant, 2021, Nat. Phys. **17**, 726.

Schlosshauer, M., 2007, *Decoherence and the Quantum-to-Classical Transition* (Springer-Verlag, Berlin).
Schollwöck, U., 2005, Rev. Mod. Phys. **77**, 259.
Schollwöck, U., 2011, Ann. Phys. (N.Y.) **326**, 96.
Schönhammer, K., 2007, Phys. Rev. B **75**, 205329.
Schreiber, M., S. S. Hodgman, P. Bordia, H. P. Lüschen, M. H. Fischer, R. Vosk, E. Altman, U. Schneider, and I. Bloch, 2015, Science **349**, 842.
Schröder, M., M. Schreiber, and U. Kleinekathöfer, 2007, J. Chem. Phys. **126**, 114102.
Schuab, L., E. Pereira, and G. T. Landi, 2016, Phys. Rev. E **94**, 042122.
Schultz, M. G., and F. von Oppen, 2009, Phys. Rev. B **80**, 033302.
Schulz, M., S. R. Taylor, C. A. Hooley, and A. Scardicchio, 2018, Phys. Rev. B **98**, 180201.
Schulz, M., S. R. Taylor, A. Scardicchio, and M. Žnidarič, 2020, J. Stat. Mech. 023107.
Schuster, B., E. Buks, M. Heiblum, D. Mahalu, V. Umansky, and H. Shtrikman, 1997, Nature (London) **385**, 417.
Schwarz, F., I. Weymann, J. von Delft, and A. Weichselbaum, 2018, Phys. Rev. Lett. **121**, 137702.
Sciolla, B., D. Poletti, and C. Kollath, 2015, Phys. Rev. Lett. **114**, 170401.
Seah, S., S. Nimmrichter, and V. Scarani, 2018, Phys. Rev. E **98**, 012131.
Seaman, B. T., M. Krämer, D. Z. Anderson, and M. J. Holland, 2007, Phys. Rev. A **75**, 023615.
Secular, P., N. Gourianov, M. Lubasch, S. Dolgov, S. R. Clark, and D. Jaksch, 2020, Phys. Rev. B **101**, 235123.
Segal, D., 2008, Phys. Rev. Lett. **100**, 105901.
Segal, D., and B. K. Agarwalla, 2016, Annu. Rev. Phys. Chem. **67**, 185.
Segal, D., A. J. Millis, and D. R. Reichman, 2010, Phys. Rev. B **82**, 205323.
Serafini, A., 2017, *Quantum Continuous Variable: A Primer of Theoretical Methods* (CRC Press, Boca Raton).
Setiawan, F., D.-L. Deng, and J. H. Pixley, 2017, Phys. Rev. B **96**, 104205.
Shahbazyan, T. V., and M. E. Raikh, 1994, Phys. Rev. B **49**, 17123.
Shastry, B. S., and B. Sutherland, 1990, Phys. Rev. Lett. **65**, 243.
Shekhter, R. I., Y. Galperin, L. Y. Gorelik, A. Isacsson, and M. Jonson, 2003, J. Phys. Condens. Matter **15**, R441.
Sierra, M. A., and D. Sánchez, 2014, Phys. Rev. B **90**, 115313.
Sigrist, M., A. Fuhrer, T. Ihn, K. Ensslin, S. E. Ulloa, W. Wegscheider, and M. Bichler, 2004, Phys. Rev. Lett. **93**, 066802.
Silva, A., Y. Oreg, and Y. Gefen, 2002, Phys. Rev. B **66**, 195316.
Silva, S. H. S., G. T. Landi, R. C. Drumond, and E. Pereira, 2020, Phys. Rev. E **102**, 062146.
Silvi, P., F. Tschirsich, M. Gerster, J. Jünemann, D. Jaschke, M. Rizzi, and S. Montangero, 2019, SciPost Phys. Lect. Notes **8**, 1.
Simine, L., and D. Segal, 2012, Phys. Chem. Chem. Phys. **14**, 13820.
Spohn, H., 1978, J. Math. Phys. (N.Y.) **19**, 1227.
Srednicki, M., 1993, Phys. Rev. Lett. **71**, 666.
Srednicki, M., 1994, Phys. Rev. E **50**, 888.
Środa, M., P. Prelovšek, and M. Mierzejewski, 2019, Phys. Rev. B **99**, 121110.
Stadler, D., S. Krinner, J. Meineke, J.-P. Brantut, and T. Esslinger, 2012, Nature (London) **491**, 736.
Starr, C., 1936, Physics **7**, 15.
Stegmann, P., J. König, and B. Sothmann, 2020, Phys. Rev. B **101**, 075411.
Stegmann, P., B. Sothmann, A. Hucht, and J. König, 2015, Phys. Rev. B **92**, 155413.
Stinespring, W. F., 1955, Proc. Am. Math. Soc. **6**, 211.
Stopa, M., 2002, Phys. Rev. Lett. **88**, 146802.
Stoudenmire, E. M., and S. R. White, 2013, Phys. Rev. B **87**, 155137.
Strasberg, P., 2019, Phys. Rev. Lett. **123**, 180604.
Strasberg, P., 2022, *Quantum Stochastic Thermodynamics* (Oxford University Press, Oxford).
Strasberg, P., G. Schaller, T. Brandes, and M. Esposito, 2017, Phys. Rev. X **7**, 021003.
Strasberg, P., G. Schaller, N. Lambert, and T. Brandes, 2016, New J. Phys. **18**, 073007.
Strasberg, P., G. Schaller, T. L. Schmidt, and M. Esposito, 2018, Phys. Rev. B **97**, 205405.
Strasberg, P., C. W. Wächtler, and G. Schaller, 2021, Phys. Rev. Lett. **126**, 180605.
Sutherland, B., and M. Kohmoto, 1987, Phys. Rev. B **36**, 5877.
Sutradhar, J., S. Mukerjee, R. Pandit, and S. Banerjee, 2019, Phys. Rev. B **99**, 224204.
Suzuki, M., 1971, Physica (Amsterdam) **51**, 277.
Svensson, S. F., E. A. Hoffmann, N. Nakpathomkun, P. M. Wu, H. Q. Xu, H. A. Nilsson, D. Sánchez, V. Kashcheyevs, and H. Linke, 2013, New J. Phys. **15**, 105011.
Switkes, M., C. M. Marcus, K. Campman, and A. C. Gossard, 1999, Science **283**, 1905.
Szegő, G., 1939, *Orthogonal Polynomials* (American Mathematical Society, Providence).
Takahashi, Y., and H. Umezawa, 1996, Int. J. Mod. Phys. B **10**, 1755.
Talarico, N. W., S. Maniscalco, and N. L. Gullo, 2020, Phys. Rev. B **101**, 045103.
Talkner, P., and P. Hänggi, 2020, Rev. Mod. Phys. **92**, 041002.
Tamascelli, D., A. Smirne, S. F. Huelga, and M. B. Plenio, 2018, Phys. Rev. Lett. **120**, 030402.
Tamascelli, D., A. Smirne, J. Lim, S. F. Huelga, and M. B. Plenio, 2019, Phys. Rev. Lett. **123**, 090402.
Tang, G., L. Zhang, and J. Wang, 2018, Phys. Rev. B **97**, 224311.
Tanimura, Y., 1990, Phys. Rev. A **41**, 6676.
Tanimura, Y., and R. Kubo, 1989, J. Phys. Soc. Jpn. **58**, 101.
Tao, N. J., 2009, *Electron Transport in Molecular Junctions* (World Scientific, Singapore).
Taylor, S. R., and A. Scardicchio, 2021, Phys. Rev. B **103**, 184202.
Terraneo, M., M. Peyrard, and G. Casati, 2002, Phys. Rev. Lett. **88**, 094302.
Thingna, J., and D. Manzano, 2021, Chaos **31**, 073114.
Thingna, J., D. Manzano, and J. Cao, 2016, Sci. Rep. **6**, 28027.
Thingna, J., D. Manzano, and J. Cao, 2020, New J. Phys. **22**, 083026.
Thingna, J., J.-S. Wang, and P. Hänggi, 2012, J. Chem. Phys. **136**, 194110.
Thingna, J., H. Zhou, and J.-S. Wang, 2014, J. Chem. Phys. **141**, 194101.
Thouless, D. J., 1983, Phys. Rev. B **27**, 6083.
Timm, C., 2009, Phys. Rev. E **80**, 021140.
Timpanaro, A. M., G. Guarnieri, J. Goold, and G. T. Landi, 2019, Phys. Rev. Lett. **123**, 090604.
Topp, G. E., T. Brandes, and G. Schaller, 2015, Europhys. Lett. **110**, 67003.
Torres, J. M., 2014, Phys. Rev. A **89**, 052133.
Torrontegui, E., and R. Kosloff, 2016, New J. Phys. **18**, 093001.
Touchette, H., 2009, Phys. Rep. **478**, 1.
Tritt, T. M., 2004, *Thermal Conductivity: Theory, Properties and Applications* (Kluwer Academic, Dordrecht).
Trushechkin, A., 2021, Phys. Rev. A **103**, 062226.
Turkington, D. A., 2013, *Generalized Vectorization, Cross-Products, and Matrix Calculus* (Cambridge University Press, Cambridge, England).

Ueda, A., I. Baba, K. Suzuki, and M. Eto, 2003, J. Phys. Soc. Jpn. **72**, 157.
Urban, D., and J. König, 2009, Phys. Rev. B **79**, 165319.
Urban, D., J. König, and R. Fazio, 2008, Phys. Rev. B **78**, 075318.
Utsumi, Y., D. S. Golubev, M. Marthaler, K. Saito, T. Fujisawa, and G. Schön, 2010, Phys. Rev. B **81**, 125331.
Van den Broeck, C., and M. Esposito, 2015, Physica (Amsterdam) **418A**, 6.
van Oudenaarden, A., and J. E. Mooij, 1996, Phys. Rev. Lett. **76**, 4947.
Varma, V. K., C. de Mulatier, and M. Žnidarič, 2017a, Phys. Rev. E **96**, 032130.
Varma, V. K., C. de Mulatier, and M. Žnidarič, 2017b, Phys. Rev. E **96**, 032130.
Varma, V. K., A. Lerose, F. Pietracaprina, J. Goold, and A. Scardicchio, 2017, J. Stat. Mech. 053101.
Varma, V. K., and M. Žnidarič, 2019, Phys. Rev. B **100**, 085105.
Verstraete, F., V. Murg, and J. I. Cirac, 2008, Adv. Phys. **57**, 143.
Vicentini, F., A. Biella, N. Regnault, and C. Ciuti, 2019, Phys. Rev. Lett. **122**, 250503.
Viciani, S., M. Lima, M. Bellini, and F. Caruso, 2015, Phys. Rev. Lett. **115**, 083601.
Vidal, G., J. I. Latorre, E. Rico, and A. Kitaev, 2003, Phys. Rev. Lett. **90**, 227902.
Vidal, J., D. Mouhanna, and T. Giamarchi, 1999, Phys. Rev. Lett. **83**, 3908.
Vidal, J., D. Mouhanna, and T. Giamarchi, 2001, Phys. Rev. B **65**, 014201.
Vinjanampathy, S., and J. Anders, 2016, Contemp. Phys. **57**, 545.
Vogl, M., G. Schaller, and T. Brandes, 2011, Ann. Phys. (N.Y.) **326**, 2827.
Vorberg, D., W. Wustmann, R. Ketzmerick, and A. Eckardt, 2013, Phys. Rev. Lett. **111**, 240405.
Vosk, R., D. A. Huse, and E. Altman, 2015, Phys. Rev. X **5**, 031032.
Wächtler, C. W., and G. Schaller, 2020, Phys. Rev. Res. **2**, 023178.
Wächtler, C. W., P. Strasberg, S. H. L. Klapp, G. Schaller, and C. Jarzynski, 2019, New J. Phys. **21**, 073009.
Wagner, T., P. Strasberg, J. C. Bayer, E. P. Rugeramigabo, T. Brandes, and R. J. Haug, 2017, Nat. Nanotechnol. **12**, 218.
Wahl, T. B., A. Pal, and S. H. Simon, 2017, Phys. Rev. X **7**, 021018.
Wang, C., J. Ren, and J. Cao, 2015, Sci. Rep. **5**, 11787.
Wang, C., and K.-W. Sun, 2015, Ann. Phys. (N.Y.) **362**, 703.
Wang, H., Y. Yang, H. Chen, N. Li, and L. Zhang, 2019, Phys. Rev. E **99**, 062111.
Wang, J.-S., B. K. Agarwalla, and H. L. Thingna, 2014, Front. Phys. **9**, 673.
Wang, K., F. Piazza, and D. J. Luitz, 2020, Phys. Rev. Lett. **124**, 100604.
Weidenmüller, H. A., 2003, Phys. Rev. B **68**, 125326.
Weimer, H., 2015, Phys. Rev. Lett. **114**, 040402.
Weimer, H., A. Kshetrimayum, and R. Orús, 2021, Rev. Mod. Phys. **93**, 015008.
Weiner, F., F. Evers, and S. Bera, 2019, Phys. Rev. B **100**, 104204.
Weis, J., R. J. Haug, K. v. Klitzing, and K. Ploog, 1993, Phys. Rev. Lett. **71**, 4019.
Weiss, U., 1993, *Quantum Dissipative Systems*, Series of Modern Condensed Matter Physics Vol. 2 (World Scientific, Singapore).
Werlang, T., M. A. Marchiori, M. F. Cornelio, and D. Valente, 2014, Phys. Rev. E **89**, 062109.
Werlang, T., and D. Valente, 2015, Phys. Rev. E **91**, 012143.
Werner, A. H., D. Jaschke, P. Silvi, M. Kliesch, T. Calarco, J. Eisert, and S. Montangero, 2016, Phys. Rev. Lett. **116**, 237201.
Wichterich, H., M. J. Henrich, H. P. Breuer, J. Gemmer, and M. Michel, 2007, Phys. Rev. E **76**, 031115.
Willms, A. R., 2008, SIAM J. Matrix Anal. Appl. **30**, 639.
Wilson, K. G., 1975, Rev. Mod. Phys. **47**, 773.
Wiseman, H. M., and G. J. Milburn, 2010, *Quantum Measurement and Control* (Cambridge University Press, Cambridge, England).
Wójtowicz, G., J. E. Elenewski, M. M. Rams, and M. Zwolak, 2020, Phys. Rev. A **101**, 050301.
Wolf, F. A., I. P. McCulloch, and U. Schollwöck, 2014, Phys. Rev. B **90**, 235131.
Wolf, M. M., 2006, Phys. Rev. Lett. **96**, 010404.
Wolff, S., A. Sheikhan, and C. Kollath, 2020, SciPost Phys. Core **3**, 10.
Woods, M. P., R. Groux, A. W. Chin, S. F. Huelga, and M. B. Plenio, 2014, J. Math. Phys. (N.Y.) **55**, 032101.
Wu, L.-A., and D. Segal, 2009a, J. Phys. A **42**, 025302.
Wu, L.-A., and D. Segal, 2009b, Phys. Rev. Lett. **102**, 095503.
Wu, L.-A., C. X. Yu, and D. Segal, 2009, Phys. Rev. E **80**, 041103.
Wu, L.-N., and A. Eckardt, 2019, Phys. Rev. Lett. **123**, 030602.
Wu, L.-N., and A. Eckardt, 2020, Phys. Rev. B **101**, 220302.
Wu, L.-N., A. Schnell, G. D. Tomasi, M. Heyl, and A. Eckardt, 2019, New J. Phys. **21**, 063026.
Xiao, D., M.-C. Chang, and Q. Niu, 2010, Rev. Mod. Phys. **82**, 1959.
Xing, B., X. Xu, V. Balachandran, and D. Poletti, 2020, Phys. Rev. B **102**, 245433.
Xu, B., and Y. Dubi, 2015, J. Phys. Condens. Matter **27**, 263202.
Xu, S., H. Z. Shen, X. X. Yi, and W. Wang, 2019, Phys. Rev. A **100**, 032108.
Xu, X., K. Choo, V. Balachandran, and D. Poletti, 2019, Entropy **21**, 228.
Xu, X., C. Guo, and D. Poletti, 2022, Phys. Rev. A **105**, L040203.
Xu, X., J. Thingna, C. Guo, and D. Poletti, 2019, Phys. Rev. A **99**, 012106.
Xu, X., J. Thingna, and J.-S. Wang, 2017, Phys. Rev. B **95**, 035428.
Xue-Ou, C., D. Bing, and L. Xiao-Lin, 2008, Chin. Phys. Lett. **25**, 3032.
Yacoby, A., M. Heiblum, D. Mahalu, and H. Shtrikman, 1995, Phys. Rev. Lett. **74**, 4047.
Yamanaka, K., and T. Sasamoto, 2021, arXiv:2104.11479.
Yan, Y., C.-Q. Wu, and B. Li, 2009, Phys. Rev. B **79**, 014207.
Yang, J., J.-T. Hsiang, A. N. Jordan, and B. Hu, 2020, Ann. Phys. (N.Y.) **421**, 168289.
Yang, Y., H. Chen, H. Wang, N. Li, and L. Zhang, 2018, Phys. Rev. E **98**, 042131.
Yeyati, A. L., and M. Büttiker, 1995, Phys. Rev. B **52**, R14360.
Yoshioka, N., and R. Hamazaki, 2019, Phys. Rev. B **99**, 214306.
Yueh, W. C., 2005, Appl. Math. E-Notes **5**, 66, https://www.emis.de/journals/AMEN/2005/040903-7.pdf.
Zanoci, C., and B. Swingle, 2021, Phys. Rev. B **103**, 115148.
Zedler, P., G. Schaller, G. Kießlich, C. Emary, and T. Brandes, 2009, Phys. Rev. B **80**, 045309.
Zhang, L., Y. Yan, C.-Q. Wu, J.-S. Wang, and B. Li, 2009, Phys. Rev. B **80**, 172301.
Zhou, C., J. Kong, E. Yenilmez, and H. Dai, 2000, Science **290**, 1552.
Zimbovskaya, N. A., 2020, J. Phys. Condens. Matter **32**, 325302.
Zimbovskaya, N. A., and M. R. Pederson, 2011, Phys. Rep. **509**, 1.
Ziolkowska, A. A., and F. H. Essler, 2020, SciPost Phys. **8**, 44.
Žnidarič, M., 2010a, J. Stat. Mech. L05002.
Žnidarič, M., 2010b, J. Phys. A **43**, 415004.
Žnidarič, M., 2011a, Phys. Rev. E **83**, 011108.
Žnidarič, M., 2011b, Phys. Rev. Lett. **106**, 220601.
Žnidarič, M., 2011c, J. Stat. Mech. P12008.
Žnidarič, M., 2013a, Phys. Rev. Lett. **110**, 070602.

Žnidarič, M., 2013b, Phys. Rev. B **88**, 205135.
Žnidarič, M., 2014a, Phys. Rev. Lett. **112**, 040602.
Žnidarič, M., 2014b, Phys. Rev. E **89**, 042140.
Žnidarič, M., 2015, Phys. Rev. E **92**, 042143.
Žnidarič, M., 2019, Phys. Rev. B **99**, 035143.
Žnidarič, M., 2020, Phys. Rev. Lett. **125**, 180605.
Žnidarič, M., 2021, Phys. Rev. B **103**, 237101.
Žnidarič, M., 2022, Phys. Rev. B **105**, 045140.
Žnidarič, M., and M. Horvat, 2013, Eur. Phys. J. B **86**, 67.
Žnidarič, M., and M. Ljubotina, 2018, Proc. Natl. Acad. Sci. U.S.A. **115**, 4595.
Žnidarič, M., J. J. Mendoza-Arenas, S. R. Clark, and J. Goold, 2017, Ann. Phys. (Berlin) **529**, 1600298.
Žnidarič, M., T. Prosen, G. Benenti, G. Casati, and D. Rossini, 2010, Phys. Rev. E **81**, 051135.
Žnidarič, M., A. Scardicchio, and V. K. Varma, 2016, Phys. Rev. Lett. **117**, 040601.
Žnidarič, M., B. Žunkovič, and T. Prosen, 2011, Phys. Rev. E **84**, 051115.
Zotos, X., F. Naef, and P. Prelovsek, 1997, Phys. Rev. B **55**, 11029.
Zwanzig, R., 1960, J. Chem. Phys. **33**, 1338.